



Treball Final de Grau

Study of the influence of secondary phases in the properties of superduplex stainless steel.

Estudio de la influencia de las fases secundarias en las propiedades de los aceros inoxidables superduplex.

Jordi Boquer Viñas

Junio 2017



UNIVERSITAT DE
BARCELONA

Aquesta obra està subjecta a la llicència de:
Reconeixement–NoComercial–SenseObraDerivada



<http://creativecommons.org/licenses/by-nc-nd/3.0/es/>

“Nothing in life is to be feared, it is only to be understood. Now is the time to understand more, so that we may fear less”

Marie Curie

I want to thank Daniella for her impressive support and distinguished assistance throughout the course of this project. In addition, i would like to thank my tutor N ria for her guidance during the whole evaluation.

CONTENTS

| | |
|---|------------|
| 1. Summary | i |
| 2. Resumen | iii |
| 3. Fundamentals | 1 |
| 3.1. Introduction | |
| 3.1.1. <i>Classification of stainless steels</i> | |
| 3.2. Duplex stainless steels (<i>DSS</i>) | |
| 3.3. Background and uses | |
| 3.4. Properties | |
| 3.5. Factors in selection of stainless steel | |
| 3.6. Chemical composition and microstructure | |
| 3.7. Metallurgy | |
| 3.8. Precipitation of intermetallic phases | |
| 3.9. Corrosion mechanisms | |
| 4. Objectives | 25 |
| 5. Experimental procedure | 26 |
| 5.1. Starting material (type and composition of steel) | |
| 5.2. Project Outline | |
| 5.3. Cutter | |
| 5.4. Isothermal heat treatments | |
| 5.5. Sample preparation | |
| 5.6. Characterization | |
| 5.6.1. <i>Scanning electron microscope (SEM)</i> | |
| 5.6.2. <i>Energy dispersion spectroscopy analysis (EDS)</i> | |
| 5.6.3. <i>Hardness test</i> | |
| 5.6.4. <i>Phase quantification</i> | |
| 5.7. Corrosion flooding essay | |
| 6. Results and discussion | 39 |
| 6.1. Evolution of microstructure upon aging and EDS microanalysis | |
| 6.2. Evolution of mechanical properties upon aging | |
| 6.3. Corrosion study | |
| 7. Conclusions | 55 |
| 8. Reference and Notes | 57 |
| 9. Appendices | 63 |

1. SUMMARY

The main focus on this project is to study the how the formation of secondary phases in superduplex stainless steel (SDSS) affects its mechanical and corrosion properties. At relatively high temperatures these high alloying stainless steels tend to have the drawback of forming certain secondary phases which can influence poorly on very significant and relevant properties of the steel. These phases, that are tough to quantify, patch together in a range of temperatures that depend on the chemical composition of the steel.

However, their stability at these temperatures has not been studied in depth. The aim of this project is to produce these secondary phases to a different extent in samples of SDSS extracted from a valve in a desalination plant, to subsequently check their thermal stability, analyze their corresponding microstructure, hardness and resistance to corrosion.

Duplex stainless steels are ferritic-austenitic steels, which mean that approximately half of their microstructure is made of ferrite and the other half austenite, thus ensuring good mechanical and corrosion properties. However, owing to their susceptibility to formation of dangerous intermetallic phases, the uses of SDSS have been narrowed down, especially in temperature range over 500°C.

At this temperature range the formation of the σ -phase is enhanced, but also other intermetallic phases such as the χ -phase and carbides and nitrides. The formation of these phases make the steel more brittle and hard, and reduce the corrosion resistance, making the steel less useful and effective in work environments. It has been demonstrated that over a certain amount of σ -phase, the toughness of the SDSS is reduced to values which are lower than the accepted standards, and so unsuitable for practical applications. Therefore, many standards relating to manufacturing (casting) and welding of SDSS require no intermetallic phases in the microstructure.

In order to achieve the formation of these secondary phases samples of this Super duplex stainless steel have been submitted to annealing isothermal treatments of temperatures of 850°C and 1050°C and different time scales. The goal was then to first observe and try to quantify the amount of secondary intermetallic phases formed due to the thermal, and then find the relationship between the growth of these phases with the increase of hardness and decrease of corrosion resistances.

Since the decade of the 80's, super duplex stainless steels is one of the metallic materials with highest corrosion resistance under saline atmospheres, and since alloy studied in this project derives from a working environment with a lot of salinity, it seemed appropriate to run corrosion tests to determine how σ -phase and χ -phase affect the metal's corrosion resistance.

The samples submitted to several thermal treatments (and therefore with a different composition in intermetallic phases) were left at first for 15 days soaked in a 4% NaCl solution, stirring the solution continuously with the help of a magnetic stirred. With this experiment we were able to simulate the behavior of SDSS in a saline and high chlorinated environment, such as the one we would be able to find in a chemical industry, in a desalination plant or in industries which are located in sea water on a marine environment. The experiment was later repeated with Mediterranean Sea water in order to compare the different states of corrosion.

The corrosion is later on studied with an optical microscope, a Scanning Electron Microscope (SEM) and EDS microanalysis. In order to figure out the effect of corrosion, our samples are examined using these microscopy techniques and characterized by the EDS analysis. Moreover, the weight gain and loss methods will be applied, measuring each samples weight at a prefixed time scale whilst performing the experiment. Corrosion by pitting is to be found considerably throughout all the samples.

The study of the microstructure was carried out using the high resolution scanning electron microscope (Field Emission SEM). Using a backscattered electron detector and EDS (energy dispersive spectroscopy) microanalysis we were able to observe and characterize all the different phases in the different samples and different thermal treatments. This way we are able to compare the amount of corrosion formed in a sample with the quantity of intermetallic phases present in the alloying constituent. Finally, hardness tests were performed utilizing the Rockwell C scale, in order to observe how the increase of hardness in each sample correlates to the formation of brittle intermetallic phases.

Keywords: *Superduplex stainless steel, thermal treatment, secondary phases, microstructure, corrosion, characterization*

2. RESUMEN

El principal enfoque de este proyecto es el estudio de como la formación de fases secundarias en los aceros inoxidable dúplex y súper dúplex (AISD) afectan a sus propiedades mecánicas y de corrosión. A temperaturas altas, estos aceros inoxidable de alta aleación son susceptibles a la formación de ciertas fases secundarias, las cuales influencia negativamente en las propiedades más significativas del acero. Estas fases, que son difíciles de cuantificar, se componen en un rango de temperaturas que depende de la composición química del acero.

Sin embargo, su estabilidad a estas temperaturas no ha sido estudiada en profundidad. El objetivo de este proyecto es producir estas fases secundarias en diferentes cantidades a lo largo de una serie de muestras de AISD, para a posteriori comprobar su estabilidad térmica, analizar la microestructura correspondiente, su dureza y la resistencia a la corrosión. Las muestras provienen de una válvula de una planta desalinizadora.

Los aceros inoxidable dúplex y súper dúplex son aceros ferrítico-austeníticos, lo que significa que la aproximadamente la mitad de su microestructura está formada de ferrita, mientras que la otra mitad está hecha de austenita, asegurando así unas buenas propiedades mecánicas y de corrosión. Sin embargo, debido a su susceptibilidad a formar fases intermetálicas no deseadas, los usos de estos aceros han sido acotados a procesos con temperaturas de servicio inferiores a los 500°C.

A estos rangos de temperaturas la formación de la fase sigma se promueve, al igual que otras fases intermetálicas con la fase chi, carburos y nitruros. La formación de estas fases hace que el acero sea más frágil y lo endurece, reduce su resistencia a la corrosión, haciendo que éste sea menos útil y efectivo en ambientes de trabajo industriales. Se ha demostrado que cuando el acero sobrepasa una determinada cantidad de fase chi, la tenacidad de dicho acero se reduce a valores por debajo de los estándares aceptados, y por tanto es inadecuado para aplicaciones prácticas. Debido a esto, muchos estándares de fabricación (fundición) y soldadura de AISD especifican que no contengan fases intermetálicas en la microestructura.

Para lograr la formación de estas fases secundarias intermetálicas, muestras de acero inoxidable súper dúplex son sometidas a tratamientos isotérmicos de recocido a temperaturas de 850°C y 1050°C durante diferentes tiempos de ensayo. El objetivo es, primero, observar la formación de estas fases secundarias debido a los tratamientos térmicos e intentar cuantificarla respecto a las demás fases. Posteriormente, se intentará encontrar la relación entre el crecimiento de estas fases con el incremento de la dureza y la disminución de la resistencia a la corrosión.

Desde la década de los 80's, el acero inoxidable súper dúplex es uno de los materiales metálicos con mayor resistencia a la corrosión en atmosferas salinas, y ya que la aleación usada en este proyecto proviene de una planta desalinizadora, y por tanto de un ambiente con una alta salinidad, pareció apropiado hacer ensayos de corrosión para determinar como la fase sigma y la fase chi afectaban a la resistencia a la corrosión del acero.

Las muestras que se trataron térmicamente (y por lo tanto contenían una composición diferente de fases intermetálicas) se dejaron 15 días en remojo en una solución de 4% de cloruro sódico, agitándose la misma continuamente con la ayuda de un agitador magnético. Con este experimento somos capaces de simular el comportamiento de AISD en un ambiente salino y con un alto porcentaje de cloruros, como el que encontraríamos en alguna industria química, en una planta desalinizadora o en industrias situadas en el mar o en un ambiente marino. Posteriormente se realizó el experimento con agua del mar Mediterráneo para poder comparar los diferentes estados de corrosión.

La corrosión se estudia más adelante con la ayuda de un microscopio óptico, un microscopio electrónico de barrido (MEB) y microanálisis de dispersión de energía de rayos X (EDX). Para determinar los efectos de la corrosión, las muestras fueron examinadas con éstas técnicas de microscopia y caracterizadas con el microanálisis EDX. Además, se completan estos métodos con el método de ganancia/pérdida de peso. Las muestras se retiran mientras se está realizando ensayo cada cierto tiempo para determinar su variación en peso. La corrosión por picadura se encuentra de una manera considerable a través de las muestras.

El estudio de la microestructura se realiza con el microscopio electrónico de barrido de alta resolución. Utilizando microanálisis EDX caracterizamos las diferentes muestras a diferentes tratamientos térmicos. De esta forma somos capaces de comparar la cantidad de corrosión que se ha formado en una muestra con la cantidad de fases secundarias intermetálicas presentes en la aleación. Por último, se realizan pruebas de dureza utilizando un durómetro en la escala Rockwell C, para observar así el crecimiento de la dureza con la cantidad de fase intermetálicas.

Palabras clave: *Acero inoxidable súper dúplex, Tratamiento térmico, fases secundarias, microestructura, corrosión, caracterización*

3. FUNDAMENTALS

3.1. Introduction to stainless steels

Most metals get rusty, Silver goes black when it oxidases, aluminum changes to white and copper oxide is of a green beautiful color. In the case of steel, iron present in the alloy combines with oxygen to form iron oxides, which is commonly known as rust or rustiness.

At the beginning of the twentieth century some metallurgists discovered that by adding a little over 10% of the metal chrome inside the steel, this alloy would not show any signs of oxidation or any rust under normal circumstances. The minimum amount of chrome necessary to provide a superior resistance to corrosion is not defined perfectly, for example, the American Iron and Steel Institute (AISI) has chosen 10% of chrome as the dividing line between regular steels and stainless steels, whilst others establish this boundary between 10,5% and 11%. Since then, every steel manufacturer realized the importance of stainless steel in many industries, and have never stopped trying to improve the steel they produced by adding different alloying elements.

A conventional grade of steel is a Fe-C alloy, but stainless steels form a group of highly alloyed steels which are based in Fe-Cr, Fe-Cr-C and Fe-Cr-Ni. Obviously there are a lot more of alloying elements in today's stainless steel, which every each and one of them provide the alloy with certain characteristics, but the basic matrix of which they are formed is basically the ones mentioned above.

In order to even be considered stainless steel these alloys must contain at least 10,5 % of chrome present in their structure. This percentage of chrome grants the formation of an outside passivating layer of chromium oxide, which protects the steel from oxidation and corrosion.

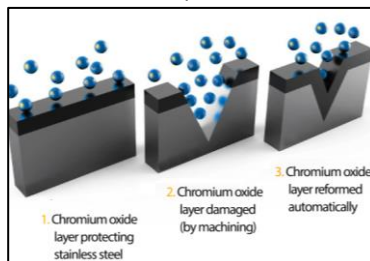


Figure 3.1. Passivation mechanism for stainless steel.

This confers the steel the property of being much more resistant to corrosion than the iron would be without the presence of this constituent. Moreover, the chromium oxide layer is restored immediately and automatically when it gets damaged or removed. The iron base contains other

elements, primarily nickel, molybdenum, manganese, silicon and titanium, all of which we will have a chance to view individually and discuss later on in this paper.

Thermal treatments in stainless steels are performed to produce changes in physical properties, mechanical properties, level of residual tensions and to restore the maximum resistance to corrosion. Frequently, with the same treatment we are able to pull off a more than satisfactory resistance to corrosion and optimal physical properties.

The higher normalization institutions regarding the world of metals and steel are the American Iron and Steel Institute (AISI) and the Society of Automotive Engineers (SAE). In the 1930s and 1940s the American Iron and Steel Institute and SAE were both involved in efforts to standardize such a numbering system for steels.

These efforts were similar and overlapped significantly. For several decades the systems were united into a joint system designated the **AISI/SAE steel grades**. The SAE steel grade system corresponds to other alloy numbering systems, such as the ASTM-SAE unified numbering system (UNS).

3.1.1. Classification of stainless steels

Stainless steels are classified in five different families, each one corresponding to their predominant microstructure formed in the alloy. The three possible phases in stainless steels are ferrite, austenite and martensite, which give name to the first three classes of steel. Within the stainless steels we can also find precipitation hardening stainless steels. These particular types owe their name due to the formation of precipitates during an ageing thermal treatment, which makes them notably harder, hence the name hardening. The latter type is the focus of this investigation paper, the duplex stainless steel. They are named like this due to a biphasic microstructure, consisting in two separate phase of austenite and ferrite roughly in equal spread.

1. Austenitic stainless steels
2. Ferritic stainless steels
3. Martensitic stainless steels
4. Precipitation hardening steels
5. Duplex stainless steels
(biphasic austenitic-ferritic)

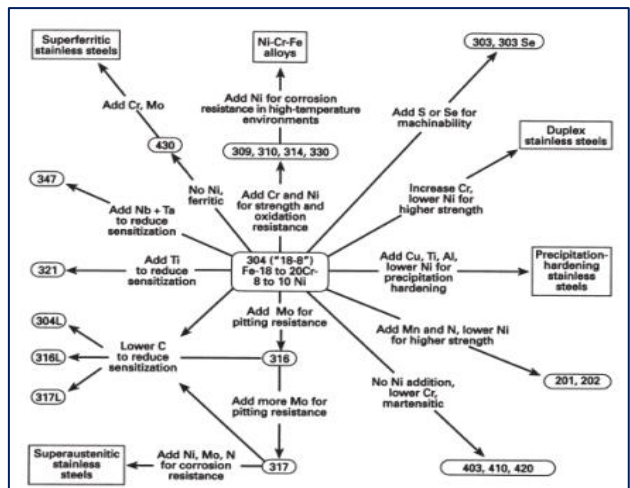


Figure 3.2. Diagram showing different types of stainless steels and how to differentiate them by their chemical composition

Austenitic stainless steels

Austenitic stainless steels represent the highest percentage of stainless steels, as they are the most common and familiar types of steel. Their metallurgic phase is austenite. These austenitic grades of steels are defined by their crystal structure. It crystallizes in a face centered cubic structure (FCC), which has one atom in the middle of each face and one in each corner of the cell, as shown in the figure below.

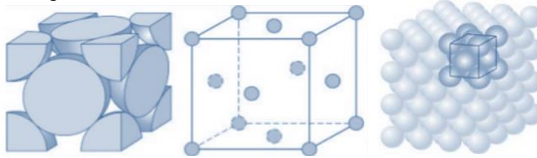


Figure 3.3. Diagram of FCC structure

This structure is formed when enough amount of nickel is added to the alloy. They have nickel content between 8 and 20% and chrome between 15% and 25%. One of the most well-known grades of austenitic stainless steels is the AISI 304 or the AISI 316, formerly used in many applications that require good hygienic conditions and in which there is a zero corrosion tolerance.

They are utterly formable and weldable and their working temperature ranges are off the charts. Their application temperature range is between -40°C to approximately 750°C , which makes them suitable for cryogenic temperatures to very high temperatures of furnaces and jet engines. They are non-magnetic steels, which may be an advantage in many situations.

As well as this austenitic steels have many advantages from a metallurgical point of view. Their strength may vary from 200-2000 MPa. They can be made very strong by cold-working the steel, which would also improve its hardness and stress resistance. An advantage to this is that at any time you may submit the steel to a solution annealing thermal treatment, followed by quenching or very fast cooling, removing segregation and restoring the steels initial condition.

The least corrosion-resistant versions can withstand the normal corrosive attack of the everyday environment while the most corrosion-resistant grades can even withstand boiling seawater. Molybdenum can also be added to improve corrosion resistance, as is the case for the AISI 316 stainless steel.

These steel grades are used in applications that require good corrosion resistance, although they are more expensive than regular ferritic or martensitic grades due to the amount of alloying elements. Nevertheless, these may experience intergranular corrosion and microbiological corrosion, amongst others. The microstructure of a 304 stainless steel grade is shown in the figure below. As you can see, the matrix is composed of one phase, meaning that this steel is fully austenitic.

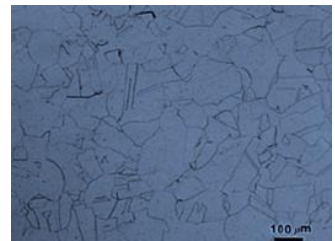


Figure 3.4. Image of austenitic matrix

To determine what grade of stainless steel ought to be used in a certain work environment lots of variables are taken into consideration, but one of the most important is the production cost and maintenance cost throughout its service life. If ferritic steels are cheaper and offer more or less the same resistance to corrosion, why ever pick austenitic steels? Even though they are cheaper, ferritic steels sometimes lack toughness and ductility in many cases, and are susceptible to high temperature embrittling phases. Austenitic steels are generally more durable and have longer service life. However, despite its elevated cost, these grades of steel offer distinctive advantages, especially regarding weldability and machinability

Duplex and super duplex grades are better than austenitic in many cases. They offer a similar, if not better, corrosion resistance and have a higher strength, but since they are more alloyed than austenitics, they run into the problem of the formation of brittle undesired secondary phases, thus making the austenitic steels more suitable for high temperature works.

Nickel is the most commonly used element in order to produce these steels grades. It is known as an 'austenite former' or 'gammagen'. This element, as well as nitrogen and manganese, help stabilize the austenitic phase. Grades of steels with low nickel and high nitrogen content are classified as the series 200. Normal austenitic grades contain a maximum carbon content of 0,08%, while the low carbon grades, also known as the famous 'L' grades, decrease it down to 0,03%, in order to avoid precipitation of carbides.

Relevant applications for each steel grade are the following:

- **304/304L:** Tanks, storage silos and pipes for corrosive chemicals, chemical and pharmaceutical production equipment, food and beverage production.
- **309/310:** Furnace, ovens and catalytic converter components.
- **316/318:** Chemical storage tanks, marine environment and piping.
- **200 series:** Kitchenware, cutlery and automobile parts.

Ferritic stainless steels

As mentioned before, ferritic stainless steels are classified this way due to the predominant metallurgic phase, the ferrite. In metallurgy ferrite or alfa-iron is one of the crystalline structures of iron. It crystallizes in a body centered cubic system and has magnetic properties.

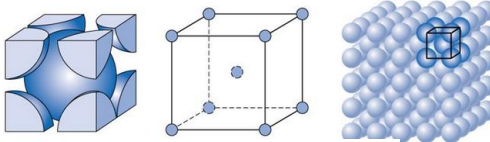


Figure 3.5. Diagram of BCC structure

These alloys provide a pretty good resistance to corrosion by several mechanisms, pitting and crevice are a notable mention in this regard, but it is also very helpful in highly chlorinated environments. This is why these steel grades are the optimal pick in car exhaust systems and washing machine drums. Exhaust pipes are submitted to high temperatures and corrosive conditions and drums have to put up with detergents and a moist environment for the major part

of the operating life-cycle. Needless to say, corrosion is undesirable in both of these examples, and ferritic stainless steel's behavior is outstanding in both cases.

Depending on the chrome percentage, ferritic steels are used in several industrial applications. Grades with low chrome percentage (10-12%) are used in automotive industry, because they provide a better corrosion resistance than carbon alloyed steels. This chrome content oscillates between the 10,5-28% mark, and there is normally very little nickel in the mix.

Special grades often include molybdenum, and maybe titanium and aluminum to certain extent. In the figure below you can find a description of the different grades of ferritic stainless steel, showing approximately the total volume produced as well as the types present in each family or group and the chrome content present.

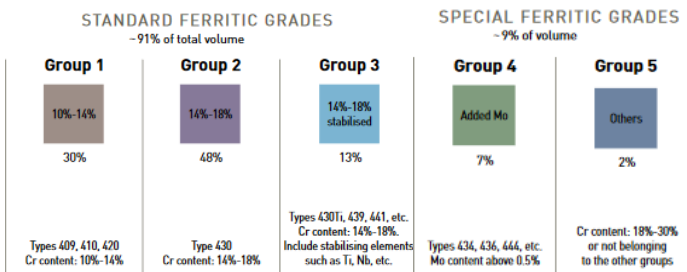


Figure 3.6.Diagram showing different groups or grades of ferritic steels.

Ferritic steels cannot be hardened or strengthened by heat treatment; otherwise they can be cold work and softened by annealing. They are normally much cheaper than austenitic steels due to the low chromium and nickel content, thus making them, by far, the largest consumed family of steels.

Ferritics have low thermal expansion and a high thermal conductivity. They are also easier to cut and work than austenitics. This is because they are softer. This also implies that they are fabricated with ease (fabrication friendliness) and have a low lifecycle cost. All of this and its excellent surface appearance and aesthetic appeal make it a good candidate for a wide variety of uses, from the automotive industry, building and construction, commercial food equipment, kitchenware, dishwashers, all the way to the transportation wagons etc.)

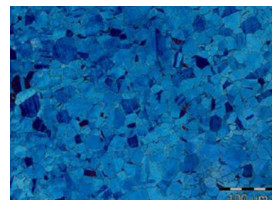


Figure 3.7.Image of ferritic matrix

These two types are the most relevant ones towards this paper, as the study of the super duplex and duplex stainless steels involve both phases, austenitic and ferritic, so a good understanding of both steels and their behavior will provide further knowledge on this subject, as both phases are present in SDSS, and have properties of both too.

3.2. Duplex stainless steel

Duplex and super duplex stainless are used in a wide range of applications, especially in the petrochemical industry, because of its high corrosion resistance and excellent mechanical properties. These alloys are based on a Fe-Cr-C-Ni-N base system and have better mechanical properties and corrosion resistance in comparison with other types of stainless steels.

Its excellent resistance to cracking by corrosion under a chlorinated atmosphere, resistance to localized corrosion, good weldability and high mechanical resistance to traction have promoted enormously the use of this type of steel throughout the modern industries, not to speak of its low maintenance cost and hygienic properties.

These alloys present a mixed structure composed of approximately 50% austenite (FCC structure) and 50% ferrite (BCC structure), which is ensured by an adequate balance of the alloying elements. This combined microstructure enhances the characteristics of each one of the both phases that are present. The austenitic phase provides the alloy with an increase of impact resistance; whilst the ferritic phase ensures a good resistance to corrosion.

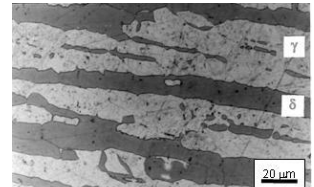


Figure 3.8. Image of ferritic/austenitic matrix representative of duplex

The microstructural balance between austenite and ferrites plays a critical role in duplex stainless steels, as the desired properties of the alloy will depend on this. If the microstructure contains a higher percentage of ferrite, the alloy will have a stronger corrosion resistance, but it will be less workable and present lower ductility. Otherwise, if the austenite content is higher, the steel will be more machinable but its corrosion resistance will be diminished.

Chemical composition of DSS is the following: 22-28% chrome, 0,5-4% molybdenum, 1-8,5% nickel, 1-6% manganese, 0,6-1% silicon and 0,05-0,3% nitrogen. Commercially, duplex steels are known for the amount or percentage of chrome and nickel that they contain. For example, the most used DSS is the grade 2205, which contains 22% chrome and 5% nickel. These percentages ensure the microstructural balance being approximately 50/50 between both phases.

Some alloying elements present in all grades of duplex stainless steels are ferrite stabilizers, also known as 'alphagens'. Some of these elements are chrome, molybdenum and wolfram, amongst others. Other alloying elements are austenite stabilizers (or gammagens), like for example nickel, carbon or nitrogen. Besides their stabilizing nature, these elements have other additional effects on the steels performance and behavior, which will be discussed in more detail further on in this paper.

New alloys of duplex have a much higher content in alloying elements in order to improve mechanical and corrosion properties, these are known by the name of super duplex. Due to this improvement, SDSS is very useful in applications that require good corrosion resistance, such as marine or highly chlorinated environments.

3.3. Background and uses

Duplex and super duplex stainless are widely used in the chemical and petrochemical industries. This is because they are able to ensure good mechanical properties and supreme resistance to corrosion. The use and application for these grades of steels have largely increased throughout the course of the last two decades, replacing austenitic and ferritic grades in many environments. Well known applications for duplex and super duplex stainless steels are as follows:

- **Desalination plants:** Desalination processes are really putting to the test the materials employed in their processes. High temperatures of the processes and the highly chlorinated environment can really punish the material being used, some equipment, like evaporators or pumps are exposed to hostile conditions, and thus require excellent properties in order to withstand the day to day use. Benefits of DSS for this application are high strength and high corrosion resistance.
- **Marine environments:** Industries that are near the sea or 'offshore' require a good corrosion resistance due to a highly chlorinated environment. Duplex steels are a natural fit, as they have an excellent resistance to corrosion.
- **Heat exchangers:** Heat exchangers normally work at high temperatures. We can find heat exchangers in many applications and industries, from heat recovery systems in large industrial plants to the radiator in your own car or in many household appliances. They are normally hard to dismantle and to clean, so keeping the tubes clean is a high priority, this is one of the reasons why SDSS is great option for this application. If you add its good thermal conductivity and low thermal expansion you can see why these grades of steel are a perfect match for these types of equipment.
- **Petrochemical plants-oil and gas:** Duplex and super duplex stainless steels have played a huge part with the tough conditions represented in the petrochemical industries. Although DSS and SDSS have outstanding corrosion resistance, what makes these alloys really appealing for this type of industry is the pitting and crevice corrosion resistance, which is much higher than regular austenitic grades. With a pitting resistance equivalent number (PREN) over 40, SDSS are the way to go if you are working with transporting corrosive gas and oil. This grade of steel may be found in piping systems and flowlines, as well as in different types of equipment such as separators, scrubbers or storage facilities.
- **Construction and architecture:** Duplex steels are crucial for the construction of bridges and other structures that require high strength and where corrosion and a saline environment are present. DSS is a 'must', due to its excellent physical and mechanical properties; it's a perfect fit for this application.

Other uses may involve the bio-fuel industry, where duplex stainless steel is replacing austenitic steels for many ethanol service applications. It is also widely used in the 'Flue gas desulfurization' process. Coal fired appliances have a major issue, exhaust gases. Large amounts of Sulphur dioxide have to be removed in order to reduce these emissions into the atmosphere. Modern FGDs work at different temperatures, chloride concentrations and pH, so an optimal corrosion resistance is what people in the industry are seeking. So the use of duplex

steels has increased in popularity for FDG absorber due to its strength, toughness and corrosion resistance.

The same properties that make it a good choice for desulfurization make it very good for different types of chemical reactors. These grades of steel can withstand the different thermal and pH conditions used in many processes inside the chemical and pharmaceutical industries. Not only can the reactor be made out of these excellent grades of steel. All the pipelines and storage silos and containers that work with a corrosive fluid should be able to withstand the test of time, as constantly having to change or clean all this systems is detrimental for business and would require a high maintenance cost.

Another important use of duplex and super duplex stainless steels is in the food and beverage industries. Food processing equipment is subject to many quality control tests and supervision. The fact is that SDSS is finding its way inside this type of machinery and equipment due to its unpolluted surface appearance and great resistance properties. It is vital for these kinds of production chains to remain as clean as possible, in order to not contaminate the aliments, so zero tolerance towards corrosion is crucial, so duplex grades and super duplex grades are a good solution to this problem.

3.4. Properties

Duplex and super duplex stainless steels were developed to upgrade or improve the technical weaknesses that other grades of stainless steel had, such as austenitic and ferritic grades. Presenting a biphasic microstructure, combining the best of both worlds, duplex steels have the following advantages:

- Very good resistance to general uniform corrosion
- Very good resistance to pitting and chloride corrosion
- High resistance to stress corrosion cracking (SCC) and fatigue corrosion
- High mechanical strength
- Good resistance to abrasion and erosion

When comparing different stainless steel families, there are many similarities between certain properties, although there are some essential differences. Stainless steels have a density hovering over the 8g/cm³ mark. The table below shows us a comparison between the mechanical properties of ferritic, austenitic and duplex stainless steels.

| UNS or AISI type | Condition | Rockwell hardness | Average tensile properties | | | | | | Charpy V-notch impact strength | |
|-----------------------------|-----------|-------------------|-----------------------------|-----|---------------------------|-----|------------------------------------|----------------------|--------------------------------|----------|
| | | | Yield strength, 0.2% offset | | Ultimate tensile strength | | Elongation in 50.8 mm (2.0 in.), % | Reduction of area, % | J | ft · lbf |
| | | | MPa | ksi | MPa | ksi | | | | |
| Austenitic stainless | | | | | | | | | | |
| Type 304 | Annealed | 81 HRB | 241 | 35 | 586 | 85 | 60.0 | 70.0 | ≥325 | ≥240 |
| N08020 | Annealed | 84 HRB | 276 | 40 | 621 | 90 | 50.0 | 65.0 | 271 | 200 |
| S20161 | Annealed | 93 HRB | 365 | 53 | 970 | 140 | 59.0 | 64.0 | ≥325 | ≥240 |
| S21800 | Annealed | 95 HRB | 414 | 60 | 710 | 103 | 64.0 | 74.0 | ≥325 | ≥240 |
| Ferritic | | | | | | | | | | |
| Type 405 | Annealed | 81 HRB | 276 | 40 | 483 | 70 | 30.0 | 60.0 | ... | ... |
| Type 430 | Annealed | 82 HRB | 310 | 45 | 517 | 75 | 30.0 | 65.0 | 217 | 161 |
| Duplex | | | | | | | | | | |
| S32950 | Annealed | 100 HRB | 570 | 82 | 760 | 110 | 38.0 | 78.0 | 157 | 116 |

Table 3.9. Table comparing mechanical properties of austenitic, ferritic, and duplex steels

Duplex and super duplex steels have exceptional mechanical properties. Their yield strength is more than double than the ones presented in regular austenitic and ferritic stainless steels. Though the toughness is small, relative to the other grades of steel, it is still far superior to alloys that have been heat treated and hardened.

It should be noted that ductile-brittle transition for DSS and SDSS occurs at -60°C or lower, which is fine for the majority of applications. Despite having relatively high strengths, duplex and super duplex steels exhibit good ductility and toughness, but are lower to pure austenitic steels.

It is to be noted as well that duplex and super duplex steels' mechanical properties are highly anisotropic. This means that properties may change and vary depending on the orientation of the different grains in the structure and crystallographic texture. The table below shows the minimum mechanical properties specifications for a duplex stainless steel plate, according to American Society for Testing and Materials (ASTM).

| Grade | ASTM | | | |
|-------|---------|-------------------------------------|----------------------------------|--------------------------|
| | UNS No. | Yield strength 0.2% MPa (ksi) | Tensile strength MPa (ksi) | Elongation in 2" % |
| 2304 | S32304 | 400 (58) | 600 (87) | 25 |
| 2205 | S32205 | 450 (65) | 655 (95) | 25 |
| 2507 | S32750 | 550 (80) | 795 (116) | 15 |

Table 3.10. Table of minimum mechanical properties of DSS according to ASTM.

Duplex and SDSS have a high level of corrosion resistance in most environments where regular stainless steel is used, but there are some applications where duplex and super duplex grade excel. This is the result of a higher chrome percentage present in these grades of steel. This higher chrome quantity present in the alloy allows these grades to be used in presence of oxidizing acids. As well as this, a relatively high amount of molybdenum and nickel provide a good resistance in mildly reducing acid environments, making the use of duplex grades much more appealing in these kinds of services.

The elevated amounts of chrome and molybdenum also grant the steel a very good resistance to chloride induced localized pitting and crevice corrosion. The biphasic metallographic structure also confers good resistance to stress corrosion cracking, so duplex and super duplex steels are far more resilient to SCC than austenitic grades such as 316 or 304. High chrome content and the presence of ferrite also give the steel good resistance to caustic environments or to strong alkaline solutions.

3.5.Factors in selection of stainless steel

There are many factors and variables regarding which grade of stainless steel should be used in a certain application or industry. However, the prime and most important factors in choosing a grade for a given application are the corrosion resistance and mechanical properties. Other factors may include product cost, availability and range of optimal work temperatures amongst others. Here is a list of characteristics to be considered in selecting a proper grade of steel in a desired application:

- Corrosion resistance and resistance to oxidation and sulfidation.
- Physical properties, magnetic properties, electrical resistivity or thermal conductivity.
- Surface finish/appearance and reflectivity.
- Strength, ductility and toughness at service temperatures and conditions.
- Resistance to erosion, abrasion and seizing.
- Total cost(product cost, installation, maintenance and life expectancy)

As mentioned earlier, corrosion resistance is the main characteristic in order to choose a grade of stainless steel, but this is much more complicated as it is difficult to quantify and hard to assess for specific applications. General corrosion resistance to different chemical solutions is not hard to evaluate, but more complex environments the gist gets much more complicated.

Localized corrosion, such as SCC, crevice, pitting and intergranular attack can cause a catastrophic failure in a small portion of the steel, while most of the structure remains unaffected. Therefore it must be a really strong consideration when selecting a steel grade. Other factors to take into consideration are not only the properties of the steel selected, but the ones of the medium in which it will perform:

- Chemical composition and physical state of medium
- Temperature and its possible variations
- Bacteria content
- Oxygen content
- Relative motion of the medium with respect to steel
- Continuity of exposure to the medium
- Surface condition of the metal and its exposure

The more you know about the alloy and its properties, and the more you know about where it will be allocated will certainly help a lot when selecting a grade of stainless steel. As mentioned before, bear in mind that not only the grade of the steel is remarkably important, but also the medium where it will be held and its work conditions and environment. Take into consideration that laboratory corrosion data is not always accurate. Even actual service data may alter slightly between one batch and another. This is because similar media may differ enormously because of a small variation in the system. It may be useful to try the grade out by means of a pilot or rather by doing 'in-service' testing, to see how it performs in the real work atmosphere or environment.

3.6. Chemical composition and microstructure

Interactions between main alloying elements, such as chrome, nickel, nitrogen and molybdenum, are fairly complex. To achieve a stable duplex microstructure (bi-phasic) that responds correctly to the fabrication process, you must be very careful and insightful when putting together alloying elements. It is of high importance to maintain the ferrite-austenite equilibrium and so the phases are more or less of equal proportions. Some authors suggest a $50\% \pm 15\%$ of variation between the ferritic phase and the austenitic phases, whilst others propose a more accurate variation of only 10%. Regardless of this fact, it is important to try and keep the phase ratio 1:1.

Besides the amount of ferritic and austenitic phases, there is another important matter regarding duplex and super duplex stainless steels and their chemical composition. This is the formation of secondary intermetallic phases, which are detrimental for the steel's properties and form at temperatures over 500°C . The amount of certain alloying elements present in the different grades of steel definitely have an influence on the quantity of intermetallic phases present after welding or thermal treatments. This subject will be studied in more depth later on in this paper.

Phase equilibrium in a binary system (or greater) depends significantly of the solubility of the alloying elements within the different crystalline structures, body centered cubic or BCC, and face centered cubic or FCC. So some elements will have a higher solubility rate in the iron's solid BCC structure, also known as ferrite, whilst other will be more soluble in the FCC structure or austenite.

This microstructure results from a ferrite-austenite solid phase transformation and is obtained by an accurate balance of chemical composition and heat treatment. Starting from a fully ferritic structure, the solid state transformation occurs during cooling and the resulting phases have different chemical composition: Fe with mainly Cr (18-28%), Ni (4-6%) and Mo (1.5-3%).

Chrome is added primordially to provide corrosion resistance in stainless steels, promoting the formation of its oxide, Cr_2O_3 on the surface of the steel, making a passivation layer to protect the metal. In the stainless steels, it also acts as a ferrite stabilizer. These types of elements are called 'alphagens'. It also provides an increase in mechanical properties, by means of the hardening mechanism of solid solution. As you are able to see in the figure below, when the amount of chrome percentage increases so does the alpha formation or ferrite.

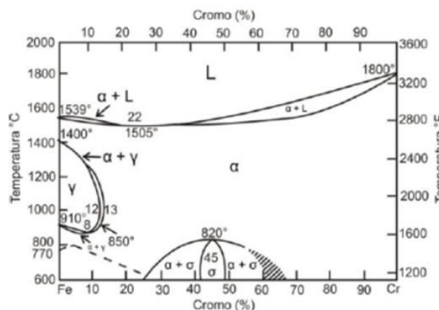


Figure 3.11. Fe-Cr equilibrium diagram

With about 10,5% of chrome, the passivating layer will protect the steel from mild atmospheric corrosion. Even if other elements may help chrome form or maintain the passivating oxide layer, chrome by its self is able to grant a certain amount of resistance to corrosion. If higher percentages of chrome wish to be added to the alloy, to give it a higher resistance to corrosion, the amount of nickel necessary to form a duplex structure increases. There is about 22% of chrome in second generation duplex.

Chrome is also one of the primary elements of secondary intermetallic phases, the most common one being the sigma phase (σ). These phases tend to form in most grades of stainless steel, however, it is mostly accepted that they form with more ease in highly alloyed austenitic steel and duplex and super duplex. Thus concluding that the higher amount of chrome present in a certain alloy, the higher the chances are that these phases form. Chrome is also present in other intermetallic phases, such as the chi phase, carbides and nitrides.

These phases tend to brittle the alloy, thus reducing toughness, ductility and most important corrosion resistance. As mentioned before, chrome tends to form carbides type $M_{23}C_6$, in most grades of stainless steels, and it is the main metallic element present in this phase. As well as this, when it combines with nitrogen, it forms nitrides, most frequent type being Cr_2N . This phenomenon has been observed in ferritic steels and mostly in duplex and super duplex grades.

Nickel is a stabilizer of the austenitic phase, these types of elements are called 'gammagens' because they tend towards the formation of the gamma phase (austenite). This means that when nickel is added to an iron based alloy it promotes a change in the crystalline structures of the steel from a body centered cubic structure to a face centered cubic structure, in this case austenite.

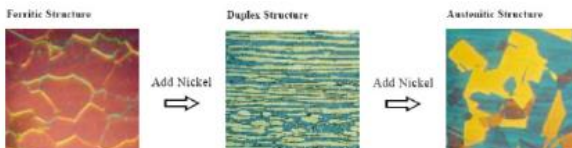


Figure 3.12. Microstructural evolution upon the addition of Ni as an alloying element

Ferritic steels contain very little or no nickel at all, whilst duplex and super duplex contains an intermediate amount, ranging from 4-7%. Austenitic steels obviously contain higher amounts of nickel, as an example, the grades from the series 300 of austenitic steels have at least 8% of it. In duplex and super duplex steels nickel contributes to the control of the microstructural balance of ferrite/austenite. As we can see in the figure beside of the equilibrium diagram between nickel and iron, nickel is responsible for the stability of the austenitic phase at room temperature. When the amount of nickel increases, the lower the temperature must be for this phase to be stable.

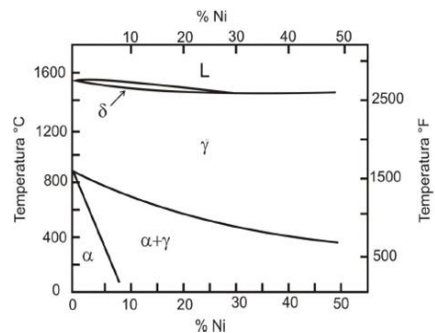


Figure 3.13. Fe-Ni equilibrium diagram

Experts suggest that the range of nickel must be between the ranges of 4% and 8% for DSS to obtain an optimal resistance to pitting corrosion. If the quantity of nickel is significantly higher, the amount of austenitic phase will rise, thus leaving a big percentage of ferrite phase highly alloyed. This phase will tend to form secondary intermetallic phases when heated or aged, and this effect is undesirable.

Nickel is a great add on to the mix. This element increase toughness and ductility at the same time that upgrades the steel's mechanical properties and hardness. Austenite's FCC structure is responsible for the excellent values of toughness. Nickel does not form undesired intermetallic compounds. All of these properties make nickel a superb element to include in iron base alloys, and that is why it is present in the majority of them.

Nitrogen increases the resistance to corrosion by pitting and crevice in austenitic and duplex stainless steels. Moreover, it also increases the alloys strength and toughness, and in fact, it is the most efficient element that hardens the steel by solid solution.

Nitrogen delays the formation of intermetallic phases enough to allow the process and fabrication of certain duplex alloys. This element is employed in austenitic and duplex steels that contain a high quantity chrome and molybdenum, in order to compensate their tendency to form intermetallic phases.

It is strong 'gammagen' element and it can partly substitute nickel in austenitic stainless steels. This is an advantage because manufacturers are able to assemble steel with good properties and a more competitive price, due to the fact that nitrogen is cheaper than nickel and a very small percentage is required. In duplex and super duplex steels, nitrogen is added till the point it reaches its solubility limit, and the quantity of nickel is adjusted to ensure the desired phase equilibrium. Third generation of duplex steels was created with the addition of nitrogen to duplex grades.

Nitrogen is found normally in the range between 2-3% for duplex stainless steels. It has also been found guilty of the formation of chrome nitrides, Cr₂N and CrN, in the ferritic matrix of the DSS. These have an adverse effect on corrosion properties, diminishing it.

Molybdenum helps chrome improving corrosion resistance to chloride attacks in stainless steels. When the chrome percentage is over 18%, the addition of molybdenum is really efficient against pitting corrosion and crevice corrosion, in environments that are highly chlorinated. So this element is essential for steels that will work in marine environments and chemical plants that work with chlorinated fluids. It also increases mechanical properties at high service temperatures.

It is an 'alphagen' element, but it also promotes the formation of unwanted intermetallic phases. This is the reason why it is found in small percentages, austenitic grades containing about 7% of it whilst duplex grades have only about 4%.

A higher percentage of this alloying element is only detrimental for the steel, as it increases the likelihood of the formation of the sigma phase. It also expands the formation field of these phases, making them precipitate at higher temperatures (over 1000°C), where we would not expect the formation of this type of precipitate.

Carbon is a good austenite stabilizer. In this regard, it is much stronger than nickel. The addition of this element increases mechanical resistance by means of the solid solution hardening mechanism. Carbon is especially good enhancing mechanical properties when working at high temperatures. It forms carbides at the grain boundaries, which cause greater susceptibility to intergranular and pitting corrosion in duplex and super duplex grades.

Other less relevant alloying elements used in modern stainless steels are for example **manganese** and **silicon**. Manganese is an element that also promotes the austenitic phase, and it is very effective to stabilize it at low temperatures. Manganese also diminishes brittleness and enhances a mechanical properties just a pinch. **Niobium** and **titanium** are also minor alloying elements for stainless steels. They are carbide stabilizers; this means that they have certain affinity for carbon, making carbide precipitation almost sure. Since carbides are going to form anyways at certain temperatures, it is best that they form these elements, rather than with chrome, thus allowing chrome to stay in the solution.

3.7. Metallurgy of DSS and SDSS

The effect of alloying elements in stainless steels is commonly expressed as 'Nickel equivalent' if these elements are gammagens, otherwise known as austenite stabilizers. On the other hand, the set of ferrite stabilizers elements are expressed as 'Chrome equivalent'.

Relative quantities of ferrite and austenite in the steel highly depend on the chemical composition and its thermal history. Small changes in the composition may lead to a great variation on the phase percentage.

Schaeffler represented the combined effect of chrome and nickel, bearing in mind that alphasen and gammagen elements would produce a similar effect than the one produced by chrome and nickel. In this fashion, he calculated a series of expressions and defined coefficients to be able to quantify the final amount of phases, starting from a known alloy's chemical composition of iron, chrome and nickel.

The following diagram shows stable zones of the different phases of duplex steels in function of the chrome equivalent alloying elements and nickel equivalent alloying elements content, also known as the Schaeffler diagram. It also exhibits the coexistence of different phases and their relative proportions.

Although this method is not very accurate, it has been around since the 1950s and it is widely used

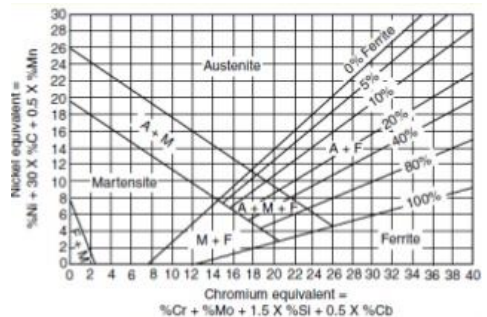


Figure 3.14. Schaeffler's diagram

as an approximate way to determine what phase or phases will most likely be present in the studied stainless steel. The lack of accuracy of this method derives from the absence of more recent and newly introduced alloying elements in today's steel. As an example, this method ignores the amount of nitrogen and titanium present in steels, the first of which we know is present in all third generation duplex steels.

A more refined and upgraded version of Schaeffler's diagram is shown in the figure below. This diagram or graph goes by the name of 'Schoefer's Diagram'. This way, the end result is a series of points in a graph that determine the amount of ferrite present in a given duplex grade in function of the chrome and nickel equivalent ratio. This method is miles ahead of its predecessor as it includes all alloying elements utilized in the fabrication of modern duplex and super duplex grades. thus making the method more accurate and acceptable.

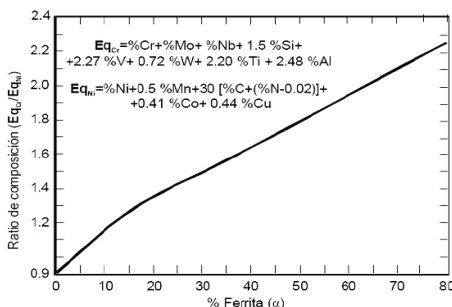


Figure 3.15. Schoefer's diagram

Due to the fact that duplex and super duplex are based on the Fe-Cr-Ni-N system, their chemical composition has to be adjusted in such a way that we are able to obtain equal parts of ferrite and austenite. Nonetheless, all duplex grades solidify basically as 100% ferrite the balance between these two phases depends on the transformation of solid states from ferrite to austenite. To enhance this transformation, nitrogen is added to the steel, stabilizing austenite as we mentioned previously. As we can see in the **Fe-Cr-Ni** ternary phase diagram, the addition of nitrogen raises the temperature where ferrite starts forming austenite. This enhances the transformation speed of austenite. At temperatures around 1300°C, austenite starts to nucleate, first in the ferrite grain boundaries and then inside the ferrite grains.

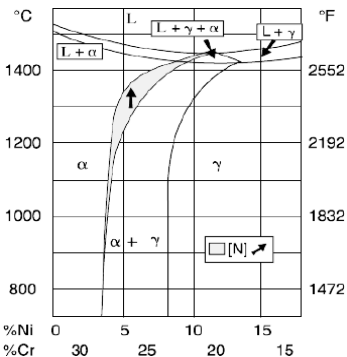


Figure 3.16. Fe-Cr-Ni ternary phase diagram

The diffusion of alloying elements takes place when the ferrite/austenite transformation begins. Ferrite stabilizing elements concentrate in the ferrite phase, whilst gammagens concentrate in the austenitic phase. Duplex steel grades have a higher percentage of alphasgen elements than gammagens, so this explains the fact that they solidify in a 100% ferritic matrix. The figure below shows that alloys having a ratio of chrome equivalence to nickel equivalence over 1,85 solidify 100% in a ferritic matrix.

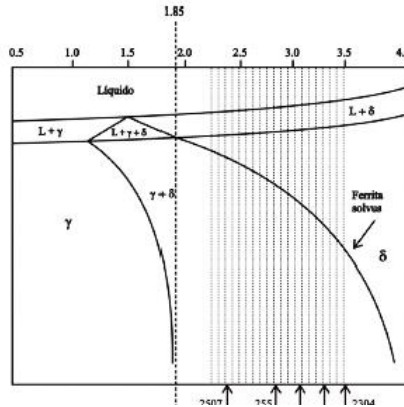


Figure 3.17. Duplex DSS bi-phasic region at high temperatures.
Some well-known DSS grades are represented on the horizontal axis.

Duplex and super duplex steels generally have this ratio (Cr_{eq}/Ni_{eq}) ranging between values of 2 and 3.5, meaning that at temperatures near the solidification temperature (around 1400°C), the alloy is bound to have a ferritic nature. Tempering treatments and hot-working in duplex steel grades are conducted well below this temperature, where austenite and ferrite are able to coexist in equilibrium. Being able to control this temperature and the temperature cooling rate allows steel manufacturers to handle the amount and distribution of ferrite/austenite in the final product.

3.8. Precipitation of intermetallic phases

The curvature in the ferrite/austenite region in the previous figure (3.17.) indicates that a higher amount of austenite will form from the ferritic phase when dropping the temperature. There will be a limit temperature in which the ferrite/austenite transformation will be at its peak; this is due to the precipitation of unwanted secondary intermetallic phases. These precipitates are detrimental for the steel's mechanical and corrosion properties and are likely to appear after welding or fabrication processes.

It is important to note that these phases form from the ferritic phase. Ferritic phase is rich in chrome and molybdenum, both of which promote the formation of secondary phases. The ease in which ferrite transforms into these secondary phases is a consequence of the high diffusion speed of alphasen elements, which is much faster than in austenite.

Chemical composition of duplex and super duplex grades heavily condition what type of ageing processes they can experience when the steel undergoes a thermal treatment, since the material's microstructure is determined by its chemical composition. As a matter of fact, depending on the composition some duplex will be more susceptible to precipitation process than others. The higher amounts of alloying elements present in the steel, the greater the tendency towards the formation of these phases.

Due to DSS and SDSS chemical composition, they are highly prone to the precipitation of intermetallic compounds, in a temperature range between 500-1000°C. The precipitation of these intermetallic phases often makes the steel much more brittle and hard, as it causes structural transformations in the steel's microstructure. This is an unfavorable feature of duplex steels because they are frequently exposed to high temperatures and are subject to this undesired precipitation.

The figure below shows a schematic TTP (time-temperature-precipitation) diagram. It summarizes the approximate temperature range in which secondary phase precipitate in a conventional grade of duplex stainless steel.

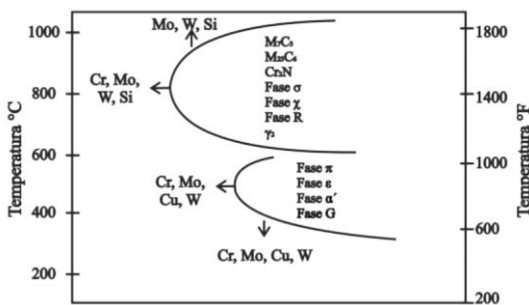


Figure 3.18. TTP diagram for precipitation of intermetallic phases

These precipitation reactions are dependent on time and temperature, as you can clearly see in the TTP diagram. In it we can distinctly see two separate zones perfectly differentiated. The first one ranging between 300-500°C, where the precipitation of phases G, pi, epsilon and alpha' is favored. The second zone is found in the temperature ranges between 500-1000°C approximately, and here is where the precipitation of carbides, nitrides, chi-phase and sigma-phase is promoted. The diagram also shows the influence of certain alloying elements to the susceptibility of precipitation of these phases. As mentioned before, higher contents of chrome and molybdenum push the precipitation curves closer to the left, therefore making the compounds precipitate at shorter times.

This top part of the diagram, or should I say the precipitation compounds found here are of more interest to us, as they are found in higher proportions and are more common than the ones below. Moreover, it has been demonstrated that the most deleterious secondary phase of all is the sigma-phase, as it significantly handicaps the steels toughness and corrosion resistance. From here on, different types of secondary phases will be discussed.

Sigma-phase is a secondary intermetallic phase with high values of hardness and consists of a tetragonal structure containing 30 atoms per unit cell. It is the most prominent phase between the intermetallic phases found amongst DSS and SDSS. This phase is formed between 600-1000°C. The mechanism in which this phase is formed corresponds to a eutectoid reaction of ferrite decomposition into sigma-phase and austenite. ($\delta \rightarrow \sigma + \gamma$). This phase tends to nucleate in ferritic grain boundaries and in austenitic/ferritic interfaces, growing in favor of the ferrite's interior.

The precipitation of this phase can be found in all commercial grades of steel, in austenitics, ferritics, but mostly in duplex and super duplex. It affects the steels toughness and ductility, decreasing hence its mechanical properties, as well it reduces the resistance to corrosion, as this phase is made mainly of chrome and molybdenum, the two key alloying elements to fight against corrosion.

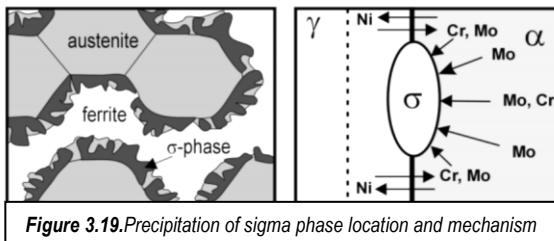


Figure 3.19. Precipitation of sigma phase location and mechanism

Its morphology or shape depends on the temperature in which it forms. At relatively low temperatures (600-700°C) sigma phase is shaped in a 'cluster' form, whilst at higher temperatures of around 800-900°C it is shaped in bigger particles and its grain size is more substantial. Moreover, there are other factors that affect upon the formation of the sigma phase. The grain size in which it starts precipitating affects its overall quantity, the smaller the grain size

the more likely it is to precipitate. Furthermore, it has been found to precipitate in high energy regions like boundaries, interphases and inclusions.

Chi-phase ($\text{Fe}_{36}\text{Cr}_{12}\text{Mo}_{10}$) may occur in austenitic, ferritic, DSS and SDSS, and its precipitation is also associated with negative effects on corrosion and mechanical properties. It has a high chrome and molybdenum percentage and has a similar impact on the steel as the sigma phase, removing these alloying elements from the matrix of the steel making more brittle and less corrosion resistant. Although its effect is hard to quantify because it generally cohabits with the sigma-phase, and its proportion regarding this one is really low.

It forms at a temperature range of 700-900°C, and as the sigma phase, its nucleation takes place in grain boundaries and ferrite/austenite interphase and grows towards the delta or ferrite matrix. It has a BCC structure just like ferrite.

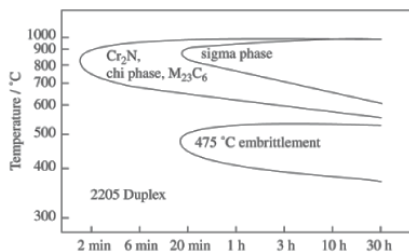


Figure 3.20. TTP diagram for 2205 DSS

As we are able to see in the TTP diagram of a 2205 duplex steel, the chi-phases precipitates at shorter time of thermal exposure, however it does at very similar or equal temperatures as the sigma-phase. It is considered to be 'metastable', as it acts as a facilitator for the formation of the sigma-phase, entirely decomposing in it after long time scales of thermal treatments. While sigma-phase is present in Fe-Cr systems, chi phase only appears in Fe-Cr-Mo ternary systems and Fe-Cr-Ni-Mo quaternary systems.

Nitrides precipitate due to the rising amount of nitrogen as an alloying element in duplex and super duplex grades. They are for the most part chrome nitrides (Cr_2N or CrN). Its precipitation is caused by the saturation of nitrogen in the ferrite.

When steel is suddenly cooled from a relatively high temperature (1000°C), nitrogen is solubilized in the ferrite matrix, and during this cooling solubility drops massively. Suddenly the ferrite matrix is saturated in nitrogen, which triggers the precipitation of these compounds in grain boundaries, which precipitates in the shape of needles following certain crystallographic directions. This precipitate has the same detrimental properties as the sigma-phase and the chi-phase.

Carbides are present in grades with high carbon content, precipitating mostly in intergranular ferrite/austenite boundaries, although it has been observed in ferrite/ferrite and austenite/austenite boundaries too, as well as inside the grains, though in very low quantity.

There are two types of carbides, M_7C_3 and $M_{23}C_6$. The first one precipitates at higher temperatures around 1000°C , whilst the other does so at smaller temperatures of $600\text{-}900^\circ\text{C}$. These precipitates are considered by some authors as starting nucleation points of the sigma-phases. Due to the low amount of carbon present in present super duplex grades, lower than $0,03\%$, carbide formation is pretty low.

In the picture below we are able to differentiate the entire different intermetallic compounds that have precipitated after an annealing thermal treatment. As we can see, the chromium nitrides have precipitated in the ferrite/austenite grain boundaries. The sigma phase has precipitated in a ferrite/ferrite boundary, as well as the chi-phase. The chi-phase also appears in a much smaller amount than the sigma-phase, as it is expected.

The carbide has precipitated in the austenitic matrix, and as we mentioned before, this is a rare outcome but it certainly can happen. In the SEM (scanning electron microscope), heavier elements appear in a brighter tone and light elements resemble to be dark. The chi-phase is the brighter component in this image, which matches the previous statement, because it contains the higher amount of molybdenum, which is in itself a relatively heavy element.

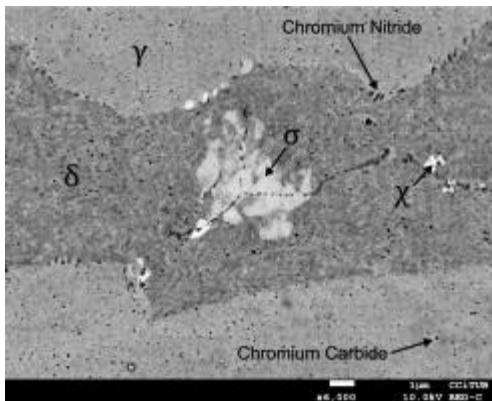


Figure 3.20. Microstructural image from SEM, showing several intermetallic phase precipitation

3.9. Corrosion mechanisms

Duplex grades have become a well-established family of steels for the usage that demands high corrosion resistance and is very suitable for such applications. These grades, as well as the super duplex grades are replacing the austenitic 300' series, as they have really cheap maintenance costs during service time and excellent mechanical properties, allowing to reduce thickness and making them even cheaper.

The standard duplex grades have had an outstanding performance throughout the last 20 years. The high chrome, molybdenum and nitrogen give the alloy a great resistance to chloride induced pitting and crevice corrosion, and their bi-phasic structure is an advantage in chloride stress corrosion cracking environments.

The Pitting Resistance Equivalent Number, also known as **PREN**, is a very useful indicator that shows the corrosion resistance of a certain alloy, particularly when considering localized corrosion. Since pitting corrosion is regarded to be very important in DSS and SDSS application, there has been a need to classify different alloys according to their resistance. PREN depends on the composition of the alloy, particularly the key elements against corrosion, according to the following formula:

$$\text{PREN} = \%Cr + 3.3\%Mo + 16\%N$$

Percentages are expressed as weight percentage in the alloy. Duplex steel grades have PREN numbers along the range of 30 to 40. One of the things that define super duplex stainless steel is precisely this indicator, which for these grades of steel is able to exceed 40. Steels with PREN values over 32 are considered to be resistant to sea water corrosion. It is important to note that PREN cannot be interpreted as an absolute value, and meaningful comparisons only withstand if they are done in the same steel family. In the table 1.1.7 shown in the appendix 1 we are able to compare different values of PREN in relation with the amount of alloying constituents present.

Corrosion is defined as a material's deterioration as a consequence of an electrochemical attack produced by its environment. Wet or aqueous corrosion is an attack on the metal by aggressive substance that is dissolved in water. A metal or alloy immersed in a liquid solution may convert into its oxidized form, transferring its metallic ions into the solution. This reaction is called anodic dissolution. Solid metal converts into ions with the most stable valence. At the same time, an electron-consuming (cathodic) reaction takes place in the surface of the metal.

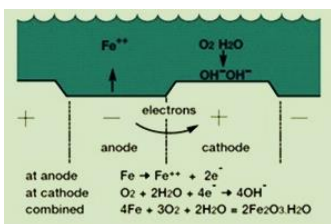


Figure 3.21. Cathodic and anodic reactions

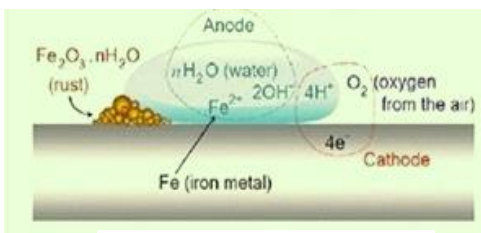


Figure 3.22. Corrosion mechanism on the surface of the steel

Corrosion is caused by an electron current that is generated by the difference of potential between one point and another. A part of the metal and the solution behaves as the anode, donating electrons to the medium. The corrosion of steel can be considered as an electrochemical process that occurs in stages. Initial attack occurs at anodic areas on the surface, where ferrous ions go into solution. Electrons are released from the anode and move through the metallic structure to the adjacent cathodic sites on the surface, where they combine with oxygen and water to form hydroxyl ions. These react with the ferrous ions from the anode to produce ferrous hydroxide, which is later oxidized in air to produce ferric oxide (red rust.) The addition of these reactions can be represented by the following equation:



So to summarize, corrosion effects are merely a REDOX reaction that use the water medium as the electrolyte. As time passes by, a humidity film layer appears over the metal's surface, creating the perfect medium for REDOX reactions.

The intensity of the reaction depends on several factors, such as pH, temperature difference of potential between the solution and the alloy, the amount of oxygen dissolved in the water and the amount of chloride concentration present as well as the metal's composition. It is important to note that chloride ion (Cl⁻) has a depassivating effect, thus will increase the corrosion rate as it damages the outside passivating layer. For corrosion to occur ions must have a medium to move in, oxygen must be present at all times and the metal gas to be willing to donate electrons to commence the process.

There are many different kinds of corrosion that can be found in industrial applications. These are present in the figure beside. In this paper we will study the effects of uniform corrosion, pitting corrosion and the effect of microbial corrosion (MIC).

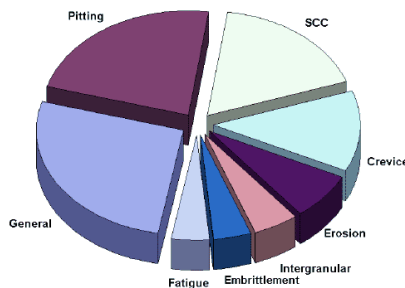


Figure 3.23. Pie chart representing approximate % of corrosion mechanisms

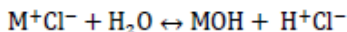
There are many different mechanism of corrosion associated with stainless steel. They are generally divided into two groups, **general** corrosion and localized **corrosion**. The general mechanism of 'wet corrosion' is always the same, an electrochemical reaction. What differs between the different types of corrosion is the initiation process, which is caused by many different ways depending on the particular conditions.

General corrosion, otherwise known as uniform corrosion occurs over the majority of the surface of the metal at a steady and predictable rate. It thins the metal, producing a regular loss of the superficial metal. It is mostly seen in highly corrosive reducing acid environments associated with chemical industries. As of today, it makes up to the 30% of failures attributed to corrosion mechanisms. It is easily controlled, as the rate of corrosion is measurable and predictable. Most common measurement of general corrosion are penetration of thickness per year (mm/year) and loss of mass in grams per square meter per day ($\text{g}/\text{m}^2 \cdot \text{day}$). Stainless steels show very low general corrosion rates.

Localized corrosion is where the loss of metallic material occurs in localized or discrete areas. This type of corrosion represents about 70% of failures associated to corrosion mechanisms. The consequences of localized corrosion are much worse than general corrosion, as the mechanical failure happens without warning and at a shorter time period. There are many types of localized corrosion, but in this paper we will only study pitting, crevice and MIC.

Pitting corrosion or pitting is a form of localized corrosion that leads to formation of small holes in the metal. This normally happens in areas where general corrosion is nonexistent. This type of corrosion is initiated by chemical or mechanical damage to the passivating film, presence of impurities in the structure such as inclusions and high concentrations of chloride.

It has an autocatalytic nature. Once the pit or hole is created by the attack of chloride ions in weak points in the passive film, a local anodic dissolution process takes place, where the metal loss is higher due to the presence of a small anode and a relatively big cathode. Then, the high concentration of metallic ions in the pit attracts chloride ions and the following reaction takes place:



As a consequence of this, the pH inside the pit decreases and a highly acidic concentration takes over the hole, thus increasing the reaction rate and making the pit larger. Studies of corrosion failures of stainless steel have indicated that pitting and crevice corrosion types are major problems, and together account for perhaps 25% of all corrosion failures. One reason why pitting corrosion is so serious is that once a pit is initiated there is a strong tendency for it to continue to grow, even though the majority of the surrounding steel is still untouched. This kind of corrosion may also lead to or facilitate the appearance of stress corrosion cracking.

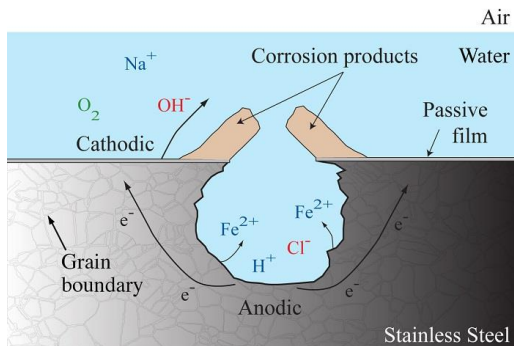


Figure 3.24. Diagram of pitting corrosion mechanism

Microbial corrosion or microbiologically influenced corrosion results from the microbiological activity of bacteria often found in water. It is defined as the electrochemical phenomenon that takes place in the presence of microorganisms. This type of localized corrosion usually takes place where metals are floating in water or flooded, or in offshore facilities where humidity is rather high.

Living biological microorganisms present in the water act in the metal's surface, accelerating the transport of oxygen, and catalyzing or producing the process of corrosion itself. The metal degradation can happen by the means of bacteria, molds and fungi or their by-products.

MIC is a common issue in many industrial processes. This is due to the presence of bacteria, adequate nutrients for this type of bacteria and secondary corrosive by-products. MIC is frequently found in water cooling systems and heat exchangers.

Microbial corrosion can be prevented through several methods, such as chemical treatment of the water if so possible. The addition of biocides in water treatment plants in order to regulate the population of bacteria will drastically prevent this type of corrosion. Good and regular mechanical cleaning will also prevent this phenomenon, as well total pipe drainage and dry storage.

The figure below shows several other corrosion mechanisms that are able to affect steel.

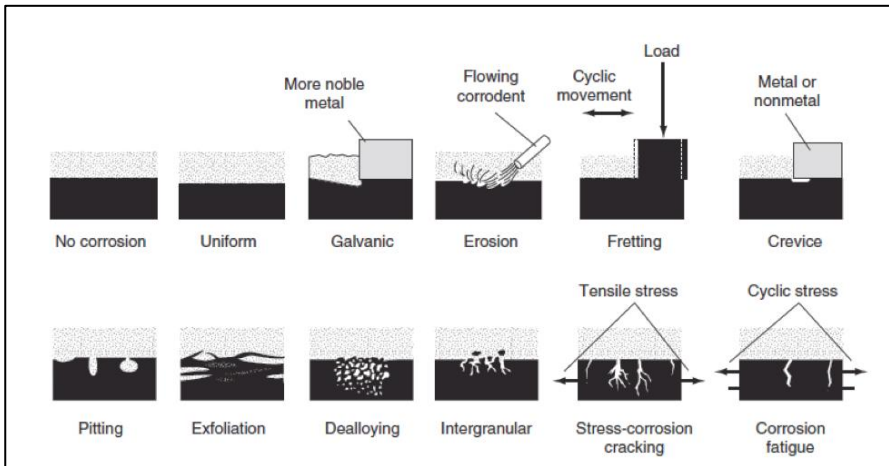


Figure 3.25. Most common corrosion mechanisms that are attributed to stainless steel.

4. OBJECTIVES

- Study the precipitation of secondary intermetallic phases of a super duplex stainless steel, corresponding to ASRM A-890 grade steel (UNS S32750 or SDSS25), through the application of short time isothermal heat treatments.
- Investigate the effect of the precipitation of the sigma phase on the super duplex stainless steel's microstructure.
- Investigate the range of temperatures in which the precipitation of sigma phase occurs, as well as its chemical composition and overall quantity throughout the different thermal treatment time scales.
- Study the differences between the steels that have been submitted to thermal treatments and the ones that haven't, thus comparing mechanical properties and their resistance to corrosion.
- To evaluate the resistance to corrosion of SDSS in a 4% NaCl solution and in a sea water solution, comparing corrosion behavior in both cases, and correlating it to the amount of brittle intermetallic phases that have precipitated.
- Observe and evaluate the main corrosion mechanism, pitting corrosion, which is regarded to be of crucial importance in SDSS applications.

5. EXPERIMENTAL PROCEDURE

5.1. Starting material

The steel that was used in this work has been the 2507 super duplex stainless steel. Also known as UNS S32750 by the ASTM unified numbering system or AST A-890 Gr5A grade steel. The particular piece of steel came from a desalination plant located in the north of Spain. More specifically, the steel was taken from a control valve found in an inverse osmosis unit in a desalination process.

The piece of steels received was cut into 22 smaller pieces with a mean surface area of the studied face of approximately 3,30 cm² and an average width of 0,6 cm in order to perform the appropriate tests and to have a large number of samples to be able to compare and contrast them throughout the different experiments.

The table below shows the maximum and minimum ranges in element compositions (in weight percentage) for this grade of stainless steel. As you can see, some spaces do not have a number, meaning that the alloy is not bound to have that specific alloying element in its composition.

| Elements | C | Cr | Cu | Fe | Mo | Mn | N | Ni | P | S | Si | W |
|----------|-------|------|------|------|------|------|------|------|-------|-------|------|------|
| Minimum | - | 24.0 | - | rest | 3.00 | - | 0.24 | 6.00 | - | - | 0.20 | - |
| Maximum | 0.030 | 26 | 0.50 | rest | 5.00 | 1.20 | 0.32 | 8.00 | 0.035 | 0.020 | 0.80 | 1.00 |

Table 5.1. Table showing max/min ranges of alloying elements in wt%

The table below shows the results obtained in the semi quantitative microanalysis of the super duplex stainless steel of the studied valve, as before, the results are shown in weight percentage (wt.). Several different parts or points of the steel where studied in order to have a more reliable calculation of its composition.

| Elements/points | Cr | Ni | Mo | Mn | Si | Fe |
|-----------------|-------|------|------|------|------|------|
| 1 | 27,4 | 6,15 | 6,17 | - | 0,70 | rest |
| 2 | 28,1 | 5,87 | 6,28 | - | 0,66 | rest |
| 3 | 27,7 | 5,65 | 6,82 | - | 0,58 | rest |
| 4 | 24,6 | 9,02 | 5,65 | 1,18 | - | rest |
| 5 | 26,7 | 7,31 | 5,29 | - | - | rest |
| 6 | 26,1 | 7,58 | 5,14 | 1,12 | - | rest |
| AVG | 26,77 | 6,93 | 5,89 | 1,15 | 0,65 | rest |

Table 5.2. Table showing 2507 SDSS microanalysis

The tables below show some information about the mechanical properties and the physical properties corresponding to this grade of steel. The below stated values for the some of the properties where not specified by the producer of the steel, but instead where retrieved from a bibliographical source. The values for the mechanical properties represent the minimum values of yield strength, UTS and elongation in order for this steel grade to be considered acceptable amongst producers.

| Physical property | Value | Mechanical property | Value |
|---|-----------------------|--|---------|
| Density (Kg.m ⁻³) | 7810 | 0.2% Yield strength (N/mm ²) | 550 |
| Young's Modulus (N/mm ²) | 199 x 10 ³ | Ultimate Tensile Strength (N/mm ²) | 800 |
| Specific Heat, 20°C (J.Kg ⁻¹ .°K ⁻¹) | 475 | Elongation (%) | 25 |
| Fracture Toughness, Kq (MPa.m) | 475 | Hardness (HRC) | 25(max) |
| Thermal conductivity, 20°C (W.m ⁻¹ .°K ⁻¹) | 14.2 | | |

Table 5.3. Tables of 2507 SDSS physical and mechanical properties

5.1.1.Applications and features of SDSS 2507

This grade of stainless steel, the SDSS 2507 has a superb resistance to corrosion in a wide variety of media, which makes it suitable for the most severe chemical conditions. Moreover, it has outstanding resistance to pitting corrosion in seawater environments, which also makes it suitable for off-shore and marine applications. Its corrosion rate in sea water and in acidic solutions is considerably lower than austenitic steels and other duplex grades.

As well as this, its high resistance to abrasion and erosion combined with exceptional resistance to SCC in chloride make SDSS 2507 perfect for oil and gas industries and other subsea equipment or subsea piping. This steel grade also has the approval for pressure vessel applications granted by ASME (American Society of Mechanical Engineers), which means that high pressure tanks and vessels are also a good application for this particular steel. Its high strength and ductility compared to austenitic and lesser alloyed duplex steels make this steel the ultimate super duplex grade.

Its applications range from a variety of sectors. This alloy is really versatile and it is used in many chemical process industries, such as nitric acids processes, polypropylene production and the handling of organic and fatty acids.

In addition to this, many duplex and super duplex grades, including this one are commonly used in the pulp and paper industry, where the medium can be pretty aggressive due to bleaching components and paints. Another use of this type of steel resides in the food industry, where corrosion resistance is a really important aspect of the metal, as it could contaminate the food in a processing plant for example.

5.2. Project outline

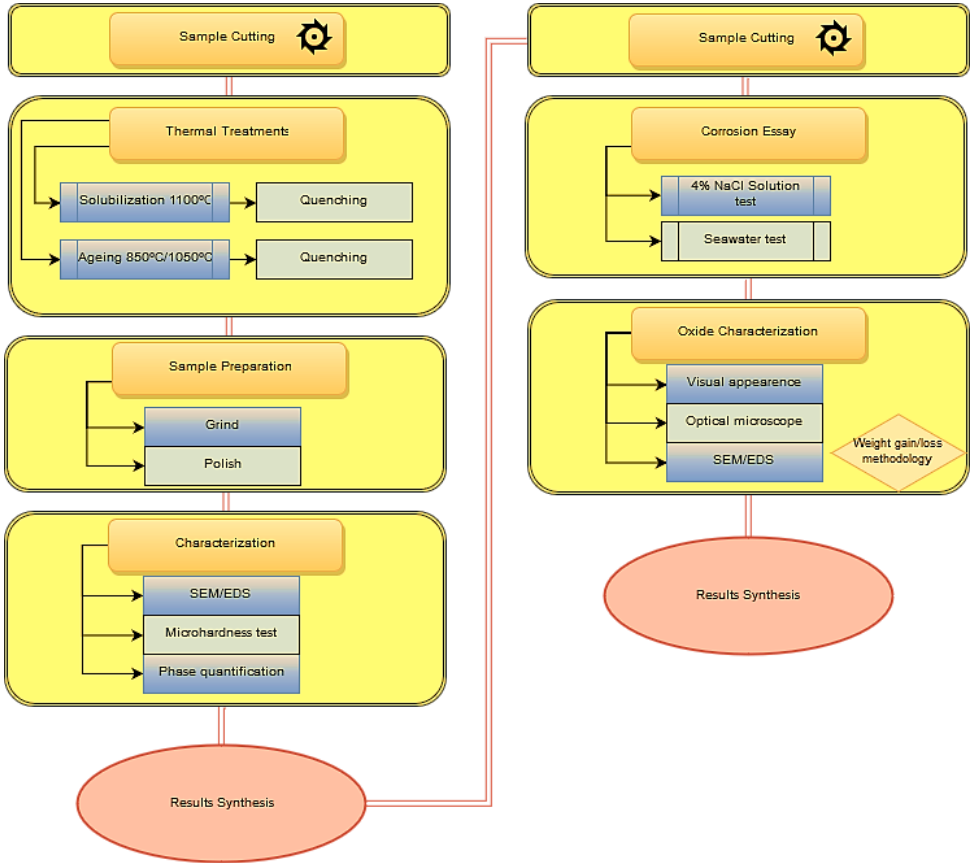


Figure 5.4. Schematic diagram of experimental process

5.3.Cutter

The initial piece of steel was first cut into 12 smaller pieces or coupons in order to perform the upcoming thermal treatments. In order to cut the pieces abrasive cutting technique was performed, using an 'AbrasiMet® 250 Manual Abrasive Cutter' from the American brand 'Buehler'.

Abrasive cutting is performed in metal samples and specimens. This device uses a silicon carbide (SiC) saw or blade in order to cut the samples. Upon cutting, the cutter tosses water on the point in which the saw and the surface of the material touch. This process takes place in order to minimize heat generation whilst cutting, as this is able to degrade the samples surface as well as lower the blade efficiency.

It is important to note that the abrasive saw is not technically a saw, as it has no teeth. The cutting action is performed by an abrasive disc and the abrasion mechanism. These discs wear off after several cutting processes and need to be replaced.

Later throughout the experiment, after performing the thermal treatments, running some tests and analysis that will later be explained in further detail, these pieces were cut again into 22 smaller pieces using the same technique. These 'third generation' pieces will be put to work in the corrosion essay performed.



Figure 5.5.Image of abrasive cutter

5.4.Isothermal heat treatments

Thermal treatments took place in **Hobersal** 'Model 12 PR/300 series 8B' oven and in a **Carbolite** 'CWF 13/05 model' oven. It is important to note that a good praxis is required in order to work with these high temperature ovens. When introducing or retrieving samples from inside the oven, safety measures were taken. The samples are placed on top of a piece of brick so they don't touch the oven's walls or floor. A big set of tweezers (over half a meter long) are used to extract and insert the samples in the oven. A fire-proof apron and fire retardant gloves are used in order to provide an extra security measure. Moreover, a plastic visor is used in order to protect the face area.



Figure 5.6.Image of Hobersal oven



Figure 5.7.Image of Carbolite oven

First of all, the 12 initial samples were submitted to a solubilization isothermal treatment of 1100°C during 30 minutes. This annealing process was performed in order to accomplish several things throughout the samples. First, any retained precipitate is dissolved in one of the phases. Moreover it eliminates any sort of segregation and relieves any residual thermal tension present in the material. After the annealing process, the samples are quenched in water and ice.

Quenching is a fast way to bring the metal back to room temperature after a thermal treatment, this allows the metal to prevent drastic changes in its microstructure from the cooling process. When fast-quenching, the metal's microstructure remains very similar to the one found in the solubilization treatment. This way, thermodynamic forces barely have the opportunity to change the microstructure.

Afterwards, an aging thermal treatment was applied to the samples. First, an 850°C isothermal ageing treatment was performed on 6 samples, then; the other 6 remaining samples were also treated at a temperature of 1050°C. Aging highly alloyed steel allows the alloying elements to diffuse throughout the microstructure and form intermetallic phases. After several time intervals, stated in the table below, the steel pieces were removed from the oven and quenched in iced water.

| <u>4 min</u> | <u>6 min</u> | <u>10 min</u> | <u>16 min</u> | <u>24 min</u> | <u>900 min</u> |
|--------------|--------------|---------------|---------------|---------------|----------------|
|--------------|--------------|---------------|---------------|---------------|----------------|

This way we are able to study the precipitation of intermetallic phases that have formed in the different samples at different time scales. One of the samples was left overnight to study the effect of a long-time treatment.

5.5. Sample preparation

In this section, the objective was to obtain a clean and polished superficial surface on one side of the samples. This will allow us to perform reliable hardness and corrosion tests as well as providing us with a good surface to observe in the optical microscope and further characterization of the sample.

First, all the samples went through a grinding and thinning process. The samples were thinned using sand paper or abrasive paper. An important concept regarding these types of papers is the grit size. This refers to the size of the particles ingrained inside the paper, the bigger the particles are, the more abrasive the paper is. Normally, bigger grain sizes are used to remove material from surfaces, whilst smaller grain sizes are used to make the surface smoother. These grains are normally made up of silicon carbide or aluminum oxide.

For our samples, we kicked things off by grinding them down with a sand paper with a P240 designation, meaning that this particular paper contained 240 particles for each squared centimeter. This is the most abrasive paper used in our testing, from here, the grits or particles embedded in the paper become smaller and smaller.

So first, we start with the bigger particle size paper and work our way down to the smallest particle size, grinding and thinning the samples along the way, with a finer and finer finish each time. The paper sequencing is the following: P240, P400, P600 and finally P1200. The usage of these papers was done manually with the aid of a grinding device. This device sprinkled water where the sandpaper was stranded in order to facilitate the manual grind. When transitioning between the different grain size papers, the samples were cleaned with distilled water, ethanol (98%) and later dried with a dryer.

Furthermore, the samples were polished at first with a 6 micron diamond particle paste and then with a 1 micron one. As with the sand paper, the 'roughest' or bigger particles were employed first, and then the smaller particle paste, leaving behind a finer finish on the surface of the steel samples. This was done using a *Buehler Metaserv 250* polisher and a *STRUERS polisher* (unknown model). When changing from one polisher to another, the samples were cleaned like in the previous step, with distilled water and ethanol in order to remove any undesired particles remaining in the surface.



Figure 5.8. Image of polisher



Figure 5.9. Image of grinding device

5.6.Characterization

Characterization introduces the concept by which a material and its properties are measured and tested. It is a core concept in materials science, as material engineers are always trying to find a way to understand substances behaviors and possible ways to improve mechanical properties; hence the understanding of the material's structure and properties is a key concept in this regard.

The understanding of this term is a little bit ambiguous, as some definitions refer to the sole use of techniques that study the microscopic structure and properties of materials, whilst others use it as a 'wild card' to attribute to any analysis process, such as mechanical testing or electrical conductivity to name a few.

In this paper we will run through three different ways of characterizing the sample: microscopy, spectroscopy and macroscopic testing. Microscopy is a characterization method that maps the surface structure of a given material. For our tests, **optical microscopy and scanning electron microscope** will be used. Spectroscopy is used for element analysis or chemical characterization, these kinds of techniques will allow the user to discover the chemical

composition and the crystallographic structure of the materials, and for our samples we will use the **energy-dispersive X-ray spectroscopy**, also known as EDX or EDS. Lastly, the macroscopic testing techniques to characterize our samples will rely upon the alloy's property of **hardness**.

5.6.1. Scanning electron microscope

The scanning electron microscope (SEM) is used for the observation and analysis of surfaces. It provides topographic and morphologic information of solid samples. Since its development, these kinds of microscopes have been largely used in many scientific fields, as it is designed for the direct study of solid object's surfaces.

The SEM is an instrument that uses a beam of electrons that falls upon the surface of the sample in order to produce an image. Once the projected electron beam impacts with the surface of the sample, an interaction takes place between the electron coming from the beam and the electrons in the atoms found inside the sample's structure. This 'clash' of electrons is the source of several distinctive signals, such as secondary electrons, backscattered electrons, characteristic X-rays and cathode luminescence.

All these different signals are later on perceived by a detector, which converts the apprehended signals into electronic signals. These are projected through a cathodic tube, allowing this way the formation of the image. All the different type of signals emitted by the interaction between the electron beam and the sample are of great use, as each and every one of them provides information and characteristics about the sample or its nature. Because of this, the SEM has specific detectors for each signal type.

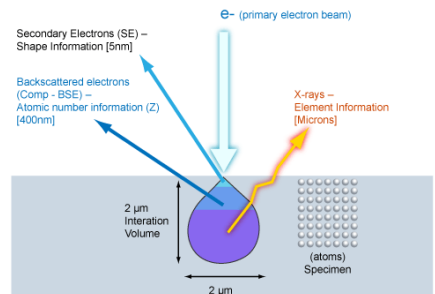


Figure 5.10. Different signals deriving from electron beam impact on the surface of the sample

Secondary electrons are used to obtain images of the surface of the sample, thus revealing the surface's topography. These electrons create a black and white image of the sample, and are captured by their detector when returning from any point, allowing then to describe the samples relieve and/or outline.

Backscattered electron's signal is received by a Backscattered Electron Detector (BED). This kind of electrons gives us picture with a contrast that both depend on the chemical composition of the surface and on its topography. In this type of technique, the image provided is one with a great contrast and very clear, where the substances or elements with the higher atomic number appear brighter and elements with a low atomic number appear to be darker.

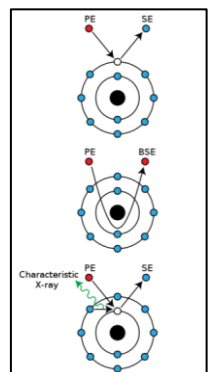


Figure 5.11. Mechanisms of emission of secondary electrons, backscattered electrons, and characteristic X-rays from atoms

5.6.2.EDS/EDX

This technique is called **energy dispersive x-ray spectroscopy**. The different X-rays generated by the interaction between the electron beam and the sample have a characteristic energy which is unique for each element.

These x-ray signals are collected by the detector and the chemical composition of the scanning zone is revealed as well as its concentration. The materials crystalline structure may also be revealed with upcoming technique. This methodology allows us to perform so called *compositional microanalysis*.



Figure 5.12. Image of SEM and EDS

5.6.3. Hardness Testing

Hardness is defined as the resistance that a material has to indentation or to surface scratches. It is measured by looking at the depth of a certain type of indentation when a load is applied. For a fixed load weight, the smaller the indentation is, the harder the metal is. Indentation hardness is obtained by measuring the depth or area of the indentation.

There are over ten different methods to measure hardness, the most common ones being Rockwell (A, B, C), Brinell or Vickers. The differences amongst them are the indenter, which come several different shapes and sizes, and the load or force applied in each case. Although it is impossible in many cases to give an exact conversion, it is possible to give an approximate comparison table for specific materials, for instance steel. (*Appendix 8-table 1.8.1*)

When running our tests we will be using the hardness scale of Rockwell C. This scale was chosen because the Rockwell Tester indicated in its specifications it was the suitable scale when working with hard metals or steels. In some cases we will make the conversion to the Vickers scale to be able to compare with other references and with bibliography.

The essay consists in disposing the steel on the base of the hardness tester, using a plain surface of the sample if possible. The tester applies a 10kg load to remove the sample's elastic deformation. Then the device applies a uniaxial load of 150 kgf of compression during 15 seconds. This uses a 120° conic indenter with a diamond point at the tip to produce a plastic deformation on the surface of the steel. The symbol for this hardness tests is represented as HRC.

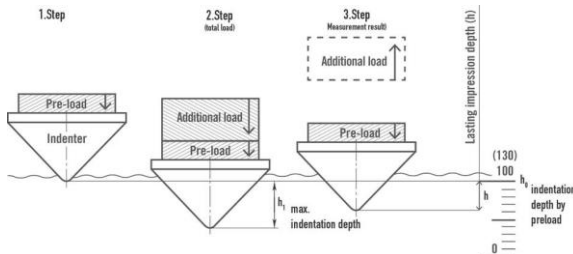


Figure 5.13. Diagram showing different steps of a Rockwell C hardness test

5.6.4. Phase quantification

In order to be able to quantify the different amounts of phases present in the steel's microstructure the computer program 'Image J' was used. This program was developed and programmed in Java and it is used as a digital image processing tool.

The program is able to calculate the given area, pixel x pixel, of a given color defined by the user. First of all, several filters are applied to smoothen the images quality. By selecting a color from the picture of your sample, the program calculates the number of pixels or units that are shaded with the same color.

For instance, if you pick a representative image of the steel's microstructure, an image where all phases were clearly visible, you just have to pick 3 or 4 different color ranges and the program maps out the number of pixels that represent that color and the total percentage, thus showing us the quantity of that specific phase present. The figure below represents an example of the use of ImageJ with one of our samples.

The average area of the images used for phase quantifications is approximately 400x400 micrometers, as they show a good and representative amount of phases present for each sample. The results for phase quantification are found in appendix 3-table 1.3.1.

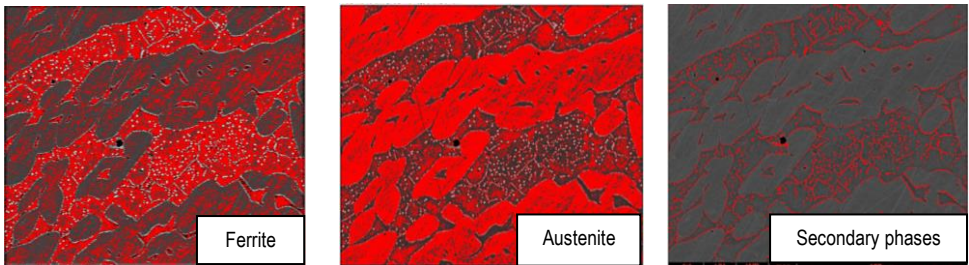


Figure 5.14. Picture provided by 'ImageJ' program, phase quantification methodology

5.7. Corrosion essay

In this particular experiment the stainless steel samples were placed inside a beaker with the help of a plastic support as shown in the figures below. Each support contains a label indicating which is sample it is holding. The samples were completely flooded by water and stirred continuously by a magnetic stirrer, simulating the conditions found inside a pipe or inside a container where water is found in constant movement. With this experiment super duplex stainless steel corrosion on the shallowness region is studied.

The magnetic stirrer promotes the movement of water inside the beaker, making the water circulate non-stop thus preventing its stagnation. As we are going to study the alloys behavior in a non-stagnant medium, such as a pipe or valve, the use of the stirrer is required. Additionally, water was removed and renewed every 48 hours, in order to clear away certain impurities and to eliminate dust or dirt particles that could provoke erosion or abrasion mechanisms on the steel samples.



Figure 5.15. Flooding corrosion device

The power of the magnetic stirrer was set to 5 bars throughout all experiments. This means that the average speed of water inside the beaker was constant through all iterations of the experiment and had an approximate value of 0,6 m/s. This was measured before mounting the plastic support and the whole device.

By measuring the circumference of the beaker at water level, and placing a few foam cubes that float and start circling around it, we are able to measure the approximate water speed. The agitation was set to the maximum speed so that a vortex would not form inside the beaker. As well as this, the temperature of the fluid was measured regularly. The measurement for all cases was around 22-23°C, very alike to the room temperature.

All the dimensions of the samples were measured with a micrometer, and are displayed in the appendix 5. The surface area of the polished face and the width of each individual sample were recorded, as well as the measurement of all their sides. This was done in order to check for general corrosion mechanisms, and to see if the sample shrunk in any way due to this procedure.



Figure 5.16. Micrometer

The samples were weighed prior to immersion, and are represented in the appendix 5 as well. The samples were weighed using a precision balance or analytical scale from Denver Instruments, model SI-114, which has an accuracy of four decimal points, or said otherwise, the scale is able to precisely measure up to milligrams.



Figure 5.17. Precision scale SI-114

First, all the steel samples were submerged in a 4% NaCl solution, in order to study how corrosion would be affect the steel under these circumstances. Every two days the solution was renewed and the experiment continued. Weight measurements were performed every five days and the total length of the experimented was 15 days.

In order to weigh the samples, they were carefully removed from the corrosion device and cleaned several times with distilled water in order to remove the salt present in the surface. It is important to note that the sample's surface was never wiped or touched, so to not remove possible corrosion products formed there. Then they were dried in a drying oven at 60°C for 20-25 minutes. This operation was repeated again as the first time wasn't enough to remove all the salt particles and crystals. Once the samples were clean and free of salt, they were weighed.

The salinity of the experiment (4%NaCl) was chosen because that is the average amount of chloride and sodium ions present in sea water throughout the world's seas and oceans. This experiment was only conducted with the samples submitted to a thermal treatment of 850°C. This will be later explained in the results and discussion area.

This whole experiment was repeated, but instead of using a 4% sodium chloride solution, real sea water fetched from the Mediterranean Sea was used. This way we will be able to compare and contrast both essays and their relation with the brittle intermetallic phases. This time around, samples submitted to both thermal treatments (850-1050°C) were employed.

Furthermore, the corrosion products in the samples will be measured by several techniques. First, microscopic observation will be executed. Finally, results will be evaluated with weight gain/weight loss methodology. If microscopic observation evaluation methods show no concluding results, corrosion effects will be also evaluated with SEM microscopy methods. According to ASTM G1-'Standard Practice for Preparing, Cleaning and Evaluation Corrosion Test Specimens' provided by ASTM and presented in the appendix 6, the chemical cleaning procedure chosen for removal of corrosion products for a stainless steel is designation C.7.1.

| | | | | |
|-------|------------------|---|--------|------|
| C.7.1 | Stainless Steels | 100 mL nitric acid (HNO ₃ , sp gr 1.42) Reagent water to make 1000 mL | 20 min | 60°C |
|-------|------------------|---|--------|------|

Table 5.18. Chemical cleaning procedure ASTM-G1

So, after studying the samples with microscopy methods, the corrosion products were cleaned or removed with a nitric acid solution, for a further evaluation of the corrosion damage that has occurred in every sample.

6. RESULTS AND DISCUSSION

6.1. Evolution of microstructure upon aging and EDS microanalysis

Samples were analyzed with the aid of the SEM, in conjunction with the backscattered electron detector BSE. The image below shows a characteristic example of a typical SEM picture. The austenite and the ferrite appear in the background, the first one having a lighter tonality than the second one, which appears darker in most of the images.

Secondary phases appear as bright smaller regions inside the ferritic matrix. As explained in previous sections of this paper, the chi-phase appears to be even brighter than the sigma-phase. This is because chi-phase has a higher content in molybdenum, which is one of the heavier elements present in our samples, and the reading performed by the detector catalogue the heavier elements as brighter zones in the pictures.

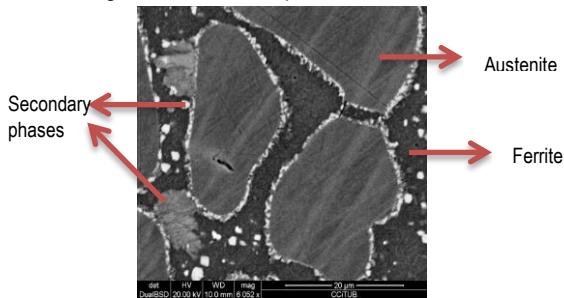


Figure 6.1. Image of microstructure from SEM

The SDSS 2507 steel provided to us had certain inclusions along its microstructure. This inclusion or defect was most likely part of the steel's microstructure before the samples were submitted to thermal treatments. It is most likely due to a flaw in the fabrication (casting) or conformation process that the stainless steel has gone through at the early stages of its life. It is appreciated that the steel's microstructure is pretty dirty, implying that the steel's manufacturer is not providing the best quality steel possible.

These types of inclusion were studied by EDS microanalysis throughout the samples, and were found to be round shaped and with a diameter around 10-20 micrometers. The EDS analysis concludes that these inclusions are made of silicon oxide (SiO_2). Very small traces of aluminum were found as well in some of the samples. This may be a residual impurity from the steel's fabrication, as aluminum is used as a deoxidizing element during steel casting, as it reduces the amount of oxygen in the steel.

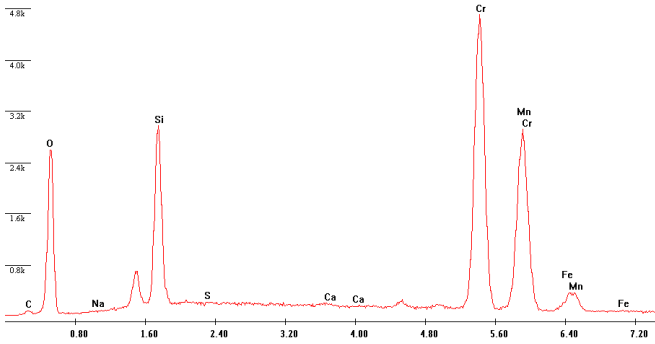


Figure 6.2. EDS diagram of SiO_2 inclusion

It is pressing to present the results from the thermal treatment of 1050°C first, as there is little to mention or talk about in the first place. The image below shows the microstructure found in a sample submitted to a high temperature thermal treatment of 1050°C . This temperature is fairly close to the one used in the solubilization thermal treatment performed on the samples before the tempering, also known as annealing.

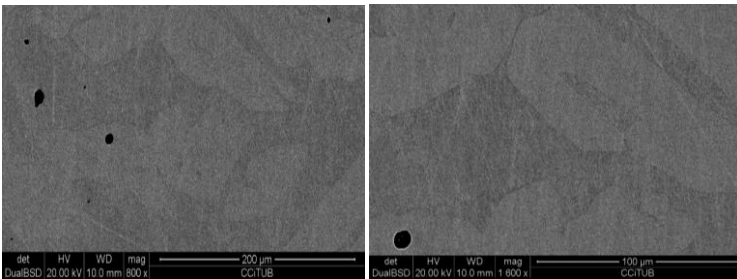


Figure 6.3. Microstructure of 1050°C -24min

These images are taken from the sample that was submitted to a TT of 1050°C at a 24 minute time scale. The differentiation between the austenitic phase and the ferritic phase is scarce. The reason behind this is that there is a lot of diffusion between both phases, meaning that alloying elements have had a lot of time to move around them and the parity between them is pretty significant. At this elevated temperatures both phases have a tendency to homogenize.

As well as this, we are able to see the inclusion of silicon oxide mentioned before. The black dots that are shown in the left part of the images are a clear indication of these. Moreover, we are able to see some secondary phases present in the microstructure. There is no trace of carbides or nitrides present in the microstructure of these samples. This phase tends to form at lower temperatures and thus is normal that they are not observed in samples that have been thermally treated at 1050°C .

At these temperatures, secondary intermetallic phases should not be present. Regardless, near some of the inclusions points sigma-phase shows up in the steel. This is because these spots or points act as a facilitator of secondary phases. These are localized around the inclusions and are nowhere to be found besides in these places. The figure below shows a detail of one of these spots. We are able to observe a white area surrounding the inclusion point. This area was further analyzed with EDS microanalysis, revealing the presence of intermetallic secondary phases, also known as sigma-phase.

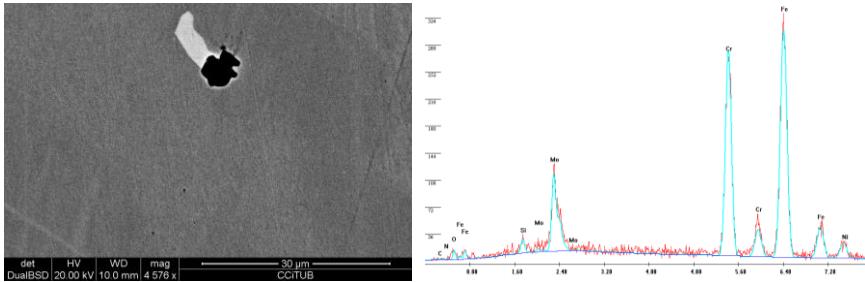


Figure 6.4. Image of secondary phase in inclusion and its EDS microanalysis

As we can see in the above figure of the EDS microanalysis, the molybdenum peak is fairly high in this phase. This is a clear indication that the presence of secondary phases is viable at these temperatures, but only if there is something that promotes or facilitates the precipitation or formation of them, as is the presence of these inclusions.

The EDS microanalysis of the austenitic and ferritic phases shows some differences between them and allows us to determine which one is which. As you can see in the diagram below, the austenitic phase microanalysis shows a higher quantity of nickel present, as it should be, because nickel is an austenite stabilizer element or gammagen. On the other hand, the ferrite EDS microanalysis shows a higher content of chrome and molybdenum, which is to be expected as both are ferrite stabilizing alloying elements.

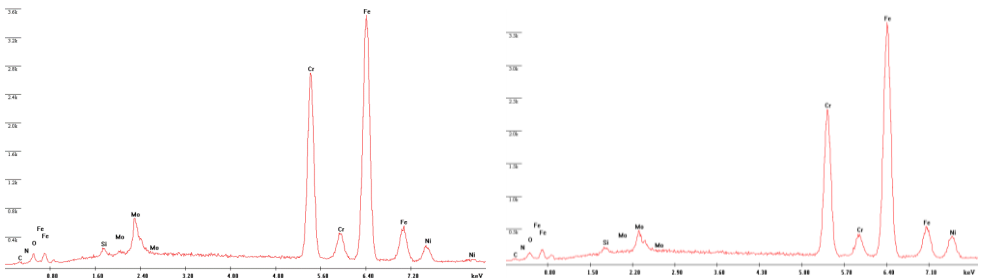


Figure 6.5. Typical EDS analysis of ferrite(left) and austenite(right)

These differences mentioned before are fairly small in comparison with other samples. This is because of the large amounts of diffusion between both phases and the tendency they have to homogenize. No further examination of samples treated at 1050°C was conducted, as they were all very similar in composition and microstructure and hardly any precipitation of secondary phases was perceived.

The study of the samples subject to 850°C is far more interesting. For this section all samples were studied at depth with the scanning electron microscope, and images for each individual sample were taken. Images corresponding to the whole thermal cycle are shown in the figure below. The first image represents a picture of the SDSS microstructure with a sample that has been in the oven for 4 minutes. The second image represents the sample for 6 minutes and so on and so forth until the last image, which is representative of the sample for 900 minutes.

For space reduction purposes, all EDS microanalysis for these images/samples is found in Appendix 7. It is important to mention that all analysis is semi quantitative and that values for all phases are found in normal ranges inside what is expected. What is meant by this is that all the EDS microanalysis corresponding to the ferritic phase, austenitic phase, sigma-phase and chi-phase present nominal values. The different peaks representing all the different alloying elements present in the phases are where they ought to be for each individual case.

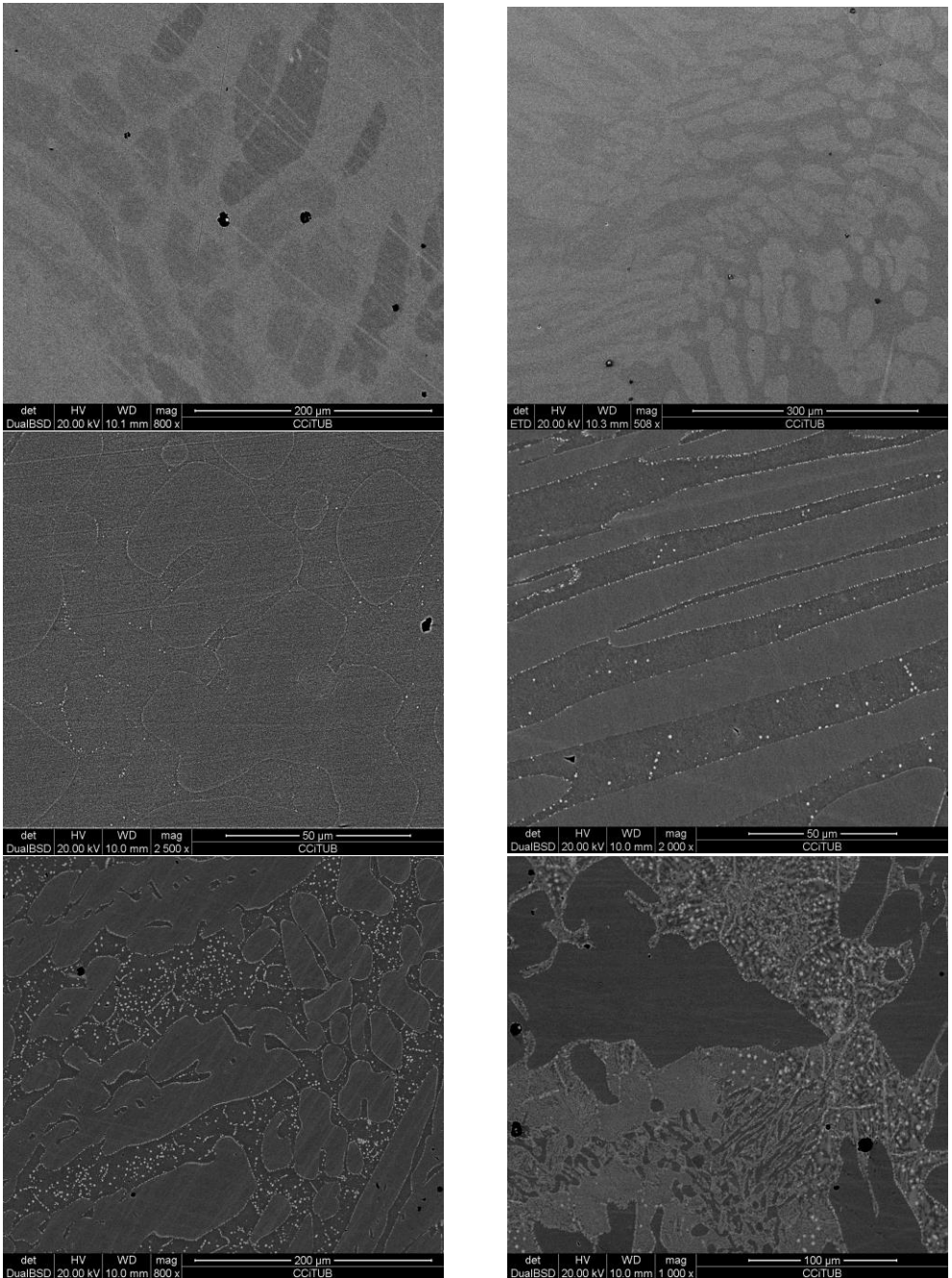


Figure 6.6. Microstructural evolution upon aging time scales

We will study and discuss these images from the shorter time period to the longer stages of thermal treatment. As we are able to see in the first image, not much is going on, the austenite and ferrite islands are about the same size and the quantity of both phases is roughly equal. There is no presence of secondary phase precipitation whatsoever in any of the images taken from the SEM at **4 minutes** time.

We can observe as well these silicon oxides inclusions that are present in all of our samples (black dots). The presence of carbides and nitrides is undetected thus far. It is safe to say that no microstructural changes have occurred yet, as the steel has more or less the same composition as its initial state.

The same can be said for the sample that is **6 minutes** in thermal treatment. There are still no signs of secondary phase precipitation in the grain boundaries. The lack of dispersion from the alloying elements force the microstructure to stay the same way as it was before and slows down the precipitation of intermetallic phases.

Finally, by the **10 minutes** mark we start to observe some changes in the microstructure. Secondary intermetallic phases start to nucleate in the ferrite/ferrite boundaries and ferrite/austenite boundaries. Most importantly, the precipitation of these phases only occurs in these boundaries at the moment. Both sigma-phase and chi-phase are present in this sample. Although it is merely impossible to distinguish them with the 'naked eye', and by this I mean by simple observation of the image provided by the SEM.

As you can see in appendix 7, tables 1.7.7 and 1.7.8, there is a clear differentiation between both phases when conducting an EDS microanalysis. It is clear that the existence of the pair of phases is viable because the sigma diagram and the chi diagram from EDS have different values of chromium quantity and molybdenum quantity.

As mentioned in the section "precipitation of intermetallic phases", the chi phase contains a large quantity of chrome and molybdenum composition in relation to the sigma phase. This way we are able to differentiate them even though their formation is quite recent, and the precipitates have nucleated but haven't yet grown.

As well as this, it is worth mentioning that the percentage of ferrite and austenite are still similar, although a slight decrease in the ferritic phase is noticed. Moreover, ferrite is showing 'compositional waters'. By this I mean that ferrite seems to be tabby or mottled, showing different tones or shades of grey on its areas. This is due to the compositional gradient of alloying elements inside it. As they are moving towards the formation of these brittle intermetallic phases, the different composition in these elements gives the ferrite different shading throughout its surface.

The **16 minutes** sample is similar to the previous one, although it harbors a few differences. First off, we are able to differentiate at plain sight the different intermetallic phases sigma and chi. These phases have different brightness, as the chi phase is nearly white, whilst the sigma phase is more greyish.

Moreover, the secondary brittle intermetallic phases are starting to grow and nucleate towards the inside of the ferritic matrix. This is clearly shown in the image corresponding to the 16 minute thermal treatment. Whilst on the 10 minute image the phase are only present in the grain boundaries, in this one they start to appear inside the ferric structure.

In addition to this, it is visible that these undesired phases are starting to grow and become bigger. During the transition of the transformation from ferrite phase to sigma phase, the ferrite's alloying elements impoverish, producing their destabilization and ultimately their transformation to secondary austenite.

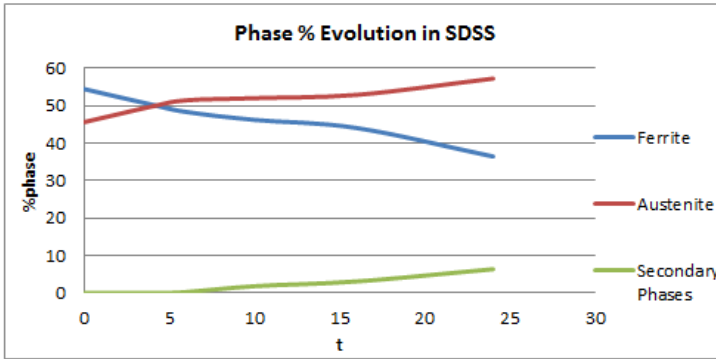
The **24 minute** image is one of the most interesting in my opinion. We can clearly observe that the amount of secondary phases is not only larger, but its grains are bigger in size as well. This big increase in the grain size of the sigma phase reduces its tendency to form, being that it runs out of ferrite to continue growing/ expanding. As a consequence of this, the quantity of ferrite present in the microstructure has clearly decreased to levels of 35%, whereas at the beginning, its initial value was over 50%.

Not only the ferrite quantity decreases, but the amounts of austenite present increases significantly. As you can see from the image at 24 minutes, the austenitic islands have a significantly larger size than in the previous pictures.

Furthermore, as the ferrite levels decrease, this inhibits and prevents the formation of intermetallic phases. At this precise moment, the microstructure has reached the point where the precipitation/formation of sigma phase kinetics is really slow. This is proven by the fact that from this point onwards until the end of the thermal treatment, the percentage increase of sigma-phase goes from roughly 9% at 25 minutes to 10% at 900 minutes.

As for the last image, after **15 hours** of thermal treatment all phases have reached equilibrium and have concluded microstructural evolution. As a matter of fact, the difference in the distribution of phases from the 24 minute mark and the 900 minute mark are relatively small. The facts stated above have led me to conclude that after about one hour of thermal treatment, the precipitation of intermetallic phases is capped and has no further continuation.

Using the **phase quantification** techniques described in the experimental procedure we are able to measure and quantify the amount of phases present in each sample and how they evolve and change during the different time scales of the thermal treatment. The table showing the phase evolution is found in appendix 3. The following graph describes the changes in the microstructure throughout the thermal treatment



Graph 6.7. Phase % evolution in SDSS

From this graph it is clear seen what was already observed in the SEM. The formation of the sigma phase goes by the following equation: $\delta \rightarrow \gamma + \sigma$. This eutectoid reaction (meaning one substance transforms into two) is represented by the graph of phase percentage evolution. As you can see, the amount of ferrite drops from around 55% to 35%. This ferrite loss is clearly transformed into an increment of austenite and secondary phases. In general most of transformations that involve the ferrite phase are primarily caused by the rapid diffusion rate of alloy elements in this phase compared with the rate for the austenite phase.

This also corroborates what we have shown before in the images of the microstructural evolution of our samples, as we observed how the amount of ferrite decrease in detriment of the growth of the austenitic phase and secondary phases such as sigma and chi-phase. The amount of secondary phase steadily grows reaching values of 8-9% at the 24 minute mark. The quantity of secondary phases keeps growing until they reach their maximum point after several hours of thermal treatment, as the percentage of secondary phases only increase by 1% from the hour mark to the end of the thermal treatment. Regardless, the substantial growth stage occurs between 10 and 25 minutes. The growth of sigma phase was enhanced by high diffusion of solute atoms and consequently this phase developed into a coarse particle after long-term aging.

A **semi quantitative** compositional analysis was carried out by EDS, to qualify and quantify each one of the phases present in the samples, as well as which elements are dominant in each one of the phases. Knowing the chemical composition of each phase and what elements they sustain will allow us to further understand the steel's behavior towards changes in the microstructure.

As an example we will perform a compositional microanalysis of the different quantity of elements present in all the phases in the sample subject to 850°C thermal treatment and 16 minutes time scale. All EDS diagrams are found in appendix 7.

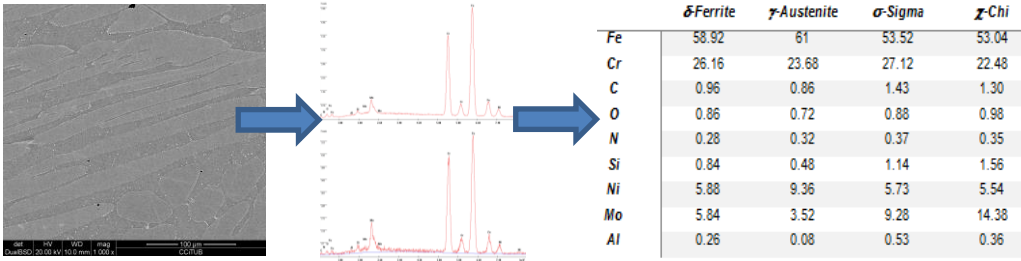
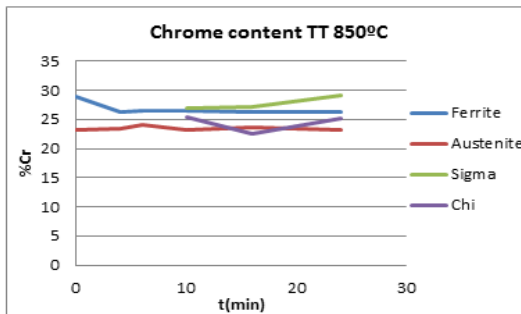


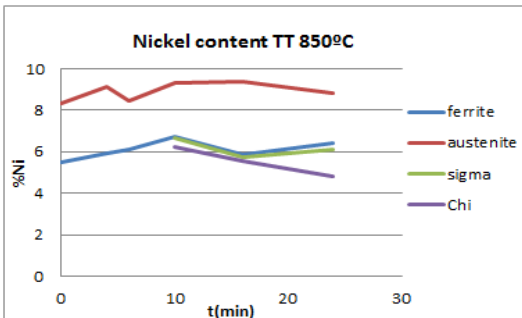
Figure 6.8. Diagram showing steps for semiquantitative analysis performed by EDS

This method was applied to all samples in order to know what alloying elements were present in each phase and how this was altered throughout the course of the thermal treatment. This way we are able to confirm what elements are austenite/ferrite stabilizers and allow us to comprehend how this move around the phases.

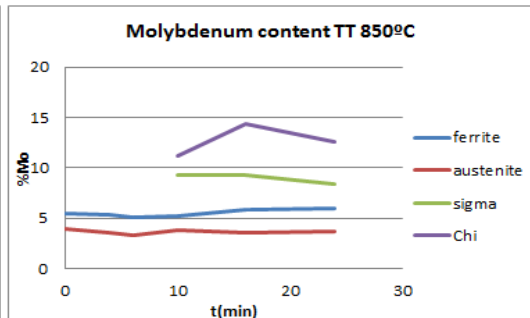
The results are shown in the graphics below and the tables can be consulted in appendix 2. It is important to point out that some readings overlap and that the data does not follow a general tendency. This is because the samples were analyzed at different points, and these may vary in composition of alloying elements, as the phases are not entirely homogenous.



Graph 6.9. Chrome content in the different phases



Graph 6.10. Nickel content in the different phases



Graph 6.11. Molybdenum content in the different phases

As expected for the austenitic phase the nickel content is significantly higher than on the other phases. The same results would show with alloying elements like nitrogen or carbon, as they all are austenite stabilizing elements or gammagens, and thus remain in higher content in this phase. The amount of nickel present in secondary phases and in the ferritic phase is very similar and could be considered constant throughout the experiment.

The higher chromium content is found in the sigma-phase. This is fairly obvious, as it is the richest phase in chromium, which is diffused from the ferritic matrix to the secondary phases. A drop in chromium content was expected for the ferritic phase, as this alloying element is ceded to the secondary phases. A slight decrease is detected but far less than what was expected. Moreover, austenite is the phase with lower chrome content, as this element is alphagens and remains in the ferritic phase.

Results from Molybdenum semi quantitative microanalysis show us what we already suspected. The chi-phase contains the higher amount of Mo as it is the richest phase in this element. Molybdenum is diffused out of the ferritic matrix towards the precipitation of intermetallic phases, thus these have a greater amount of it than ferrite and austenite. As this alloying element is a ferrite stabilizer, the lowest amount of Mo is found in the austenitic phase, as expected from the beginning.

6.2.Evolution of mechanical properties upon aging

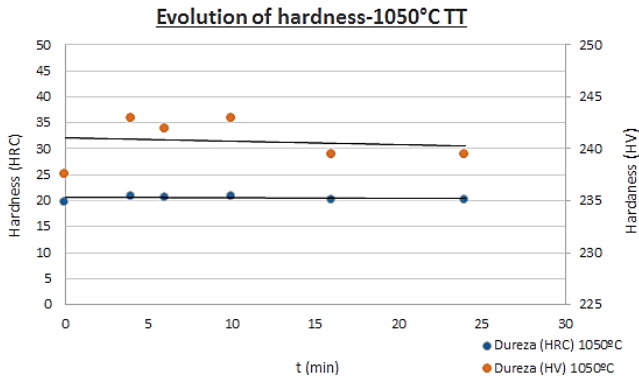
What grants super duplex steels its excellent mechanical properties is the austenite/ferrite equal phase distribution. As we have seen in previous sections of this paper, as a consequence of thermal treatments the percentage of these phases increase and decrease throughout the course of the treatment. Additionally, the appearance of secondary phases also has an impact on the mechanical properties of these alloys.

Hardness values depend on the alloy's microstructure and its chemical composition variation, as certain element tend to concentrate in several areas or phases. The diffusion of these elements throughout the phases by means of different mechanisms (grain boundary diffusion, surface diffusion etc.) creates internal stress in the phases, hardening the material even more.

Therefore, hardness tests were performed throughout the samples to be able to compare the microstructural evolution to the values of hardness. It has been proven that the precipitation of secondary intermetallic phases is detrimental to the steel's mechanical properties, as it increases the hardness of the steel, making it more brittle and fragile and thus reducing its toughness and ductility. The test performed in the samples hope to prove the above statement.

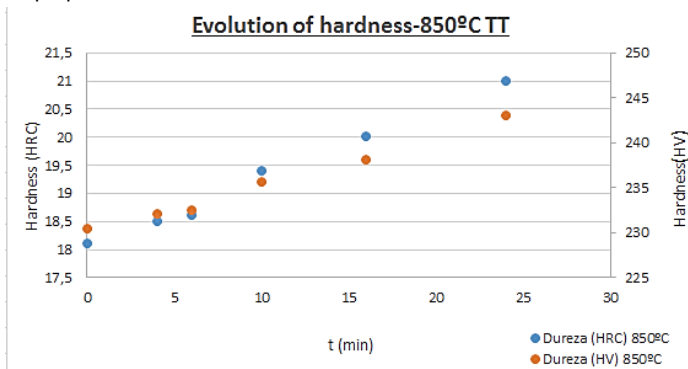
As we did in the previous section, we will begin analyzing the samples belonging to the thermal treatment of 1050°C. As no secondary phase precipitations was seen in the samples submitted to this thermal treatment and phase evolution remained quite steady, we expect to see no changes in the hardness values. The table containing these values is present in appendix 4.

The graph below shows us exactly this. The values of hardness remain constant around 20 HRC or 240 HV and remain in a linear fashion. These ranges of hardness correspond to the standard nominal values of hardness for duplex stainless steels.



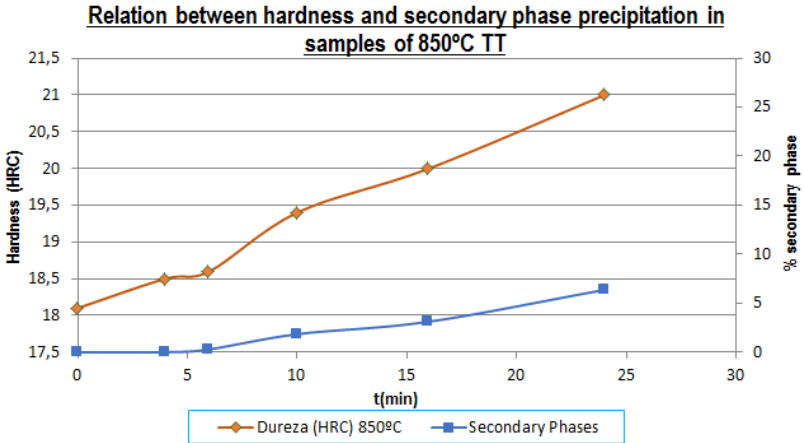
Graph 6.12. Changes in hardness after thermal treatment 1050°C

Then the samples submitted to thermal treatments of 850°C were analyzed and studied. As shown in section 6.1. Graph 6.7, the variation and evolution of phases is pretty hefty. As secondary phases start precipitating, the amount of austenite increases and the quantity of ferrite decreases. Due to these changes in the microstructure, we expect to see a variation in the mechanical properties of the steel.



Graph 6.13. Changes in hardness after thermal treatment 850°C

As we are able to see in the above graph, the hardness of the samples increases during the different time scales of the thermal treatment. The above presented facts lead me to conclude that as the amount of secondary intermetallic phases increases, so does the hardness of the steel. The value of hardness for 900 minutes is not presented in the graph, but you can check it out in appendix 3. After several hours of thermal treatment, the values of hardness continue to increase, reaching a maximum value of 37,2 HRC at 15h of thermal treatment, even though the evolution of phases and the kinetics of secondary phase precipitation have been reduced vigorously. This is due to the fact that diffusion of alloying elements still takes place in certain areas of the microstructure, thus creating internal stresses and hardening the alloy even more.



Graph 6.14. Correlation between hardness and secondary phase ppt.

The above graphic has been developed, which shows the relation or correlation between the precipitation of secondary phases and the values of hardness presented in Rockwell C scale. This graph is a hybrid between *graph 6.7* and *graph 6.9*. This has been done in order to verify that the formation of sigma phase affects the increases in hardness of these steels.

As we can see in the *graph 6.10.*, there is a correlation between the hardness and the precipitation of secondary phases, as the increase in the latter also promotes an increase in hardness. As we can see, the values of hardness and secondary phases remain more or less the same until the 7 minute mark, which is where sigma and chi phase precipitations starts. From here on, the values of hardness increase proportionally with the percentage of secondary phases.

It would have been interesting to perform other mechanical tests to these steels to be able to study the evolution of other properties, such a Charpy-impact test to see the evolution of toughness or tensile strength tests to be able to compare ductility and brittleness through a stress-strain graphic.

6.3. Corrosion study

For this section first we will study the samples submitted to the corrosion experiment with a 4% NaCl solution. Then we will proceed to the examination of the samples subject to the corrosion experiment with sea water that were previously treated at a temperature of 1050°C. To conclude we will complete the study with those samples that were treated at a temperature of 850°C and subject to the sea water corrosion experiment.

The first thing that was done was a visual examination of the samples with the help of an optical microscope. Prior to the examination, samples were cleaned with alcohol in order to remove dirt. Not much information was extracted by this method, as it was impossible to differentiate the pits created by the pitting corrosion mechanism from impurities and dirt or salt that has been deposited on the surface of the sample. Some examples are shown in appendix 10.

What is a fact for all samples of 850°C TT is that the amount of black dots on the surface when observed with an optical microscope increases as the amount of time submitted to thermal treatment also increases. Images are shown in appendix 10. As mentioned before, there is no way to see what a pit is and what dirt in the surface is without EDS analysis. Nevertheless, as all samples have been submitted to the same procedure, it is expected that all sustain the same amount of dirt or impurities on its surface. Thus the increasing number of black dots indicates that more corrosion products have been formed. This method is a qualitative method nonetheless, but we are looking to find a more accurate way to measure in order to achieve higher precision.

We hereby conclude that optical examination of the samples is found to be an inconclusive method in order to assess or evaluate numerically the corrosion products that have formed throughout our samples. Moreover, weight gain/loss methodology is also found to be inconclusive after all. For all three experiments, the amount of weight gained at the end of these was pretty insignificant.

The amount of weight won by the samples after spending 15 days inside the corrosion device averages at 18 mg. The amount of weight lost for all three experiments after performing the chemical cleaning procedure of corrosion products averages at about 30 mg. These values are too low in comparison with the weight of the samples in order to be meaningful. The mean mass of the samples is about 15,6 grams, which has a magnitude order of five more times over the weight gain/loss, thus making these reading unreliable. Besides, when working with variations that are this tiny, a small human error or experimental error can vary the result so drastically that it doesn't make sense to totally rely on these results.

One experimentation method that has been found conclusive is the testing for general corrosion. Samples' dimensions were measured using a micrometer. After the conclusion of the 15 days experiments, they were measured again by the same means. The volume variation of the samples is null. This result extends itself through the three experiments.

The assumption made for the reasoning of this phenomenon is that the samples were exposed to corrosive media for a very short time, taking into consideration that steel's corrosion resistance is superb. The corrosion rate found in bibliography for this superduplex steel grade in a sea water medium is under $0,1 \text{ mm.y}^{-1}$, so it is logical that in only 15 days this type of corrosion mechanism hasn't even begun.

So then the last experimental method we have available to check for corrosion products is with a SEM examination with a EDS microanalysis in order to truly corroborate that what we are observing are really oxides and other corrosion products. In order to make the explanation of each sample more comprehensible samples are named after the following guidelines:

| 4% NaCl | | | Sea Water | | | | | |
|---------|-----|------|-----------|-----|------|--------|-----|------|
| TT | Min | Name | TT | Min | Name | TT | Min | Name |
| 850°C | 4 | A.1. | 850°C | 4 | B.1. | 1050°C | 4 | C.1 |
| 850°C | 6 | A.2. | 850°C | 6 | B.2. | 1050°C | 6 | C.2 |
| 850°C | 10 | A.3. | 850°C | 10 | B.3. | 1050°C | 10 | C.3 |
| 850°C | 16 | A.4. | 850°C | 16 | B.4. | 1050°C | 16 | C.4 |
| 850°C | 24 | A.5. | 850°C | 24 | B.5. | 1050°C | 24 | C.5 |
| 850°C | 900 | A.6. | 850°C | 900 | B.6. | - | - | - |

Graph 6.15. Names of samples for corrosion experiment

Starting by the samples that were treated with a 4% NaCl solution, we are able to see that corrosion products and/or pits are barely non-existent for all time intervals of thermal treatments. Sample A.1 is practically the same as sample A.5.

For sample A.1. the only corrosion products observed are formed inside the inclusions or impurities found in the microstructure. All the rest of the surface is free from pits and no traces of other corrosion mechanisms where found. As represented in the figure below by the EDS microanalysis diagram, inside the silicon oxide inclusion we are able to find chrome oxides.

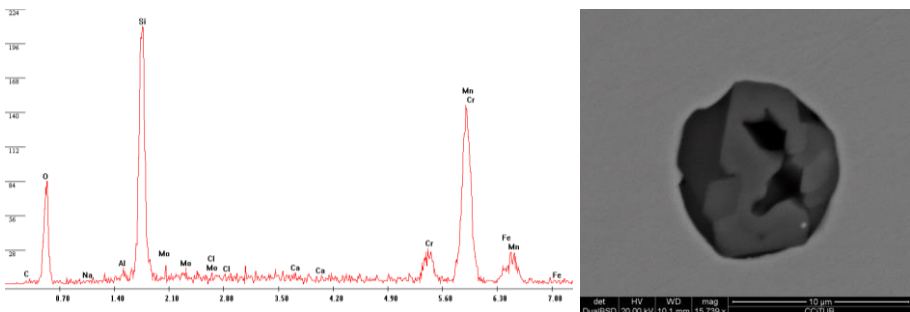


Figure 6.15. EDS diagram of inclusion and inclusion image

At the moment no there is no indication or signs of Cl⁻ ions detected by EDS so it is clear to us that the corrosion mechanism is not pitting. We observe exactly the same for sample A.2. (*Appendix 10-diagram 1*). This leads us to believe that these inclusions facilitate the formation of oxides in them or near them. For the next sample, A.3., we don't see any particular changes respecting the previous two samples. It may be said so far that all samples are showing the same results independently of the TT time, so instead we tried a different approach this time.

Instead of analyzing the polished side of the sample, we went ahead at checked out one of the other sides that was not grinded or polished on the edge of the piece. The results are found in *Appendix 10-diagram 2*. For the first time we are able to see leads of the pitting corrosion mechanism. First of all we see the presence of a high amount of chrome and oxygen, which indicates the formation of corrosion products.

As well as this we are able to see chlorine, sodium and potassium. This indicates that the corrosion mechanism is in fact pitting. This is found on the edge and not on the surface because this side of the piece has interphases with more tensions, due to cutting and not being polished. Moreover, the area has more porosity so corrosion mechanisms act easier than on the polished face, as this relieves superficial energy.

For all other samples (A.4 through A.6) the amounts of pits or corrosion found in the polished surface it identical. We also observe corrosion products inside inclusions. As well as on the other samples, no traces of chloride or sodium, so we can safely affirm that corrosion mechanism found inside the inclusions are not due to the chloride ion but of mere contact with water. All EDS diagrams for inclusions zones are really alike. In the figure below, thanks to overlaying technique we are able to see the depth of the 'hole' left behind in one of these inclusions.

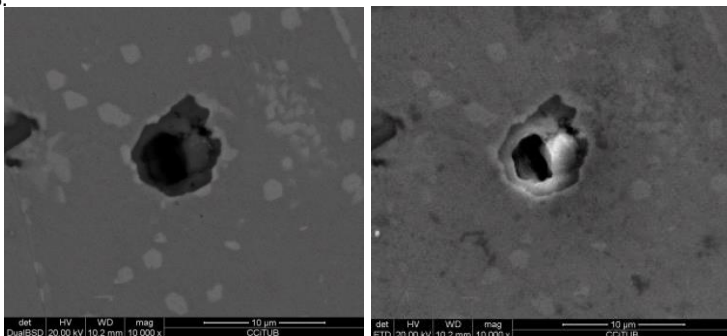


Figure 6.15. Image of inclusion showing its depth after corrosion

The samples treated with sea water tell us a very different tale. For the samples B.1. through B.6. we are able to see traces of NaCl throughout all of the different samples. All images and EDS microanalysis is found in appendix 10-figure 10.3 to figure 10.6.

As we can see in these figures, all the black zones or areas are corrosion products or related. The further you go down the list, the more corrosion products and pits you are likely to find. This means that for higher time scales of thermal treatments, the higher the amount of secondary phases present in the steel sample and the lower corrosion resistance it has.

Secondary phases take away chrome and molybdenum from the ferritic matrix. The latter grants excellent corrosion resistance to the steel, so when it is removed from the matrix, it is left more vulnerable to corrosion mechanisms. In the images found in appendix 10 for samples B.3. to B.6., we see austenite islands are 'cleaner' and have developed less corrosion product. It seems as if corrosion mechanisms are enhanced in the ferritic matrix. This is perfectly understandable because this phase is lacking its primary element to fight against corrosion.

In these samples we can also observe that inclusions are a 'hot spot' for corrosion to occur, just as in the previous experiment. On the EDS diagram corresponding to these samples the carbon peak is very high as well. This is attributed to a biomass film of living microorganisms such as ferrobacteria or ferro reducer microorganisms.

Samples corresponding to sea water experiment and TT of 1050°C are a complete success for our predictions. Samples C.1 through C.5 are studied by the same techniques. These samples show none or very few corrosion products across all images. The most we can see are salt crystal deposited on the surface of the steel. As there are little to none secondary phases present in these pieces, corrosion resistance is much higher than the B samples and thus no products are found. Images found in *appendix 10-figure 10.7* onwards. The results from these samples are very alike to the sample that has not been submitted to thermal treatment, which presents no secondary phases and no corrosion products.

In general, a larger amount of pits and corrosion products are found in the experiments that contained seawater rather than 4% NaCl solution. Moreover, the samples with higher times of thermal treatments and thus more secondary phases contained larger amounts of pits. From the above stated we are able to conclude that the precipitation of secondary phases and the depletion of the ferritic matrix from good alloying elements to this regard diminish the steel's resistance to corrosion.

7. CONCLUSIONS

In this project, the evolution of super duplex SDSS 2507's microstructure was investigated after submitting small samples of this steel grade to short time isothermal treatments of 850°C and 1050°C and different time scales. Furthermore, the precipitation of secondary intermetallic phases was studied and observed with microscopy techniques. The quantity of intermetallic substances that have precipitated was afterwards correlated to a difference in the steel's hardness and resistance to corrosion. The influence of these phases affects the alloy's properties in different manners. The conclusions withdrawn are the following:

- The first ounces of secondary phases (sigma and chi) were first observed at a 4 minute time scale for the 850°C thermal treatment. From the above statement we are able conclude that these phases precipitation kinetics is fast, as they start to precipitate in heat affected zones in a time scale under five minutes. This is due to the high percentage of alloying elements present in the ferritic matrix of super duplex steels.
- Precipitation of secondary intermetallic phases always takes place in the ferrite/austenite interfaces or ferrite/ferrite interfaces at first, and then grows towards the interior of the ferrite matrix. The kinetics of intermetallic phase formation is favored by grain boundaries diffusion. In this fashion, the formation of these phases depletes the surrounding ferritic matrix from alloying elements like chrome and molybdenum, thus reducing the alloys resistance to corrosion, making it more brittle and hardening it.
- A small precipitation of these undesired phases is enough to increase hardness values attributed to the steel. It has been shown that the higher the percentage content in secondary phases, the more the hardness increases throughout the samples. Reducing its toughness in the process.
- It has been demonstrated that the formation of sigma phases results from the following eutectoid reaction: $\delta \rightarrow \gamma + \sigma$. This is proven by the fact that the intermetallic precipitates consume the ferrite after its nucleation. As the thermal treatment time increases, so does the amount of sigma and chi-phases, whilst the ferrite content decreases.
- Secondary phases and corrosion products are detected using BED (backscattered electron detector) and their composition is characterized or confirmed by EDS/EDX microanalysis. This methodology allows us to observe at first glance the secondary

phases or corrosion products to then later corroborate their chemical composition and thus ensure that what we are seeing is in fact what we thought it was.

- Samples submitted to thermal treatment of 1050°C show no signs of secondary intermetallic phase precipitation. This case is later on ensured by the fact that the hardness of these samples remains the same for every time scale of the thermal treatment.
- Against our belief, no signs of carbides and nitride precipitation were found in the samples. The non-presence of chromium carbides is understandable because of the very low amount of carbon present in SDSS 2507, which ranges of 0-0, 03% in weight.
- No general corrosion mechanisms were initiated or found in our examination, as samples measurements of dimensions and size remained the same as before the corrosion experiments were conducted.
- As expected, a higher corrosion index was found in samples that were treated at 850°C than samples treated at 1050°C. The reason behind this is the greater amount of intermetallic phases present. Moreover, more corrosion products were found in samples that were submitted to corrosion testing by flooding of sea water instead of a regular 4% sodium chloride solution. This is due to the living biological microorganisms present in the sea water, such as ferrobacteria and others. As well as this, other de-passivating ions are present in sea water in small amounts, such as bromide (Br⁻) and iodide (I⁻), which can also attack the protecting oxide layer in SDSS.
- Overall, SDSS 2507 has an excellent resistance to corrosion, as not many pits were found during the SEM analysis and optical observation. Moreover, weight gain/loss methods conclude that samples practically don't lose weight after the chemical cleaning procedure of corrosion products (mean weight loss is on the order of 30mg approximately, which is insignificant in relation to the weight of the sample). The results confirm the fact that 2507 SDSS does not suffer severe damage from corrosion effects in the flooding region. This outcome was already expected as this grade of super duplex steel is rated as one of the best against pitting and localized corrosion. As proven, this grade of steel is superb for marine industry applications, as well as chemical processing industry applications.

8. REFERENCES AND NOTES

1. S.Duarte, Brandi, Giraldo, C.P. Serna, and. "Precipitación de fases intermetálicas de aceros inoxidable dúplex sometidos a tratamientos térmicos a temperatura de 850° c." *Scientia et Technica* 1.36 (2007).
2. M. P Rodríguez, et al. "Cinéticas de transformación de fases a 850 °C de aceros inoxidable dúplex clásicos (2205 y 2507) y de uno nuevo con bajo contenido en níquel y alto en manganeso (DBNi)." *Boletín de la Sociedad Española de Cerámica y Vidrio* 43.2 (2004): 237-242
3. I. Calliari, M. Zanezco, E. Ramous. "Influence of isothermal aging on secondary phases precipitation and toughness of a duplex stainless Steel SAF 2205." *Jmater Sci* 41 (2006): 7643-7649
4. D.M. Escriba, E. Materna-Morris, R.L. Plaut, A.F. Padilha. "Chi-phase precipitation in a duplex stainless steel." *Materials Characterization* 60 (2009): 1214-1219
5. E.J Chun, H.Baba, Kazutoshi Nishimoto, Kazuyoshi Saida. "Precipitation of sigma and chi phases in d-ferrite of Type 316FR Weld metals." *Materials Characterization* 89 (2013): 152-166
6. A. Swierczynska, Ms.C and S. Topolska, Ph.D. "Effect of microstructure on mechanical properties and corrosion resistance of 2005 duplex stainless Steel." *Behavior Polish maritime research* 4(84) (2014) vol.21: 108-112
7. J.M. Bonnel.; Pease N.C.; Atament, S.Welding superduplex stainless steels with flux-cored and metal cored wires. *Stainless Steel World 99 Conference. Proceedings.* (1999): 219-36
8. J. Basumatary, M. Nie, R. J. K. Wood. "The Synergistic Effects of Cavitation Erosion-Corrosion in Ship Propeller Materials." *J bio Tribo Corros* (2015): 1-12
9. J.-O. Nilsson, P. Kangas, T. Karlsson, and A. Wilson. "Mechanical Properties, Microstructural Stability and Kinetics of s-Phase Formation in 29Cr-6Ni-2Mo-0.38N Superduplex Stainless Steel." *Metallurgical and Materials Transactions A* vol 31A (2000): 35-45
10. K. O. Oparaodu, G. C. Okpokwasili. "Comparison of Percentage Weight Loss and Corrosion Rate Trends in Different Metal Coupons from two Soil Environments." *International Journal of Environmental Bioremediation & Biodegradation*, 2.5 (2014): 243-249.
11. ASM International. "Alloy Digest Sourcebook: Stainless Steels." Ohio USA
12. S. J. Morrow. "Materials Selection for Seawater Pumps." Chief Metallurgist & Global Manager of Materials Technology
13. J. L Garin, R. L. Mannheim y M.A. Camus. "Formación de fase sigma en unions soldadas de acero inoxidable súper dúplex fundido." *Revista de metalurgia*, 47.4 (2011): 293-306

14. A. M. Orellana. "Microanálisis por Dispersión de Energías de Rayos-X (XEDS)." Servicio de Microscopía Electrónica. SCAI. Universidad de Málaga (2010)
15. G. Jean-Ives, Chairman. "The Ferritic Solution. " International Stainless Steel Forum
16. E. Otero 2012, *Corrosión y degradación de materiales*, Madrid, España, Editorial Síntesis
17. YU. M. Laitin 1973, *Metalografía y Tratamiento Térmico de los Metales*, Moscú, Mir editorial
18. IMOA (International Molybdenum Association) 2012, Directrices prácticas para la fabricación de aceros inoxidables duplex, Londres, Reino Unido.
19. Schaeffler technical documentation 2014, *Schaeffler Technical Pocket Guide*, Herzogenaurach, Alemania, Schaeffler Technologies GmbH & Co. KG
20. astm G1-90 (1999), Standard Practice for Preparing, Cleaning, and Evaluation Corrosion Test Specimens, American Society for Testing and Materials
21. Foundry-lexicon (2017): Sigma Phase
<http://www.giessereilexikon.com/en/foundrylexicon/Encyclopedia/show/sigma-phase-3594/>
22. The Online Hub for Corrosion Professionals (2017):
<https://www.corrosionpedia.com/>
23. SASSDA 2017: Stainless Steel and Corrosion:
<http://sassda.co.za/stainless-steel-and-corrosion/>
24. Langley Alloys 2017: Super Duplex, Nickel Alloys, Austenitic Stainless Steels, Duplex Stainless, Bronzes, Super Duplex UK <http://www.langleyalloys.com/>
25. Antidesgast:http://antidesgast.com/downloads/pag_37.pdf
26. Corrotherm:<https://www.corrotherm.co.uk/hubfs/resources/corrotherm-introduction-super-duplex-stainless-steels.pdf>

8.1.ACRONYMS

- **SDSS:** Super Duplex Stain Steel
- **DSS:** Duplex Stain Steel
- **α :** Ferrite phase(low temperature)
- **δ :** Ferrite phase (high temperature)
- **γ :** Austenite phase
- **σ :** Sigma phase
- **χ :** Chi phase
- **Cr_{eq} :** Chrome equivalent
- **Ni_{eq} :** Nickel equivalent
- **SEM:** Scanning Electron Microscope
- **EDS:** Energy Dispersive Spectroscopy
- **BED:** Backscattered Electron Detector
- **AISI:** American Iron Steel Institute
- **SAE:** Society of Automotive Engineers
- **ASTM:** American Society for Testing and Materials
- **FCC:** Face Centered Cubic
- **BCC:** Body Centered Cubic
- **MPa:** Mega Pascal
- **UNS:** Unified Numbering System
- **PREN:** Pitting Resistance Equivalent Number
- **FGD:** Flue Gas Desulfurization
- **SCC:** Stress Corrosion Cracking
- **$^{\circ}C$:** degrees Celsius
- **TTP/TTT:** Time-Temperature-Precipitation/Time-Temperature-Transformation
- **J:**Jules
- **m/s:** meters per second
- **ASME:** American Society of Mechanical Engineers
- **REDOX:** Reduction-Oxidation
- **MIC:** Microbial Influence Corrosion
- **Mm/year:** millimeters per year
- **g/m².day:** grams per meter squared per day
- **wt:** weight percentage
- **UTS:** Ultimate Tensile Strength
- **HRC:** Rockwell C Hardness
- **HV:** Vickers Hardness
- **TT:** Thermal Treatment
- **Kgf:** kilogram-force or kilopond
- **Mg:** milligrams

9. APPENDICES

9.APPENDICES

APPENDIX 1: AUSTENITIC, FERRITIC AND DUPLEX STAINLESS STEEL GRADES

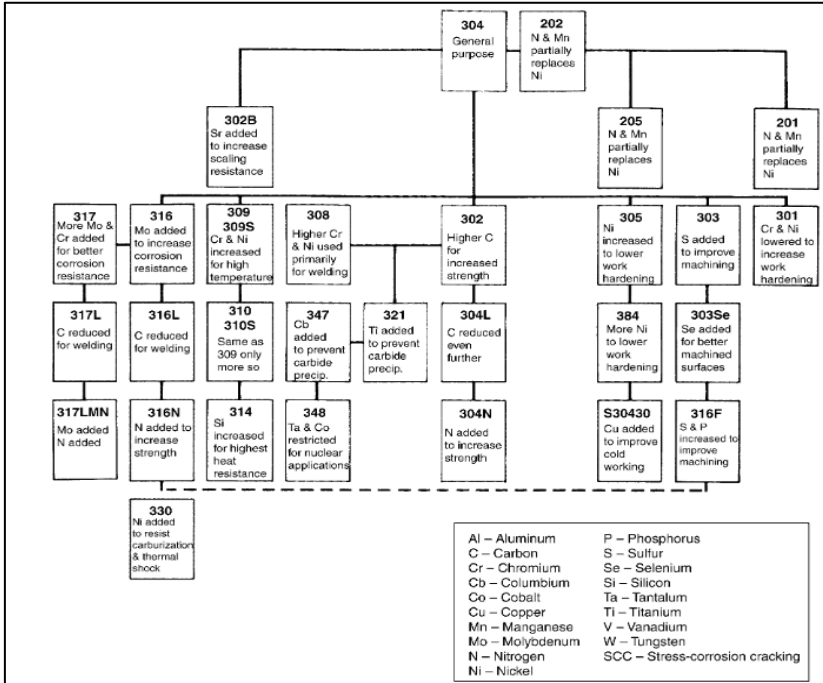


Figure 1.1.1. Diagram representing several austenitic steel grades

| Properties | Ferritic | Austenitic |
|--------------------------------------|----------------|--------------|
| Toughness | Moderate | Very high |
| Ductility | Moderate | Very high |
| Weldability | Limited | Good |
| Thermal expansion | Moderate | High |
| Stress corrosion cracking resistance | Very high | Low |
| Magnetic properties | Ferro magnetic | Non-magnetic |

Table 1.2. Table showing differences in mechanical and physical properties between ferritic and austenitic steels

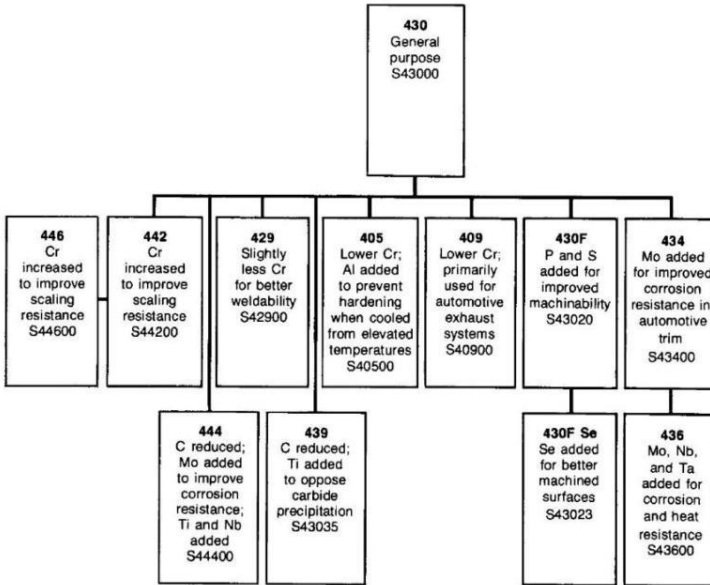


Figure 1.1.3. Diagram representing several ferritic steel grades



A 995/A 995M – 98 (2003)

TABLE 2 Chemical Requirements

| Grade | 1B | 2A | 3A | 4A | 5A ^A | 6A ^A |
|-----------------|------------------|----------------|---------------|---------------|-----------------|-----------------|
| Type | 25Cr-5Ni-Mo-Cu-N | 24Cr-10Ni-Mo-N | 25Cr-5Ni-Mo-N | 22Cr-5Ni-Mo-N | 25Cr-7Ni-Mo-N | 25Cr-7Ni-Mo-N |
| UNS | J93372 | J93345 | J93371 | J92205 | J93404 | J93380 |
| ACI | CD4MCuN | CE8MN | CD6MN | CD3MN | CE3MN | CD3MWCuN |
| Composition: | | | | | | |
| Carbon, max | 0.040 | 0.080 | 0.060 | 0.030 | 0.030 | 0.030 |
| Manganese, max | 1.00 | 1.00 | 1.00 | 1.50 | 1.50 | 1.00 |
| Silicon, max | 1.00 | 1.50 | 1.00 | 1.00 | 1.00 | 1.00 |
| Phosphorus, max | 0.040 | 0.040 | 0.040 | 0.040 | 0.040 | 0.030 |
| Sulfur, max | 0.040 | 0.040 | 0.040 | 0.020 | 0.040 | 0.025 |
| Chromium | 24.5-26.5 | 22.5-25.5 | 24.0-27.0 | 21.0-23.5 | 24.0-26.0 | 24.0-26.0 |
| Nickel | 4.7-6.0 | 8.0-11.0 | 4.0-6.0 | 4.5-6.5 | 6.0-8.0 | 6.5-8.5 |
| Molybdenum | 1.70-2.30 | 3.0-4.5 | 1.75-2.50 | 2.5-3.5 | 4.0-5.0 | 3.0-4.0 |
| Copper | 2.7-3.3 | ... | ... | 1.00, max | ... | 0.50-1.00 |
| Tungsten | ... | ... | ... | ... | ... | 0.50-1.00 |
| Nitrogen | 0.10-0.25 | 0.10-0.30 | 0.15-0.25 | 0.10-0.30 | 0.10-0.30 | 0.20-0.30 |

^A% Cr + 3.3 % Mo + 16 % N ≥ 40.

TABLE 3 Tensile Requirements

| Grade | 1B | 2A | 3A | 4A | 5A | 6A |
|--|------------------|----------------|---------------|---------------|---------------|---------------|
| Type | 25Cr-5Ni-Mo-Cu-N | 24Cr-10Ni-Mo-N | 25Cr-5Ni-Mo-N | 22Cr-5Ni-Mo-N | 25Cr-7Ni-Mo-N | 25Cr-7Ni-Mo-N |
| Tensile strength, ksi [MPa], min | 100 [690] | 95 [655] | 95 [655] | 90 [620] | 100 [690] | 100 [690] |
| Yield strength (0.2 % offset), ksi [MPa], min | 70 [485] | 65 [450] | 65 [450] | 60 [415] | 75 [515] | 65 [450] |
| Elongation in 2 in. [50 mm], %, min ^A | 16 | 25 | 25 | 25 | 18 | 25 |

^A When ICI test bars are used in tensile testing as provided for in this specification, the gage length to reduced section diameter ratio shall be 4:1.

Table 1.1.4. Table representing several chemical compositions and mechanical requirements for DSS

| UNS Number Duplex Grades | Type ^b | C | Mn | P | S | Si | Cr | Ni | Mo | N | Cu | Other |
|--------------------------|-------------------|-------|---------|-------|-------|------|-----------|-----------|-----------|-----------|-----------|------------|
| S31200 | ... | 0.030 | 2.00 | 0.045 | 0.030 | 1.00 | 24.0-26.0 | 5.5-6.5 | 1.20-2.00 | 0.14-0.20 | ... | ... |
| S31260 | ... | 0.03 | 1.00 | 0.030 | 0.030 | 0.75 | 24.0-26.0 | 5.5-7.5 | 2.5-3.5 | 0.10-0.20 | 0.20-0.80 | W0.10-0.20 |
| S31803 | ... | 0.030 | 2.00 | 0.030 | 0.020 | 1.00 | 21.0-23.0 | 4.5-6.5 | 2.5-3.5 | 0.08-0.20 | ... | |
| S32001 | ... | 0.030 | 4.0-6.0 | 0.040 | 0.030 | 1.00 | 22.0-23.0 | 1.00-3.00 | 0.60 | 0.05-0.17 | 1.00 | |
| S32205 | 2205 | 0.030 | 2.00 | 0.030 | 0.020 | 1.00 | 19.5-21.5 | 4.5-6.5 | 3.0-3.5 | 0.14-0.20 | ... | |
| S32304 | 2304 | 0.030 | 2.50 | 0.040 | 0.030 | 1.00 | 21.5-24.5 | 3.0-5.5 | 0.05-0.60 | 0.05-0.20 | 0.05-0.60 | |
| S32520 | ... | 0.030 | 1.50 | 0.035 | 0.020 | 0.80 | 24.0-26.0 | 5.5-8.0 | 3.0-4.0 | 0.20-0.35 | 0.50-2.00 | |
| S32550 | 255 | 0.04 | 1.50 | 0.040 | 0.030 | 1.00 | 24.0-27.0 | 4.5-6.5 | 2.9-3.9 | 0.10-0.25 | 1.5-2.5 | |
| S32750 | 2507 | 0.030 | 1.20 | 0.035 | 0.020 | 0.80 | 24.0-26.0 | 6.0-8.0 | 3.0-5.0 | 0.24-0.32 | 0.50 | |
| S32760 | ... | 0.030 | 1.00 | 0.030 | 0.010 | 1.00 | 24.0-26.0 | 6.0-8.0 | 3.0-4.0 | 0.20-0.30 | 0.50-1.00 | c |
| S32900 | 329 d | 0.06 | 1.00 | 0.040 | 0.030 | 0.75 | 23.0-28.0 | 2.5-5.0 | 1.0-2.0 | ... | ... | |
| S32950 | ... | 0.03 | 2.00 | 0.035 | | | | | | | | |

Table1.1.5. Table representing chemical composition of DSS and SDSS

The various Alloys

Super-Duplex falls under the Duplex stainless steel grouping.

Duplex stainless steels are graded for their corrosion performance depending on their alloy content. Today, modern Duplex stainless steel can be divided into four groups:

- Lean Duplex such as 2304, which contains no deliberate Mo addition;
- 2205, the work-horse grade accounting for more than 80% of duplex usage;
- 25 Cr duplex such as Alloy 255 and DP-3;
- Super-Duplex; with 25-26 Cr and increased Mo and N compared with 25 Cr grades, including grades such as 2507, Zeron 100, UR 52N+, and DP-3W

| FAMILY | USA | EURONORM | Cr | Mo | Ni | Mn | Cu | N | Others | PRE | PREN |
|--|---------|----------|------|-----|-----|-----|------|------|--------|-----|------|
| 300 | 304L | 1.4307 | 18 | 0 | 9 | 1 | 0 | | | 18 | 18 |
| | 316L | 1.4401 | 17 | 2 | 11 | 1 | 0 | | | 24 | 24 |
| | 904LN | 1.4539 | 20 | 4 | 25 | 1 | 1.5 | 0.1 | | 33 | 35 |
| Standard DUPLEX (1996) | S 32304 | 1.4362 | 23 | 0.3 | 4 | 1 | | 0.13 | | 23 | 25 |
| | S 32205 | 1.4462 | 22 | 3 | 6 | 1 | | 0.17 | | 32 | 35 |
| | S 32750 | 1.4410 | 25 | 3.5 | 7 | 1 | | 0.27 | | 37 | 41 |
| | S 32760 | 1.4501 | 25 | 3.8 | 7 | 1 | 0.7 | 0.27 | 0.7 W | 38 | 42 |
| S 32520 | 1.4507 | 25 | 3.5 | 7 | 1 | 1.5 | 0.25 | | 37 | 41 | |
| New DUPLEX (EX) | S 31500 | | 18.5 | 2.7 | 5 | 1 | | 0.1 | | 27 | 29 |
| | S 32101 | 1.4162 | 21 | 0.3 | 1.5 | 5 | | 0.2 | | 21 | 24 |
| | S 32001 | | 20 | 0.3 | 1.7 | 5 | 0.3 | 0.15 | | 21 | 23 |
| | S 32003 | | 20 | 1.7 | 3.5 | 2 | | 0.15 | | 26 | 28 |
| | S 31260 | | 27 | 3 | 7 | 1 | 0.5 | 0.16 | 0.3 W | 37 | 39 |
| | S 39274 | | 25 | 3 | 7 | 1 | 0.6 | 0.27 | 2 W | 35 | 39 |
| S 32906 | 1.4362 | 29 | 2 | 6 | 1 | | 0.4 | | 36 | 42 | |
| PRE = %Cr + 3.3%Mo ; PREN = %Cr + 3.3%Mo + 16%N | | | | | | | | | | | |

Table1.1.7. Table representing values of PREN for different steel alloys

Table1.1.6. Classification of DSS and SDSS

APPENDIX 2: EDS MICROANALYSIS

SDSS without Thermal Treatment

| | δ -Ferrite | γ -Austenite | σ -Sigma | χ -Chi |
|-----------|-------------------|---------------------|-----------------|-------------|
| Fe | 54.51 | 59.28 | | |
| Cr | 28.8 | 23.09 | | |
| C | 3.35 | 4.87 | | |
| O | 1.99 | 0 | | |
| N | 0.98 | 0 | | |
| Si | - | - | | |
| Ni | 5.16 | 8.42 | | |
| Mo | 5.5 | 3.58 | | |
| Al | - | - | | |

Table1.2.1.EDS microanalysis no TT

SDSS 4 min 850°C

| | δ -Ferrite | γ -Austenite | σ -Sigma | χ -Chi |
|-----------|-------------------|---------------------|-----------------|-------------|
| Fe | 59.75 | 60.87 | | |
| Cr | 26.30 | 23.48 | | |
| C | 1.01 | 1.12 | | |
| O | 0.71 | 0.70 | | |
| N | 0.32 | 0.33 | | |
| Si | 0.68 | 0.8 | | |
| Ni | 5.95 | 9.13 | | |
| Mo | 5.28 | 3.56 | | |
| Al | - | - | | |

Table1.2.2.EDS microanalysis 4 min 850°C

SDSS 6 min 850°C

| | δ -Ferrite | γ -Austenite | σ -Sigma | χ -Chi |
|-----------|-------------------|---------------------|-----------------|-------------|
| Fe | 59.62 | 61.42 | | |
| Cr | 26.82 | 24.08 | | |
| C | 0.74 | 0.86 | | |
| O | 0.66 | 0.63 | | |
| N | 0.23 | 0.46 | | |
| Si | 0.66 | 0.78 | | |
| Ni | 5.59 | 6.11 | | |
| Mo | 5.68 | 5.04 | | |
| Al | - | - | | |

Table1.2.3.EDS microanalysis 6 min 850°C

SDSS 10 min 850°C

| | δ -Ferrite | γ -Austenite | σ -Sigma | χ -Chi |
|-----------|-------------------|---------------------|-----------------|-------------|
| Fe | 59.66 | 61.92 | 54.51 | 53.90 |
| Cr | 26.53 | 23.16 | 26.90 | 25.28 |
| C | - | - | - | - |
| O | 0.73 | 0.65 | 0.91 | 0.85 |
| N | 0.19 | 0.32 | 0.43 | 0.30 |
| Si | 0.92 | 0.80 | 1.35 | 1.67 |
| Ni | 6.70 | 9.34 | 6.69 | 6.23 |
| Mo | 5.27 | 3.80 | 9.22 | 11.12 |
| Al | - | - | | |

Table1.2.4.EDS microanalysis 10 min 850°C

SDSS 16 min 850°C

| | δ -Ferrite | γ -Austenite | σ -Sigma | χ -Chi |
|-----------|-------------------|---------------------|-----------------|-------------|
| Fe | 58.92 | 61 | 53.52 | 53.04 |
| Cr | 26.16 | 23.68 | 27.12 | 22.48 |
| C | 0.96 | 0.86 | 1.43 | 1.30 |
| O | 0.86 | 0.72 | 0.88 | 0.98 |
| N | 0.28 | 0.32 | 0.37 | 0.35 |
| Si | 0.84 | 0.48 | 1.14 | 1.56 |
| Ni | 5.88 | 9.36 | 5.73 | 5.54 |
| Mo | 5.84 | 3.52 | 9.28 | 14.38 |
| Al | 0.26 | 0.08 | 0.53 | 0.36 |

Table1.2.4.EDS microanalysis 16 min 850°C

SDSS 24 min 850°C

| | δ -Ferrite | γ -Austenite | σ -Sigma | χ -Chi |
|-----------|-------------------|---------------------|-----------------|-------------|
| Fe | 59.05 | 61.34 | 53.90 | 53.68 |
| Cr | 26.24 | 23.17 | 29.07 | 25.21 |
| C | 0.27 | 1.29 | 0.76 | 0.86 |
| O | 0.64 | 0.78 | 0.92 | 0.93 |
| N | 0.28 | 0.36 | 0.10 | 0.00 |
| Si | 0.85 | 0.52 | 0.63 | 0.98 |
| Ni | 6.45 | 8.82 | 6.09 | 5.39 |
| Mo | 5.95 | 3.63 | 8.35 | 12.54 |
| Al | 0.26 | 0.09 | 0.19 | 0.40 |

Table1.2.5.EDS microanalysis 24 min 850°C

SDSS 900 min 850°C

| | δ -Ferrite | γ -Austenite | σ -Sigma | χ -Chi |
|-----------|-------------------|---------------------|-----------------|-------------|
| Fe | 60.09 | 62.81 | 53.93 | 52.55 |
| Cr | 27.45 | 23.50 | 29.14 | 26.79 |
| C | - | - | - | 1.30 |
| O | - | - | - | - |
| N | 0.11 | - | 0.25 | - |
| Si | 0.62 | - | 1.19 | 1.02 |
| Ni | 5.68 | 9.32 | 3.89 | 3.62 |
| Mo | 6.05 | 3.77 | 11.60 | 14.71 |
| Al | - | - | - | - |

Table1.2.6.EDS microanalysis 900 min 850°C

APPENDIX 3: PHASE QUANTIFICATION

SDSS 2507

| <i>t (min)</i> | <i>δ-Ferrite</i> | <i>γ-Austenite</i> | <i>Secondary Phases</i> |
|----------------|------------------|--------------------|-------------------------|
| 0 | 54,4 | 45,6 | 0 |
| 4 | 50,23 | 49,57 | 0 |
| 6 | 48,29 | 51,17 | 0 |
| 10 | 46,19 | 51,97 | 1,84 |
| 16 | 44,01 | 52,87 | 3,12 |
| 24 | 36,44 | 57,19 | 6,37 |
| 900 | 40,66 | 49,14 | 10,2 |

Table1.3.1.Phase quantification developed by Image J

APPENDIX 4: ROCKWELL C HARDNESS TEST

SDSS 2507 850°C

| <i>t (min)</i> | 0 | 4 | 6 | 10 | 16 | 24 | 900 |
|-----------------|----------|----------|----------|-----------|-----------|-----------|------------|
| | 17,75 | 18 | 18,75 | 19,5 | 22,5 | 19 | 37,25 |
| | 18 | 18,5 | 18,5 | 19,8 | 18 | 22,5 | 38 |
| | 18,5 | 19 | 18,5 | 19 | 19,5 | 21,5 | 36,25 |
| Avg. | 18,1 | 18,5 | 18,6 | 19,4 | 20,0 | 21,0 | 37,2 |
| Desvest. | 0,382 | 0,500 | 0,144 | 0,404 | 2,291 | 1,803 | 0,878 |

Table1.4.1. Hardness tests for different 850 °C TT times

SDSS 2507 1050°C

| <i>t (min)</i> | 0 | 4 | 6 | 10 | 16 | 24 |
|-----------------|----------|----------|----------|-----------|-----------|-----------|
| | 19,8 | 20 | 18,5 | 20 | 20,5 | 20,5 |
| | 20 | 21 | 21,5 | 22 | 20 | 20,5 |
| | 20 | 22 | 22,5 | 21 | 20,5 | 20 |
| Avg. | 19,9 | 21,0 | 20,8 | 21,0 | 20,3 | 20,3 |
| Desvest. | 0,115 | 1,000 | 2,082 | 1,000 | 0,289 | 0,289 |

Table1.4.2. Hardness tests for different 1050°C TT times

APPENDIX 5: WEIGHT GAIN/LOSS METHODOLOGY

4% NaCl SOLUTION-850°C T.T.

| SDSS 850°C | Area (cm ²) | Width(cm) | Volume (cm ³) | Weight(g) | | | | | ASTM-G1 / C.7.1 |
|------------|-------------------------|-----------|---------------------------|-----------|---------|---------|---------|---------|-----------------|
| | | | | Day 0 | Day 5 | Day 10 | Day 15 | | |
| 4(min) | 2,865 | 0,701 | 2,008 | 15,3941 | 15,3953 | 15,3964 | 15,3975 | 15,3927 | |
| 6(min) | 3,337 | 0,701 | 2,339 | 18,8038 | 18,8048 | 18,8089 | 18,8089 | 18,8029 | |
| 10(min) | 2,970 | 0,755 | 2,242 | 16,4915 | 16,4929 | 16,4977 | 16,4956 | 16,4902 | |
| 16(min) | 3,929 | 0,668 | 2,625 | 20,0870 | 20,0883 | 20,0926 | 20,0899 | 20,0856 | |
| 24(min) | 4,529 | 0,658 | 2,980 | 21,7039 | 21,7075 | 21,7156 | 21,7095 | 21,7019 | |
| 900(min) | 2,177 | 0,616 | 1,341 | 10,3446 | 10,3486 | 10,3503 | 10,3443 | 10,3444 | |

Table1.5.1.Weight gain/loss throughout experiment. 850°C TT-NaCl solution

SEA WATER SOLUTION-850°C T.T.

| SDSS 850°C | Area (cm ²) | Width (cm) | Volume (cm ³) | PESO (g) | | | | | ASTM-G1/C.7.1 |
|------------|-------------------------|------------|---------------------------|----------|---------|---------|---------|---------|---------------|
| | | | | Day 0 | Day 5 | Day 10 | Day 15 | | |
| 4 (min) | 3,359 | 0,696 | 2,338 | 17,2404 | 17,2415 | 17,2598 | 17,2397 | 17,2395 | |
| 6 (min) | 3,381 | 0,562 | 1,900 | 13,8090 | 13,8101 | 13,8096 | 13,8105 | 13,8083 | |
| 10 (min) | 3,513 | 0,575 | 2,020 | 13,5195 | 13,5205 | 13,5201 | 13,5209 | 13,5184 | |
| 16(min) | 3,083 | 0,67 | 2,065 | 15,3668 | 15,3674 | 15,3672 | 15,3680 | 15,3661 | |
| 24 (min) | 3,873 | 0,651 | 2,521 | 18,7359 | 18,7362 | 18,7377 | 18,7385 | 18,7351 | |
| 900 (min) | 3,022 | 0,62 | 1,874 | 13,6978 | 13,6982 | 13,6992 | 13,6998 | 13,6972 | |

Table1.5.2.Weight gain/loss throughout experiment. 850°C TT-sea water solution

SEA WATER SOLUTION-1050°C T.T. / No T.T.

| SDSS 1050°C | Area (cm ²) | Width(cm) | Volume (cm ³) | Weight (g) | | | | | ASTM-G1 / C.7.1 |
|-------------|-------------------------|-----------|---------------------------|------------|---------|---------|---------|---------|-----------------|
| | | | | Day 0 | Day 5 | Day 10 | Day 15 | | |
| 4(min) | 4,074 | 0,621 | 2,530 | 18,5094 | 18,5098 | 18,5093 | 18,5096 | 18,5085 | |
| 6(min) | 3,005 | 0,592 | 1,779 | 13,1591 | 13,1597 | 13,1593 | 13,1601 | 13,1586 | |
| 10(min) | 2,785 | 0,575 | 1,601 | 12,1679 | 12,1684 | 12,1681 | 12,1689 | 12,1669 | |
| 16(min) | 3,105 | 0,562 | 1,745 | 12,4291 | 12,4292 | 12,4294 | 12,4299 | 12,4284 | |
| 24(min) | 3,465 | 0,522 | 1,809 | 13,5610 | 13,5614 | 13,5613 | 13,5624 | 13,5609 | |
| SDSS No TT | Area (cm ²) | Width(cm) | Volume (cm ³) | Weight (g) | | | | | ASTM-G1 / C.7.1 |
| 3.1 | 3,869 | 0,528 | 2,043 | 13,0354 | 13,0352 | 13,0348 | 13,0351 | 13,0338 | |

Table1.5.2.Weight gain/loss throughout experiment. 1050°C TT and no TT-sea water solution

APPENDIX 6: CHEMICAL CLEANING PROCEDURES FOR CORROSION PRODUCTS REMOVAL

TABLE A1.1 CHEMICAL CLEANING PROCEDURES FOR REMOVAL OF CORROSION PRODUCTS

| Designation | Material | Solution | Time | Temperature | Remarks |
|-------------|--------------------------------|---|--------------|-----------------|--|
| C.1.1 | Aluminum and Aluminum Alloys | 50 mL phosphoric acid (H ₃ PO ₄ , sp gr 1.69) 20 g chromium trioxide (CrO ₃) Reagent water to make 1000 mL | 5 to 10 min | 90°C to Boiling | If corrosion product films remain, rinse, then follow with nitric acid procedure (C.1.2). |
| C.1.2 | | Nitric acid (HNO ₃ , sp gr 1.42) | 1 to 5 min | 20 to 25°C | Remove extraneous deposits and bulky corrosion products to avoid reactions that may result in excessive removal of base metal. |
| C.2.1 | Copper and Copper Alloys | 500 mL hydrochloric acid (HCl, sp gr 1.19) Reagent water to make 1000 mL | 1 to 3 min | 20 to 25°C | Deaerate of solution with purified nitrogen will minimize base metal removal. |
| C.2.2 | | 4.9 g sodium cyanide (NaCN) Reagent water to make 1000 mL | 1 to 3 min | 20 to 25°C | Removes copper sulfide corrosion products that may not be removed by hydrochloric acid treatment (C.2.1). |
| C.2.3 | | 100 mL sulfuric acid (H ₂ SO ₄ , sp gr 1.84) Reagent water to make 1000 mL | 1 to 3 min | 20 to 25°C | Remove bulky corrosion products before treatment to minimize copper redeposition on specimen surface. |
| C.2.4 | | 120 mL sulfuric acid (H ₂ SO ₄ , sp gr 1.84) 30 g sodium dichromate (Na ₂ Cr ₂ O ₇ ·2H ₂ O) Reagent water to make 1000 mL | 5 to 10 s | 20 to 25°C | Removes redeposited copper resulting from sulfuric acid treatment. |
| C.2.5 | | 54 mL sulfuric acid (H ₂ SO ₄ , sp gr 1.84) Reagent water to make 1000 mL | 30 to 60 min | 40 to 50°C | Deaerate solution with nitrogen. Brushing of test specimens to remove corrosion products followed by re-immersion for 3 to 4 s is recommended. |
| C.3.1 | Iron and Steel | 1000 mL hydrochloric acid (HCl, sp gr 1.19) 20 g antimony trioxide (Sb ₂ O ₃) 50 g stannous chloride (SnCl ₂) 50 g sodium hydroxide (NaOH) 200 g granulated zinc or zinc chips Reagent water to make 1000 mL | 1 to 25 min | 20 to 25°C | Solution should be vigorously stirred or specimen should be brushed. Longer times may be required in certain instances. |
| C.3.2 | | 200 g granulated zinc or zinc chips Reagent water to make 1000 mL | 30 to 40 min | 80 to 90°C | Caution should be exercised in the use of any zinc dust since spontaneous ignition upon exposure to air can occur. |
| C.3.3 | | 200 g sodium hydroxide (NaOH) 20 g granulated zinc or zinc chips Reagent water to make 1000 mL | 30 to 40 min | 80 to 90°C | Caution should be exercised in the use of any zinc dust since spontaneous ignition upon exposure to air can occur. |
| C.3.4 | | 200 g diammonium citrate ((NH ₄) ₂ HC ₆ H ₇ O ₇) Reagent water to make 1000 mL | 20 min | 75 to 90°C | Depending upon the composition of the corrosion product, attack of base metal may occur. |
| C.3.5 | | 500 mL hydrochloric acid (HCl, sp gr 1.19) 3.5 g hexamethylene tetramine Reagent water to make 1000 mL | 10 min | 20 to 25°C | Longer times may be required in certain instances. |
| C.3.6 | | Molten caustic soda (NaOH) with 1.5–2.0 % sodium hydride (NaH) | 1 to 20 min | 370°C | For details refer to Technical Information Bulletin SP29-370, "DuPont Sodium Hydride Descaling Process Operating Instructions." |
| C.4.1 | Lead and Lead Alloys | 10 mL acetic acid (CH ₃ COOH) Reagent water to make 1000 mL | 5 min | Boiling | ... |
| C.4.2 | | 50 g ammonium acetate (CH ₃ COONH ₄) Reagent water to make 1000 mL | 10 min | 60 to 70°C | ... |
| C.4.3 | | 250 g ammonium acetate (CH ₃ COONH ₄) Reagent water to make 1000 mL | 5 min | 60 to 70°C | ... |
| C.5.1 | Magnesium and Magnesium Alloys | 150 g chromium trioxide (CrO ₃) 10 g silver chromate (Ag ₂ CrO ₄) Reagent water to make 1000 mL | 1 min | Boiling | The silver salt is present to precipitate chloride. |
| C.5.2 | | 200 g chromium trioxide (CrO ₃) 10 g silver nitrate (AgNO ₃) 20 g barium nitrate (Ba(NO ₃) ₂) Reagent water to make 1000 mL | 1 min | 20 to 25°C | The barium salt is present to precipitate sulfate. |
| C.6.1 | Nickel and Nickel Alloys | 150 mL hydrochloric acid (HCl, sp gr 1.19) Reagent water to make 1000 mL | 1 to 3 min | 20 to 25°C | ... |
| C.6.2 | | 100 mL sulfuric acid (H ₂ SO ₄ , sp gr 1.84) Reagent water to make 1000 mL | 1 to 3 min | 20 to 25°C | ... |
| C.7.1 | Stainless Steels | 100 mL nitric acid (HNO ₃ , sp gr 1.42) Reagent water to make 1000 mL | 20 min | 60°C | ... |
| C.7.2 | | 150 g diammonium citrate ((NH ₄) ₂ HC ₆ H ₇ O ₇) Reagent water to make 1000 mL | 10 to 60 min | 70°C | ... |
| C.7.3 | | 100 g citric acid (C ₆ H ₈ O ₇) 50 mL sulfuric acid (H ₂ SO ₄ , sp gr 1.84) 2 g inhibitor (diorthotolyl thiourea or quinoline ethyl iodide or betanaphthol quinoline) Reagent water to make 1000 mL | 5 min | 60°C | ... |
| C.7.4 | | 200 g sodium hydroxide (NaOH) 30 g potassium permanganate (KMnO ₄) Reagent water to make 1000 mL followed by 100 g diammonium citrate ((NH ₄) ₂ HC ₆ H ₇ O ₇) Reagent water to make 1000 mL | 5 min | Boiling | ... |
| C.7.5 | | 100 mL nitric acid (HNO ₃ , sp gr 1.42) 20 mL hydrofluoric acid (HF, sp gr 1.199–48 %) Reagent water to make 1000 mL | 5 to 20 min | 20 to 25°C | ... |
| C.7.6 | | 200 g sodium hydroxide (NaOH) 50 g zinc powder Reagent water to make 1000 mL | 20 min | Boiling | Caution should be exercised in the use of any zinc dust since spontaneous ignition upon exposure to air can occur. |

APPENDIX 7: EDS DIAGRAMS FOR SDSS 850°C TT

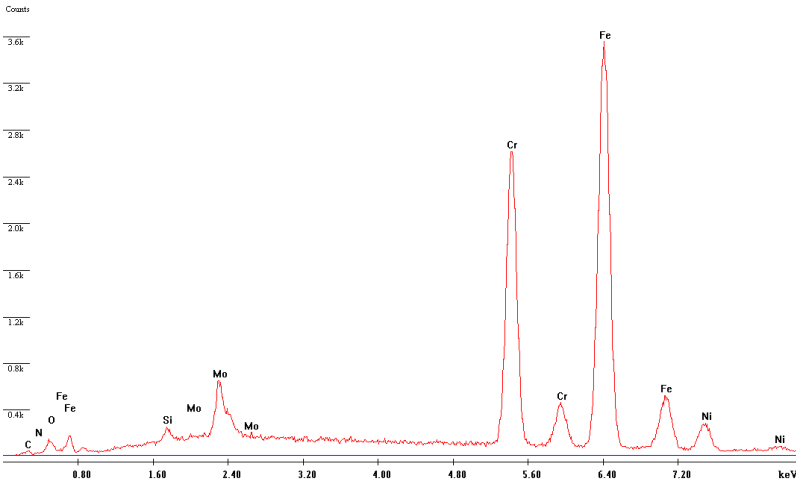


Figure 1.7.1 Ferrite 4 min 850°C SDSS

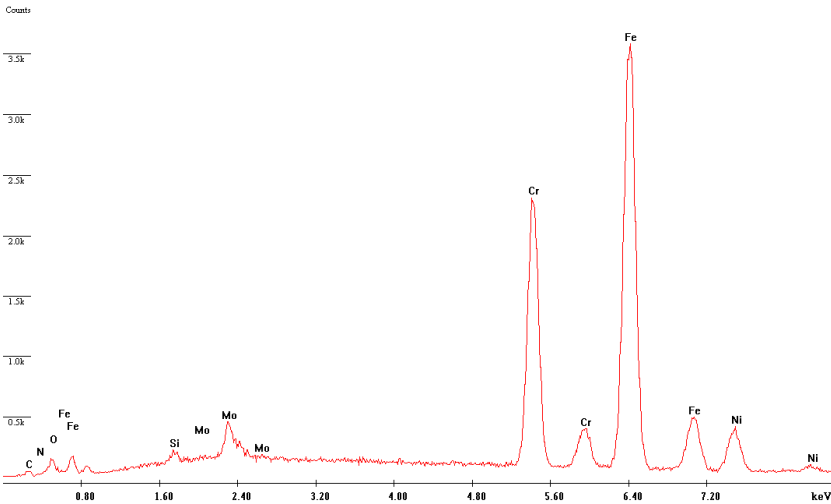


Figure 1.7.2. Austenite 4 min 850°C SDSS

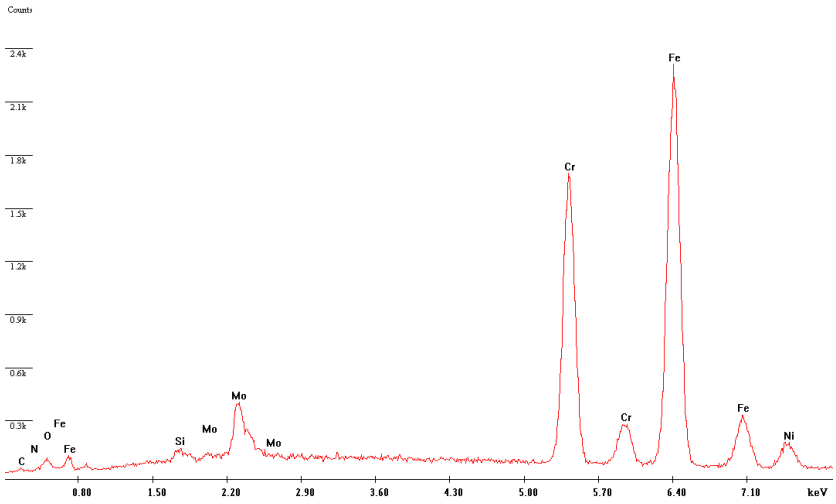


Figure 1.7.3. Ferrite 6 min 850°C SDSS

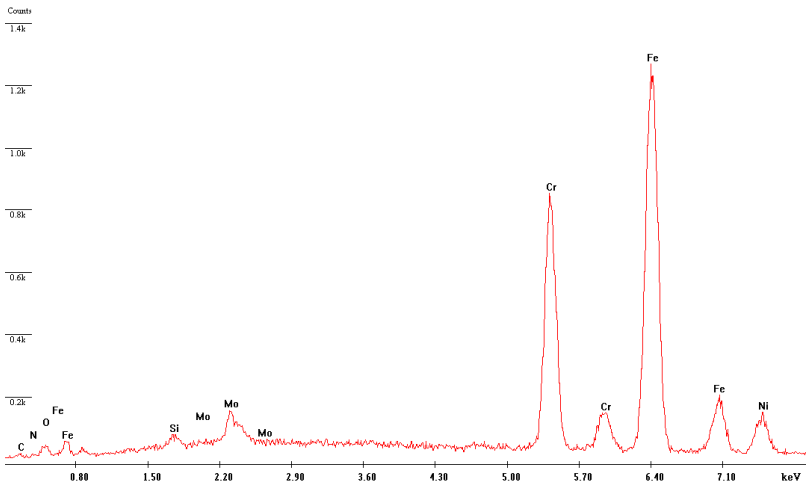


Figure 1.7.4. Austenite 6 min 850°C SDSS

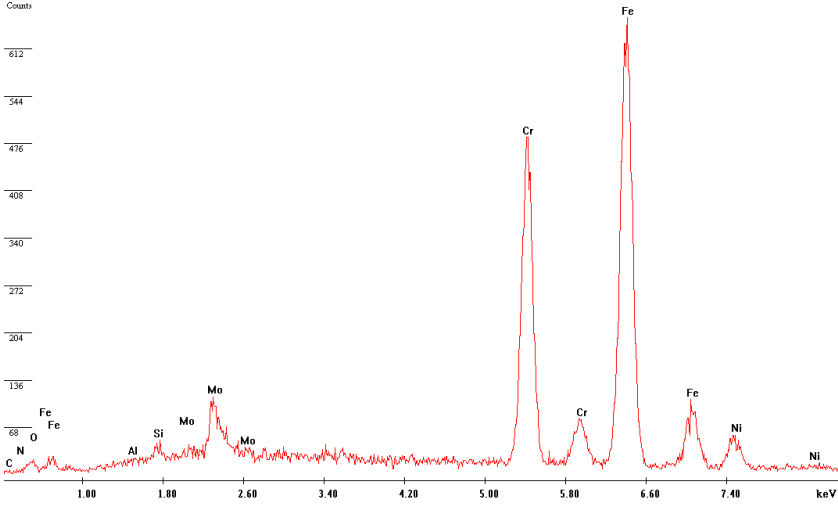


Figure 1.7.5. Ferrite 10 min 850°C SDSS

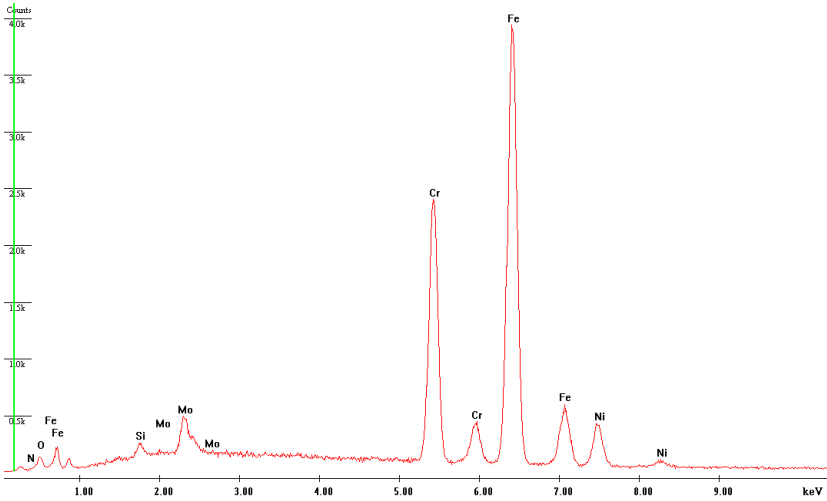


Figure 1.7.6. Austenite 10 min 850°C SDSS

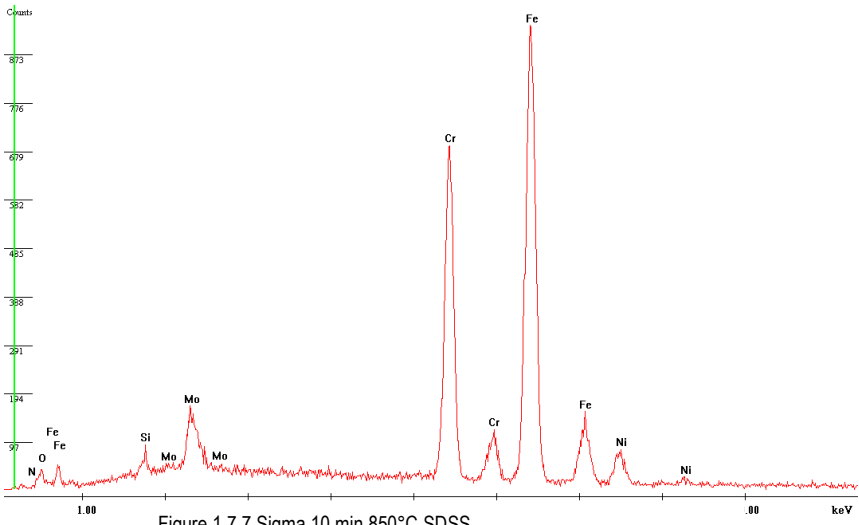


Figure 1.7.7. Sigma 10 min 850°C SDSS

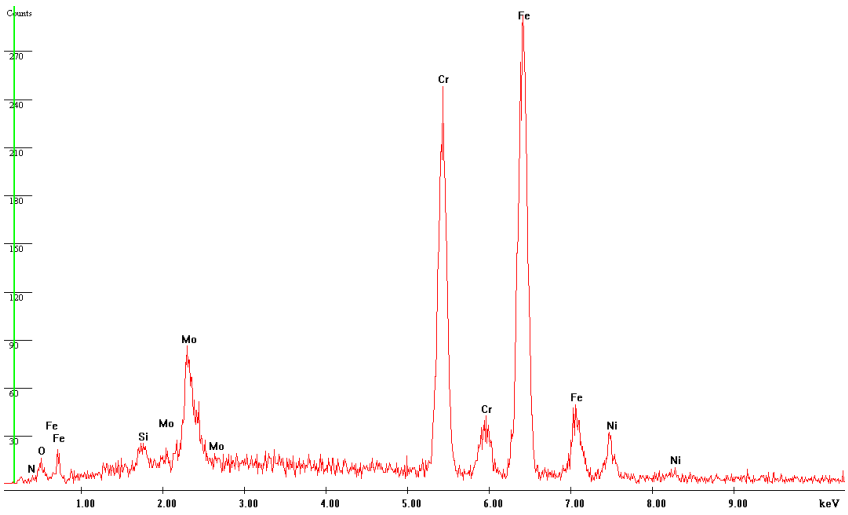


Figure 1.7.8. Chi 10 min 850°C SDSS

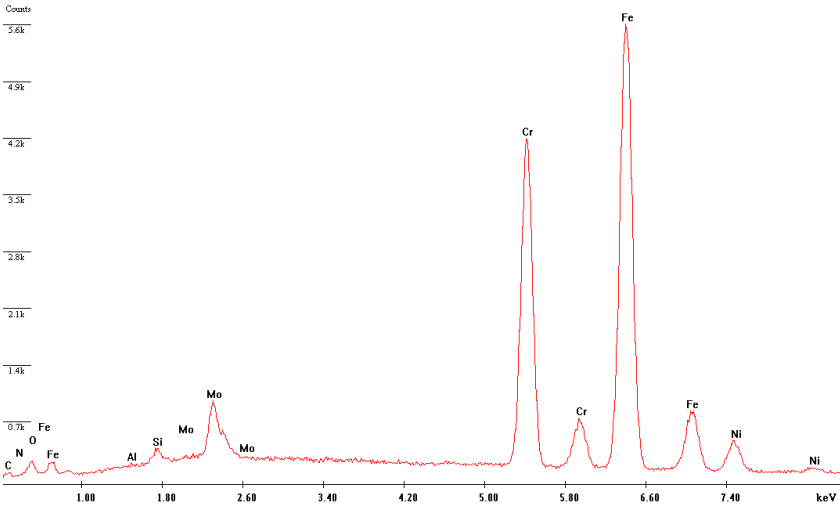


Figure 1.7.9. Ferrite 16 min 850°C SDSS

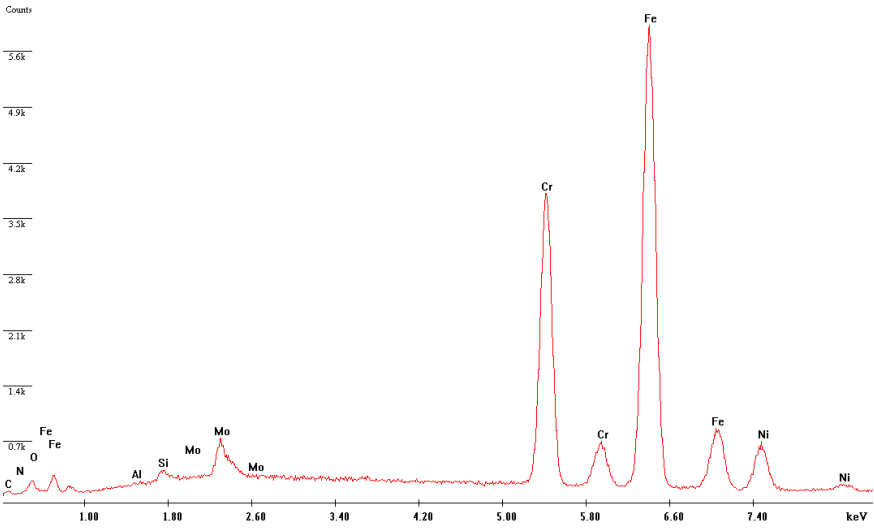


Figure 1.7.10. Austenite 16 min 850°C SDSS

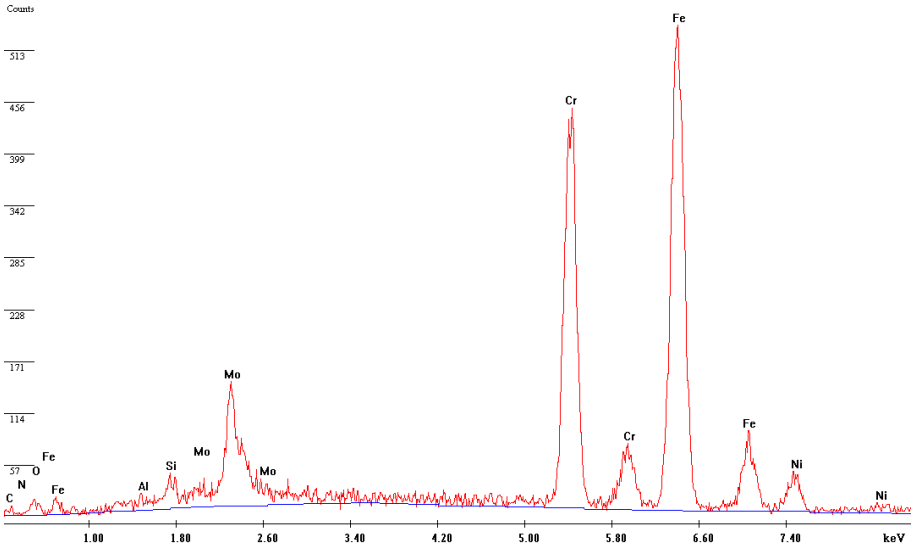


Figure 1.7.11. Sigma 16 min 850°C SDSS

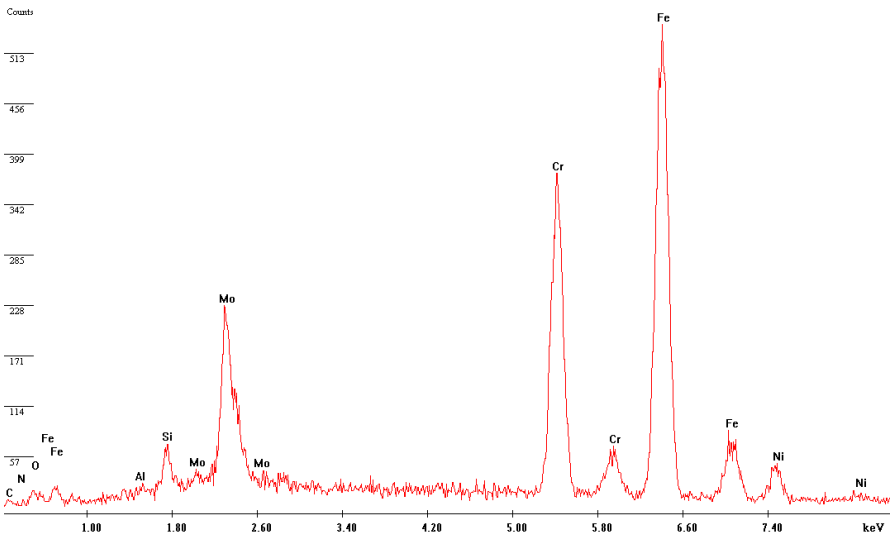


Figure 1.7.12. Chi 16 min 850°C SDSS

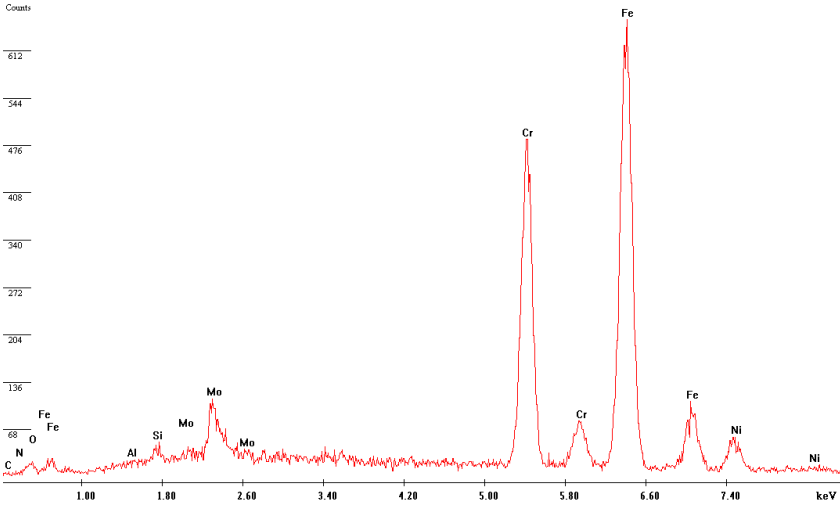


Figure 1.7.13. Ferrite 24 min 850°C SDSS

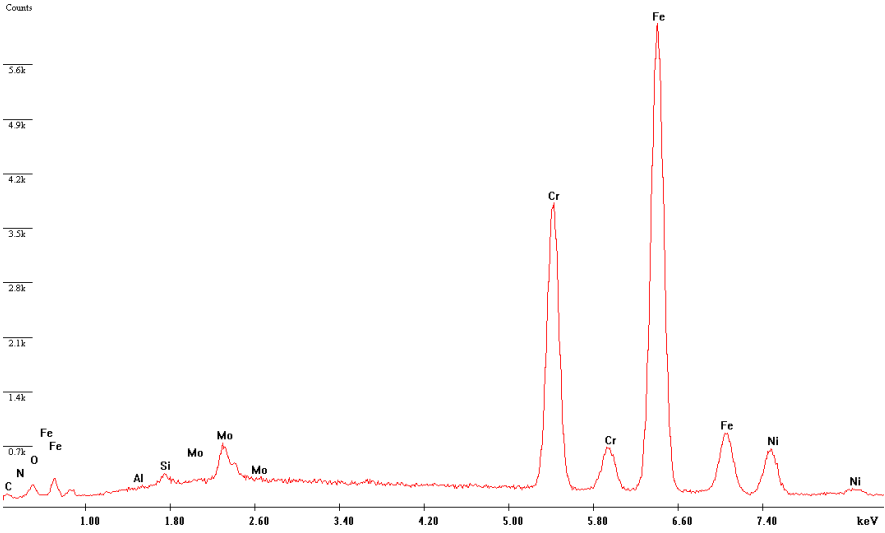


Figure 1.7.14.austenite 24 min 850°C SDSS

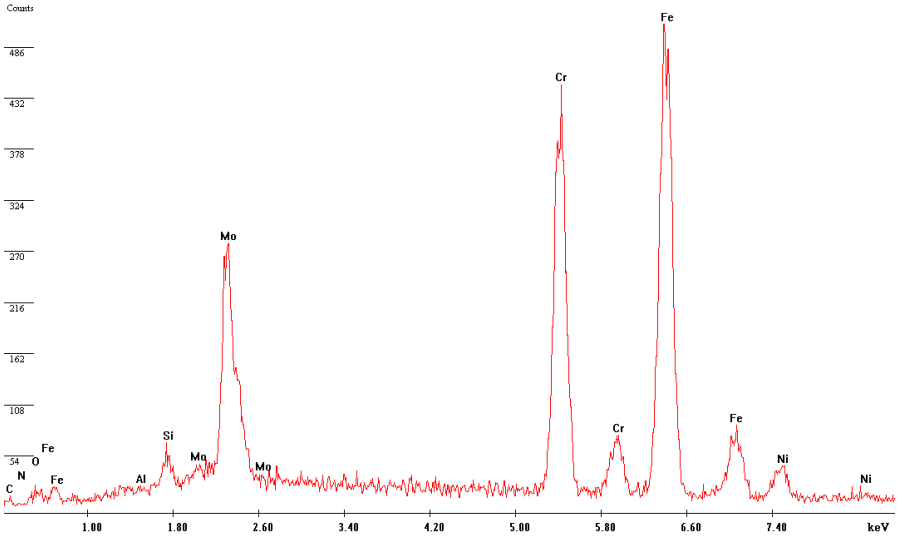


Figure 1.7.15 Sigma 24 min 850°C SDSS

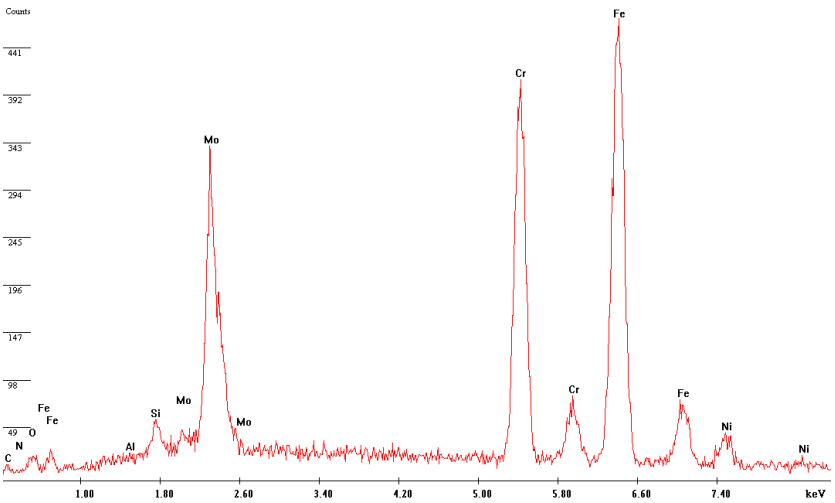


Figure 1.7.16. Chi 24 min 850°C SDSS

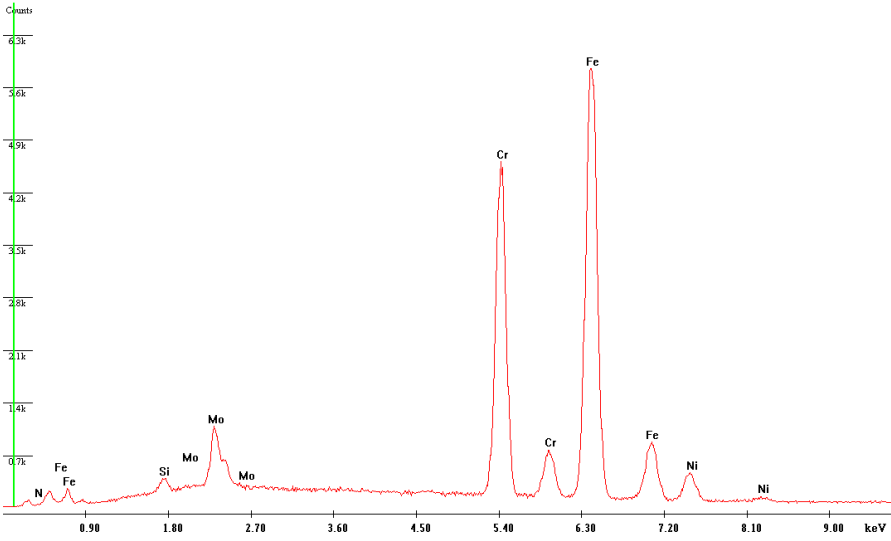


Figure 1.7.17. Ferrite 900 min 850°C SDSS

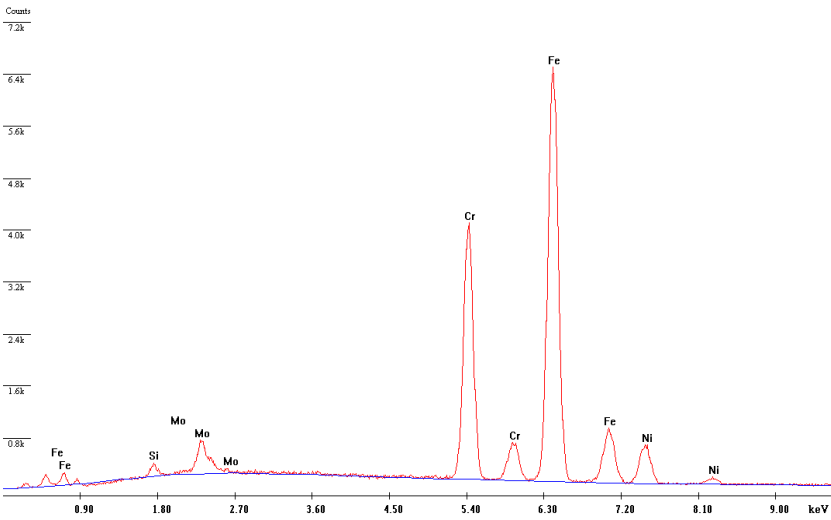


Figure 1.7.18. Ferrite 900 min 850°C SDSS

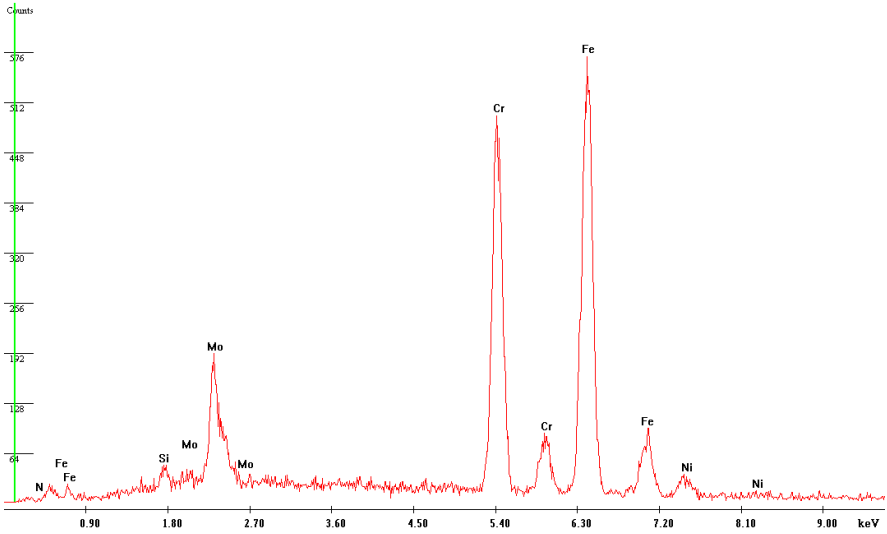


Figure 1.7.19. sigma 900 min 850°C SDSS

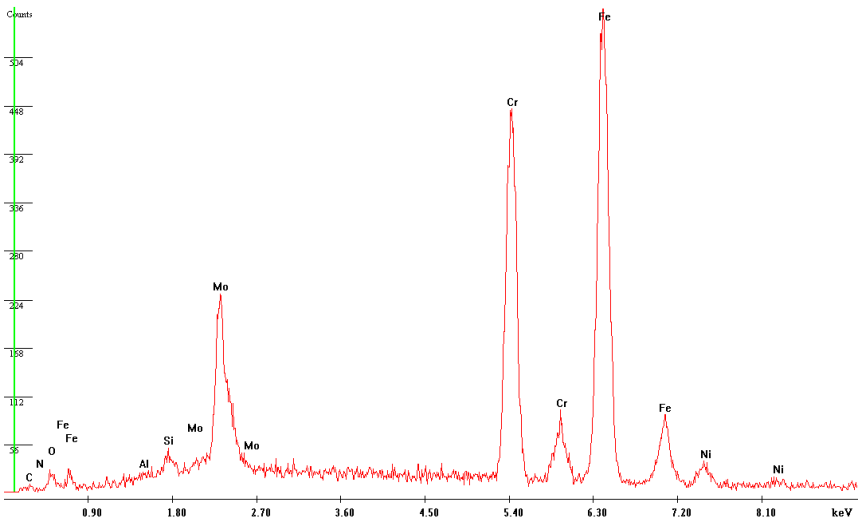


Figure 1.7.20. Chi 900 min 850°C SDSS

APPENDIX 8: HARDNESS EQUIVALENCE

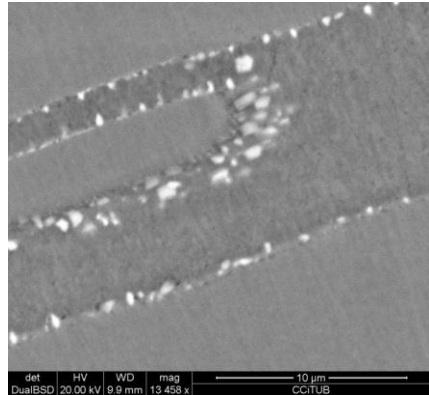
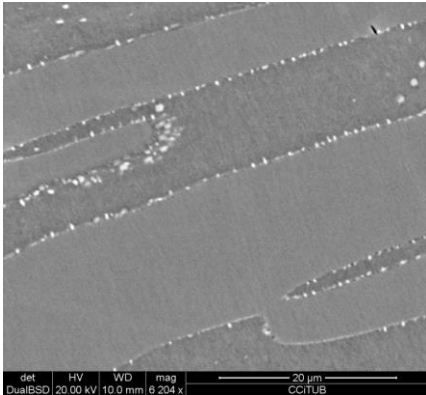
| ROCKWELL HARDNESS | | | | ROCKWELL SURFACE HARDNESS | | | Vickers Hardness | Brinell Hardness P: 3.000 kg. steel ball Ø 10 mm | | Resistance to Traction Mpa |
|---------------------------------------|--|--------------------------------------|---------------------------------------|--|--|--|--------------------------------|---|---------------|-------------------------------|
| HRC | HRB | HRA | HRD | Scale 15-N P.15 kg. Diamond cone | Scale 30-N P.30 kg. Diamond cone | Scale 45-N P.45 kg. Diamond cone | HW | Standard Ball | Tungsten Ball | |
| Escale C P.150 kg. Diamond cone | Escale B P.100 kg. Steel ball Ø 1/16" | Escale A P.60 kg. Diamond cone | Escale D P.100 kg. Diamond cone | | | | P.30 kg. Diamond Pyramid | | | |
| 68 | --- | 85,6 | 76,9 | 93,2 | 84,4 | 75,4 | 940 | --- | --- | --- |
| 67 | --- | 85,0 | 76,1 | 92,9 | 83,6 | 74,2 | 900 | --- | --- | --- |
| 66 | --- | 84,5 | 75,4 | 92,5 | 82,8 | 73,3 | 865 | --- | --- | --- |
| 65 | --- | 83,9 | 74,5 | 92,2 | 81,9 | 72,0 | 832 | --- | (739) | --- |
| 64 | --- | 83,4 | 73,8 | 91,8 | 81,1 | 71,0 | 800 | --- | (722) | --- |
| 63 | --- | 82,8 | 73,0 | 91,4 | 80,1 | 69,9 | 772 | --- | (705) | --- |
| 62 | --- | 82,3 | 72,2 | 91,1 | 79,3 | 68,8 | 746 | --- | (688) | --- |
| 61 | --- | 81,8 | 71,5 | 90,7 | 78,4 | 67,7 | 720 | --- | (670) | --- |
| 60 | --- | 81,2 | 70,7 | 90,2 | 77,5 | 66,6 | 697 | --- | (654) | --- |
| 59 | --- | 80,7 | 69,9 | 89,8 | 76,6 | 65,5 | 674 | --- | (634) | --- |
| 58 | --- | 80,1 | 69,2 | 89,3 | 75,7 | 64,3 | 653 | --- | 615 | --- |
| 57 | --- | 79,6 | 68,5 | 88,9 | 74,8 | 63,2 | 633 | --- | 595 | --- |
| 56 | --- | 79,0 | 67,7 | 88,3 | 73,9 | 62,0 | 613 | --- | 577 | --- |
| 55 | --- | 78,5 | 66,9 | 87,9 | 73,0 | 60,9 | 595 | --- | 560 | 2075 |
| 54 | --- | 78,0 | 66,1 | 87,4 | 72,0 | 59,8 | 577 | --- | 543 | 2015 |
| 53 | --- | 77,4 | 65,4 | 86,9 | 71,2 | 58,6 | 560 | --- | 525 | 1950 |
| 52 | --- | 76,8 | 64,6 | 86,4 | 70,2 | 57,4 | 544 | (500) | 512 | 1880 |
| 51 | --- | 76,3 | 63,8 | 85,9 | 69,4 | 56,1 | 528 | (487) | 496 | 1820 |
| 50 | --- | 75,9 | 63,1 | 85,5 | 68,5 | 55,0 | 513 | (475) | 481 | 1760 |
| 49 | --- | 75,2 | 62,1 | 85,0 | 67,6 | 53,8 | 498 | (464) | 469 | 1695 |
| 48 | --- | 74,7 | 61,4 | 84,5 | 66,7 | 52,5 | 484 | 451 | 455 | 1635 |
| 47 | --- | 74,1 | 60,8 | 83,9 | 65,8 | 51,4 | 471 | 442 | 443 | 1580 |
| 46 | --- | 73,6 | 60,0 | 83,5 | 64,8 | 50,3 | 458 | 432 | 432 | 1530 |
| 45 | --- | 73,1 | 59,2 | 83,0 | 64,0 | 49,0 | 446 | 421 | 421 | 1480 |
| 44 | --- | 72,5 | 58,5 | 82,5 | 63,1 | 47,8 | 434 | 409 | 409 | 1435 |
| 43 | --- | 72,0 | 57,7 | 82,0 | 62,2 | 46,7 | 423 | 400 | 400 | 1385 |
| 42 | --- | 71,5 | 56,9 | 81,5 | 61,3 | 45,5 | 412 | 390 | 390 | 1340 |
| 41 | --- | 70,9 | 56,2 | 80,9 | 60,4 | 44,3 | 402 | 381 | 381 | 1295 |
| 40 | --- | 70,4 | 55,4 | 80,4 | 59,5 | 43,1 | 392 | 371 | 371 | 1250 |
| 39 | --- | 69,9 | 54,6 | 79,9 | 58,6 | 41,9 | 382 | 362 | 362 | 1215 |
| 38 | --- | 69,4 | 53,8 | 79,4 | 57,7 | 40,8 | 372 | 353 | 353 | 1180 |
| 37 | --- | 68,9 | 53,1 | 78,8 | 56,8 | 39,6 | 363 | 344 | 344 | 1160 |
| 36 | (109,0) | 68,4 | 52,3 | 78,3 | 55,9 | 38,4 | 354 | 336 | 336 | 1115 |
| 35 | (108,5) | 67,9 | 51,5 | 77,7 | 55,0 | 37,2 | 345 | 327 | 327 | 1080 |
| 34 | (108,0) | 67,4 | 50,8 | 77,2 | 54,2 | 36,1 | 336 | 319 | 319 | 1055 |
| 33 | (107,5) | 66,8 | 50,0 | 76,6 | 53,3 | 34,9 | 327 | 311 | 311 | 1025 |
| 32 | (107,0) | 66,3 | 49,2 | 76,1 | 52,1 | 33,7 | 318 | 301 | 301 | 1000 |
| 31 | (106,0) | 65,8 | 48,4 | 75,6 | 51,3 | 32,5 | 310 | 294 | 294 | 980 |
| 30 | (105,5) | 65,3 | 47,7 | 75,0 | 50,4 | 31,3 | 302 | 286 | 286 | 950 |
| 29 | (104,5) | 64,7 | 47,0 | 74,5 | 49,5 | 30,1 | 294 | 279 | 279 | 930 |
| 28 | (104,0) | 64,3 | 46,1 | 73,9 | 48,6 | 28,9 | 286 | 271 | 271 | 910 |
| 27 | (103,0) | 63,8 | 45,2 | 73,3 | 47,7 | 27,8 | 279 | 264 | 264 | 880 |
| 26 | (102,5) | 63,3 | 44,6 | 72,8 | 46,8 | 26,7 | 272 | 258 | 258 | 860 |
| 25 | (101,5) | 62,8 | 43,8 | 72,2 | 45,9 | 25,5 | 266 | 253 | 253 | 840 |
| 24 | (101,0) | 62,4 | 43,1 | 71,6 | 45,0 | 24,3 | 260 | 247 | 247 | 825 |
| 23 | 100,0 | 62,0 | 42,1 | 71,0 | 44,0 | 23,1 | 254 | 243 | 243 | 805 |
| 22 | 99,0 | 61,5 | 41,6 | 70,5 | 43,2 | 22,0 | 248 | 237 | 237 | 785 |
| 21 | 98,5 | 61,0 | 40,9 | 69,9 | 42,3 | 20,7 | 243 | 231 | 231 | 770 |
| 20 | 97,8 | 60,5 | 40,1 | 69,4 | 41,5 | 19,6 | 238 | 226 | 226 | 760 |
| (18) | 96,7 | --- | --- | --- | --- | --- | 230 | 219 | 219 | 730 |
| (16) | 95,5 | --- | --- | --- | --- | --- | 222 | 212 | 212 | 705 |
| (14) | 93,9 | --- | --- | --- | --- | --- | 213 | 203 | 203 | 675 |
| (12) | 92,3 | --- | --- | --- | --- | --- | 204 | 194 | 194 | 650 |
| (10) | 90,7 | --- | --- | --- | --- | --- | 196 | 187 | 187 | 620 |
| (8) | 89,5 | --- | --- | --- | --- | --- | 188 | 179 | 179 | 600 |
| (6) | 87,1 | --- | --- | --- | --- | --- | 180 | 171 | 171 | 580 |
| (4) | 85,5 | --- | --- | --- | --- | --- | 173 | 165 | 165 | 550 |
| (2) | 83,5 | --- | --- | --- | --- | --- | 166 | 158 | 158 | 530 |
| (0) | 81,7 | --- | --- | --- | --- | --- | 160 | 152 | 152 | 515 |

Table 1.8.1. Hardness equivalence table

APPENDIX 9: DETAILS OF MICROSTRUCTURE

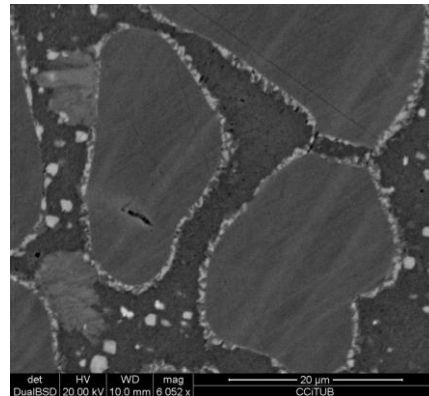
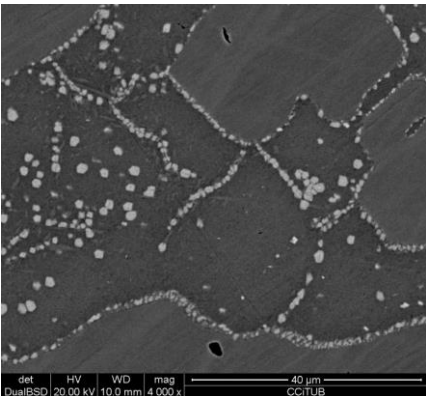
Detail for sample **4/6 min-850°C**.

No further images or information is provided because there was no change in the microstructure and no precipitation of intermetallic phases was detected.



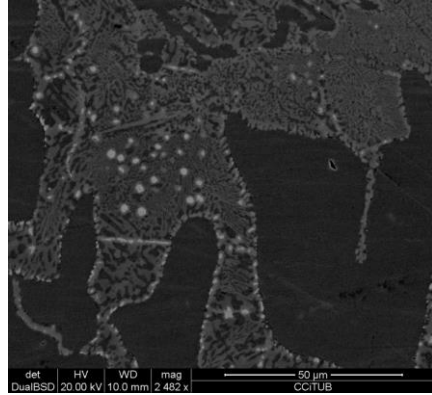
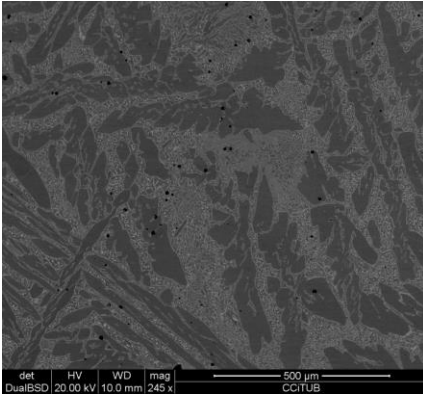
Detail for sample **16 min-850°C**.

The formation of intermetallic phase is clearly formed in the ferrite/austenite boundaries, but is commencing its formation towards inside the ferritic matrix. Different shades of grey/white located in the second image are a clear indication of both sigma and chi-phase presence.



Detail for sample **24 min-850°C**.

In the image we can appreciate that the formation of sigma phase also happens in the ferrite/ferrite grain boundaries. Moreover, its grain size is considerably larger than in samples with a lesser thermal treatment. Again, different shades present in secondary phases indicates the formation of sigma and chi, which is later on corroborated by EDS microanalysis.

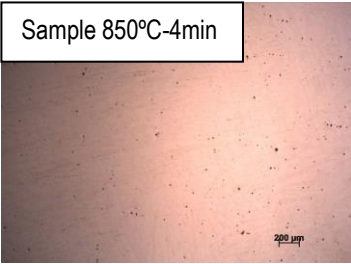


Detail for sample **900 min-850°C**.

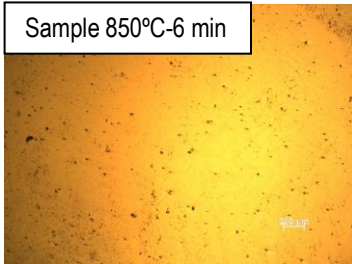
In this image we can see many silicon oxide inclusions which are a defect on the steel's microstructure. For purposes of phase quantification these inclusion were left out and not counted, as they don't evolve with different time scales of TT. As well as this an increase in the amount of austenite is fairly clear in comparison with other samples. We can also see the ferritic matrix is disappearing in order to form austenitic matrix.

APPENDIX 10: CORROSION

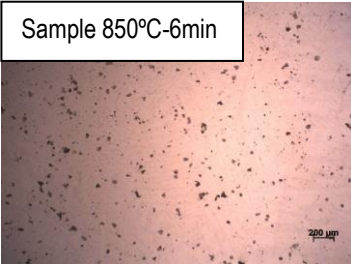
Sample 850°C-4min



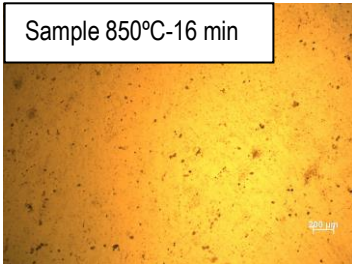
Sample 850°C-6 min



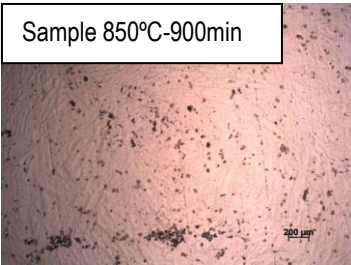
Sample 850°C-6min



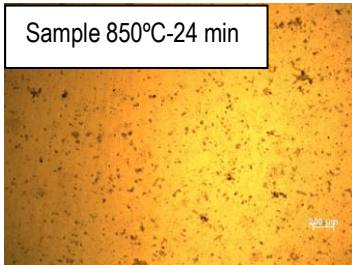
Sample 850°C-16 min



Sample 850°C-900min

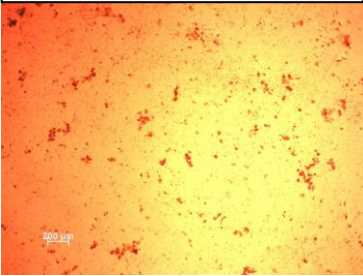


Sample 850°C-24 min

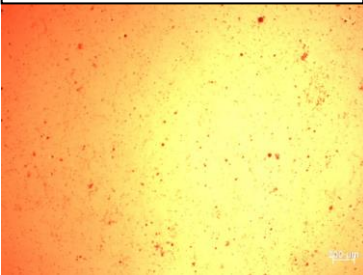


Samples in a pink tone correspond to the 4% NaCl solution experiment, whilst the ones with the pink tone correspond to the experiment with sea water. As you are able to see, the bigger the time scale of TT the more dots appear on the surface. Moreover, when comparing samples with the same TT time and different corrosion experiments, the ones in sea water solution present a much higher amount of potential corrosion.

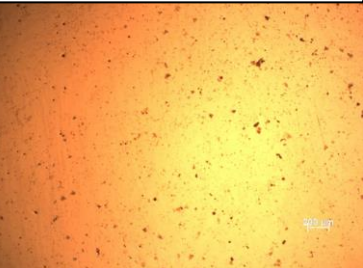
Sample No TT



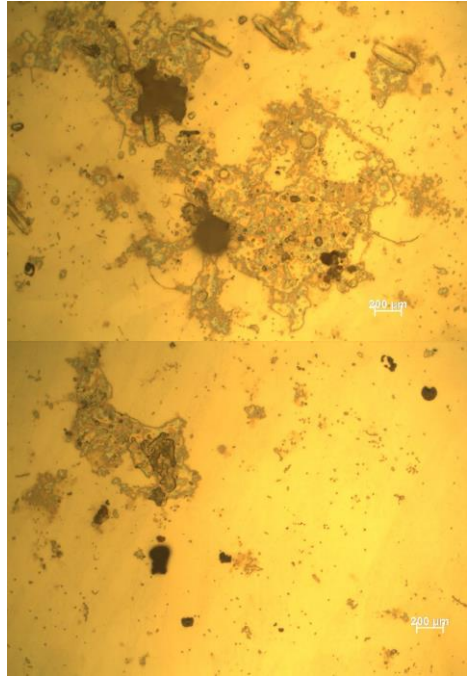
Sample 1050°C-16 min



Sample 1050°C-24 min



Samples of TT 1050°C have much less dots; hence less corrosion products than the ones with the same time scale but different TT. This is because these samples lack formation of secondary phases and are more resistant to corrosion.



Sample 850 ° C-24 min big pit

These pits were found in the sample B5. They are very big in comparison to those found in other samples undergoing the same experiment. A very high concentration of salt (chlorides) is found in their surroundings.

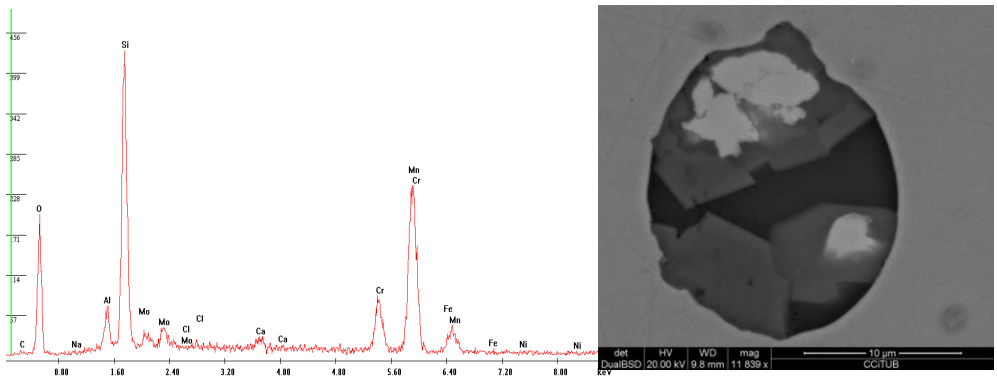


Diagram 10.1-Sample A2

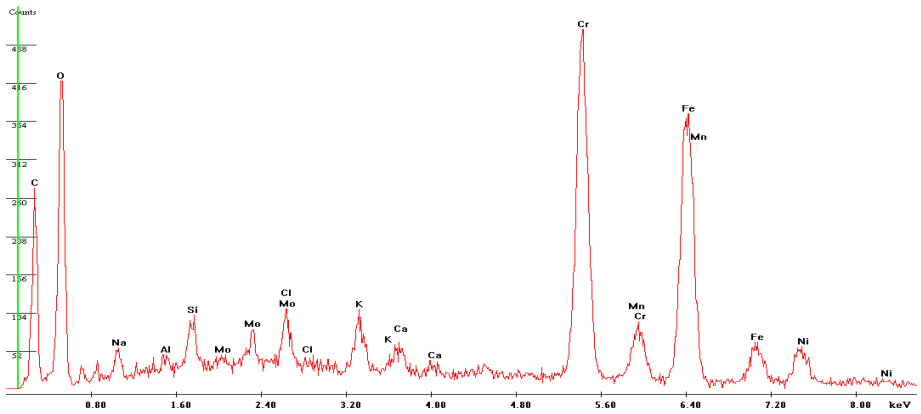


Diagram 10.2-Sample A3-edge of sample

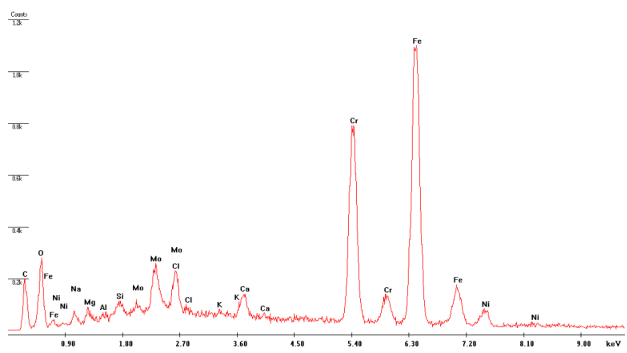
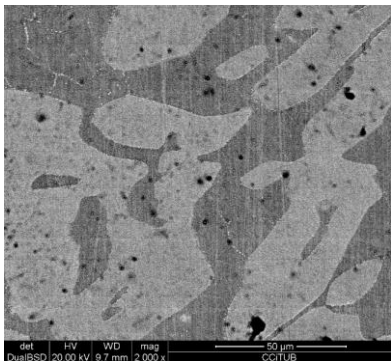


Figure 10.3. 10 min 850°C

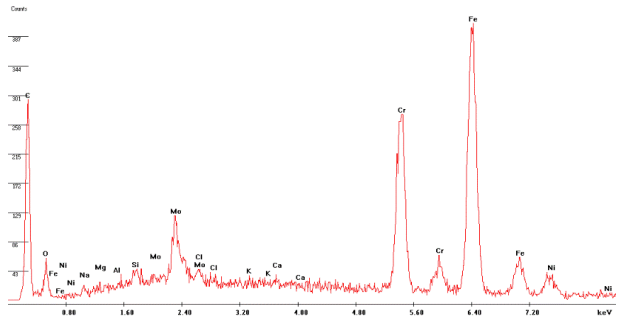
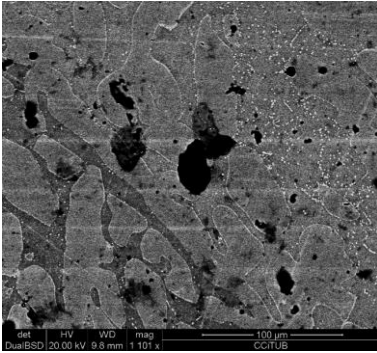


Figure 10.4 16 min 850°C

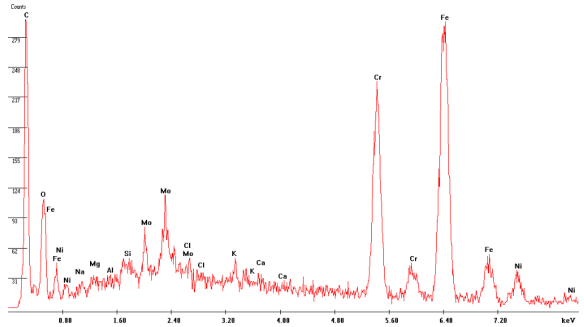
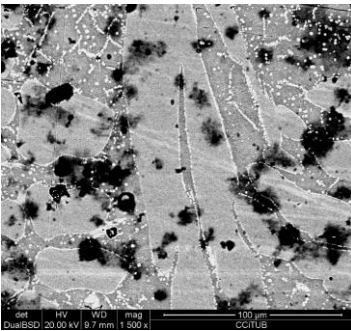


Figure 10.5 24 min 850°C

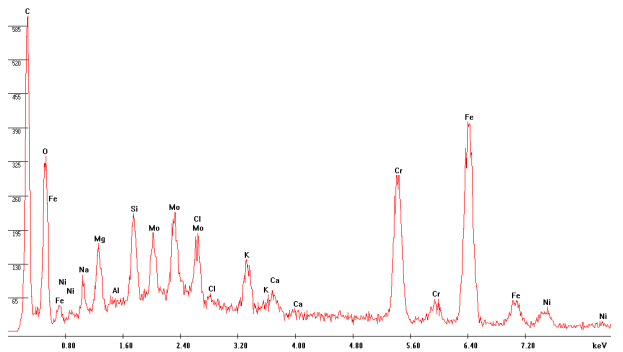
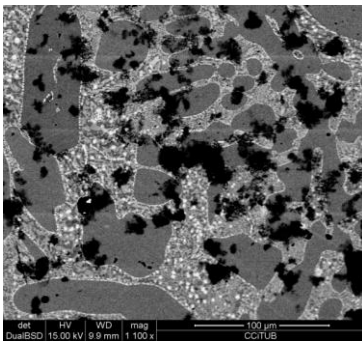


Figure 10.6 90 min 850°C

